Spring 2020

# Effects of Material Characteristics and Equipment Configuration on Profilometry Scanning Results for Error Mitigation in Automated Fiber Placement

Jacob Ondeck

# Effects of Material Characteristics and Equipment Configuration on Profilometry Scanning Results for Error Mitigation in Automated Fiber Placement

by

Jacob Ondeck

Bachelor of Science
Boston University, 2014

---

Submitted in Partial Fulfillment of the Requirements

For the Degree of Master of Science in

Mechanical Engineering

College of Engineering and Computing

University of South Carolina

2020

Accepted by:

Michel van Tooren, Major Professor

Wout De Backer, Reader

Darun Barazanchy, Reader

Cheryl L. Addy, Vice Provost and Dean of the Graduate School

# ACKNOWLEDGEMENTS

I would like to thank the following for their help throughout the project; Wout De Backer, Michel van Tooren, Saurabh Vaidya, Darun Barazanchy, the entirety of the Multifunctional Materials and Structures team, Kris Czaja, Ingersoll Machine Tools, and the McNair Support Staff. Additionally, a special thanks is owed to my friends and family, especially my wife Charlie, for their continual support.

# ABSTRACT

The Automated Fiber Placement manufacturing process is a method for constructing layered composite parts. This is done by placing tapes of material on a tool using a compaction roller and heat to tackify the material [1]. This manufacturing process is not new, but latest equipment generations can still introduce randomly occurring defects, presenting often as tow twists, gaps, unintentional overlaps and even missing tows during the layup process. These defects deviate the manufactured structure from the as-designed structure, and have been proven to introduce stress concentration sources, which can ultimately undermine the performance of a structure [2]. To detect and avert these defects during manufacturing, a profilometry driven topology analysis system can be used to scan the placed tows, check for layup defects, and record a history of the part [3,4]. However, for certain materials and environmental conditions, it has been shown that the utilized profilometers do not currently return reliable readings of the material topology. An experimental investigation into the feasibility of improving scan results of specific thermoset composite materials is summarized by investigating settings on commercially available profilometry scanners. Additionally, the impacts of material characteristics including surface quality are explored. Presented are the challenges, analysis, and potential solutions discovered to improve scanning results.

# TABLE OF CONTENTS

# LIST OF TABLES

# LIST OF FIGURES

# LIST OF EQUATIONS

# LIST OF ABBREVIATIONS

ACSIS ..... Automated Composite Structure Inspection System

AFP ..... Automated Fiber Placement

ATL ..... Automated Tape Laying

CED ..... Canny Edge Detection

CFTP ..... Composite Fourier-transform Profilometry

FEA ..... Finite Element Analysis

FTP ..... Fourier-transform Profilometry

IFTP ..... Improved Fourier-transform Profilometry

IMT ..... Ingersoll Machine Tools

MFTP ..... Modified Fourier-transform Profilometry

NOAA ..... National Oceanic and Atmospheric Administration

# CHAPTER 1

# INTRODUCTION

Automatic Fiber Placement (AFP) has become an increasingly widely used manufacturing process as the aerospace industry, as shown by its rapid adoption of the new technology, benefits greatly from its obvious improvements to traditional composite manufacturing [4]. The AFP process of placing tows of composite material onto a mandrel or mold, while using heat to tackify the material and a compaction roller to compress (shown in Figure 1.1 and Figure 1.2) [1], is not perfectly reliable. Defects can arise due to manufacturing parameters such as part geometry and material type, occurring as the misplacement of tows or unintended modification of tow geometry (section 2.1) [2]. The detection and recording of these defects, automated in the current generation of inspection systems by incorporating laser based profilometry scanners (section 2.2), is vital to the success of AFP manufacturing. However, certain materials have proven to produce inauthentic results when subjected to this scanning. Introduced in this section, and discussed in depth throughout the subsequent sections, are the considerations, purpose, and experimental goals of this thesis.

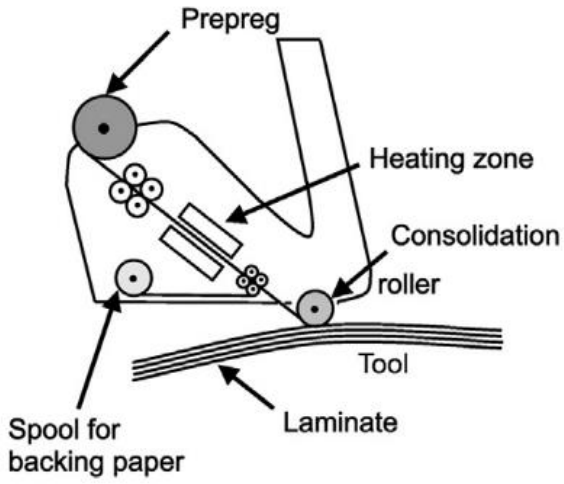


*Figure 1.1: AFP Head and Tooling Interface (Schematic)* [1]

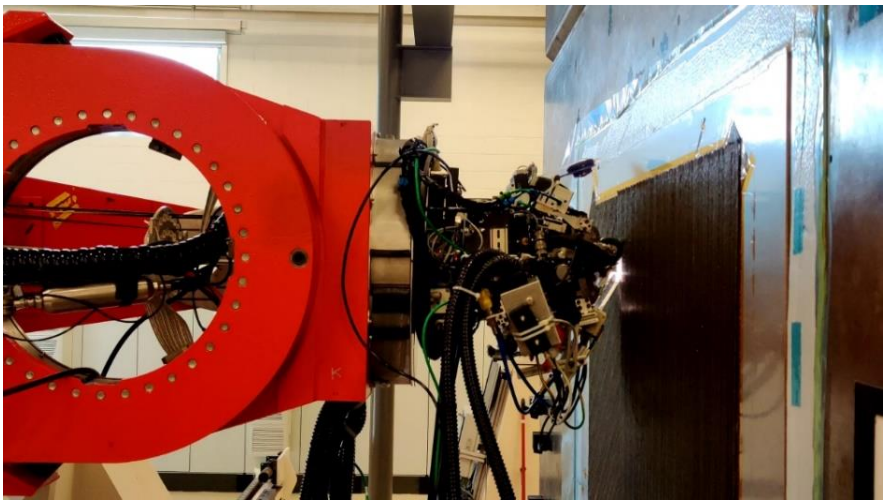

*Figure 1.2: AFP Head and Tooling Interface*

## 1.1 LAYUP DEFECTS AND INSPECTION SYSTEMS

In the current generation of the AFP process, an attentive operator is necessary during manufacturing to look for any process defects that may occur. These defects can be in many forms, including twisting of the tows or tows that are missing. Furthermore, these defects can cause voids or stress concentrations within a part (section 2.1), which are disadvantageous as they can undermine the performance of a structure.

To reduce the intensity of operator attention, Ingersoll Machine Tools (IMT) developed an automated composite structure inspection system (ACSIS) that scans the placed tows of each ply, checks for layup defects, and records a history of the part. This system, shown in Figure 1.3, consists of a scanning head mounted to a robotic arm which sends data to a computer for processing (section 2.2). The sensing end of this system is built from digital profilometry scanners that measure the surface of the structure. These 3D topography measurement tools are used ubiquitously across multiple industries for quality control, including but not limited to composites manufacturing and automotive part inspection. Additionally, this inspection system is ideally able to be utilized regardless of material, as AFP manufacturing is not limited to one specific reinforced polymer.


*Figure 1.3: ACSIS Developed by IMT*

## 1.2 SCANNING ERRORS AND SPECULATIVE CAUSES

During operationalizing of this ACSIS system, IMT observed that the scanning of certain materials produced erroneous scan results. These scanning issues were termed “noisy” as the unreadable data often appeared intermittently, sporadically manifesting within single scans. In some cases, materials were found to be completely unreadable, resulting in a void in the entirety of scan data (section 3.1).

The cause of this effect is due to the way in which the profilometry scanner collect data. From analysis of the scanner’s manual, Figure 1.4, and the topography tool’s data sheet, the scanner's measurement relies on the target object’s ability to scatter light [3]. All light emitted from the scanner, once it reaches the target object’s surface, is either reflected, refracted, or absorbed. This is shown in Figure 1.5 and Equation 1.1. Reflected light, the focus of this report, experiences either specular reflection of diffuse reflection. Due to this understanding of how the profilometry scanners operate, an investigation into material and equipment impact of light reflectance.

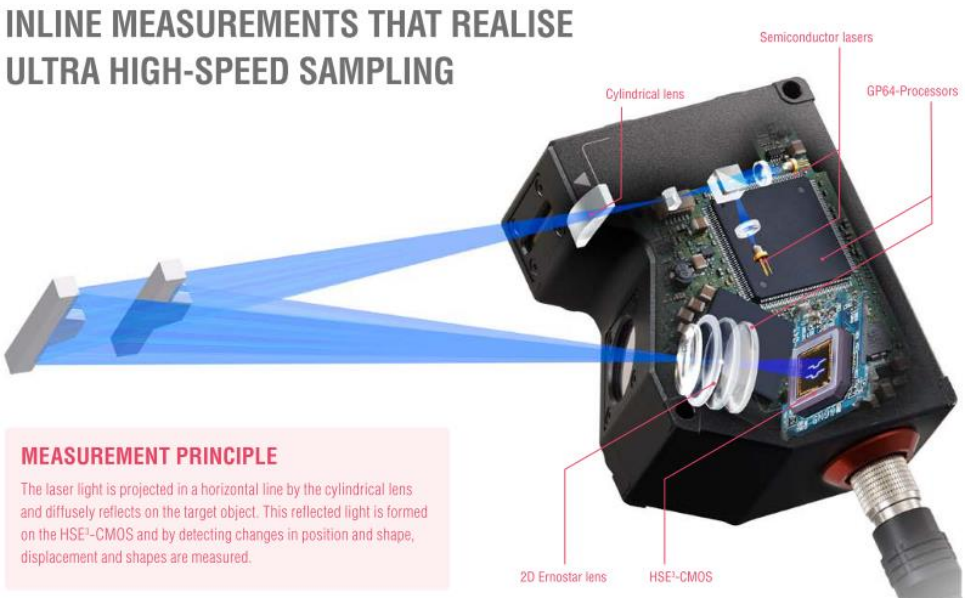


*Figure 1.4: Excerpt from Keyence Scanner Manual* [3]

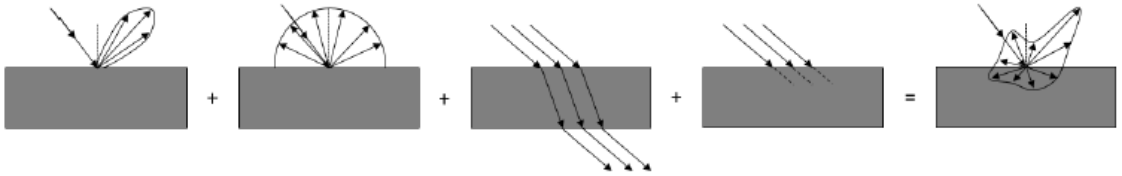

*Figure 1.5: The Summation of (from left) Specular Reflection, Diffuse Reflection, Refraction, and Absorption*

$$\Sigma\ Specular\ Reflection + \Sigma\ Diffuse\ Reflection + \Sigma\ Refraction + \Sigma\ Absorption + Statistical\ Scatter = \Sigma\ Total\ Light$$

*Equation 1.1: The summation of light reflected, refracted, and absorbed equals the total light*

## 1.3 THESIS FOCUS AND RESEARCH QUESTIONS

The focus of this research is to investigate the reason for which certain materials produce noisy image results when inspected by IMT's ACSIS. This scanning inspection system, due to the various material manufacturers and types used in composite manufacturing, is required to provide consistent results across a broad selection. For this reason, the source of the errors needs to be determined, as well as a set of possible solutions implemented in an effort to mitigate the impact of these errors during manufacturing. The overall goal of this report is to present a better understand of profilometry scanning anomalies, as well as to introduce possible solutions and suggestions gleaned from the study and findings. In completion of this goal, three research questions will be addressed. They are presented below along with an accompanying topics map (Figure 1.6), which serves to highlight a selection of topics related to the research.

Research Questions:

1. What is error in profilometry scanning and how can it be quantified?
2. What are the causes and dependencies of profilometry scanning error?
3. How can profilometry scanning error be mitigated?

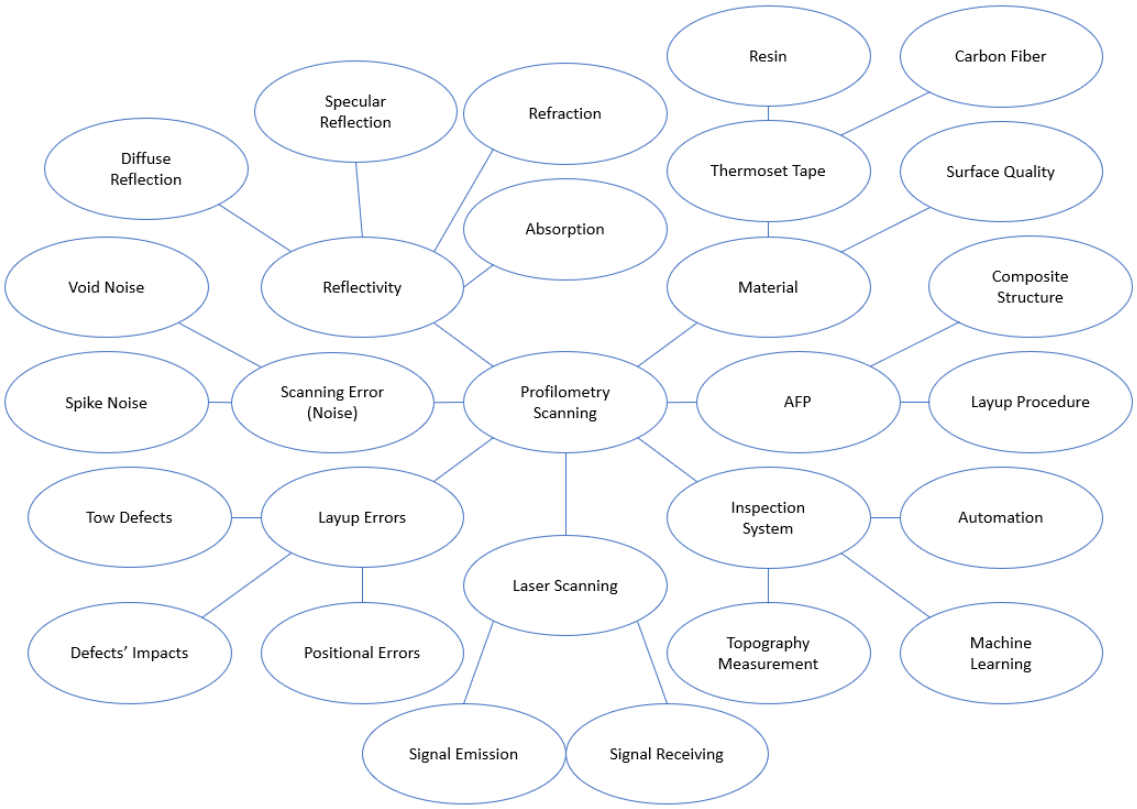


*Figure 1.6: Research Topics Map*

The following sections of this thesis report explain in detail the background and theory, experimental setup, data analysis methods, experiments performed, and overall conclusions and final observations of this research.

Chapter 3 of this report details the methods by which data was collected. This firstly includes the material selection and justification thereof. A brief discussion of scanning noise is presented here. The physical experimental setup of a constructed profilometry gantry system is detailed in this section. Additionally, material layup procedures, sample mounting techniques, and storage considerations are discussed here.

Chapter 4 of this report discusses in great detail the scan data analysis script which was developed and implemented through this research. Here, profilometry scan data noise is defined with examples of the varying manifestations. These are presented to

directly respond to research question 1. The initial design of the algorithm implemented to quantify this noise is presented along with corner cases and developed solutions and improvements. Lastly within this chapter, a baseline measurement of profilometry scan noise is plotted. This serves as a useful tool in better defining a significant level or change in scanning noise.

Chapter 5 presents the first of three major experimental investigations performed in an effort to relate profilometry scanning noise to equipment, directly responding to research questions 2 and 3. This experiment analyzes scans performed at varying pitch to determine a relationship between pitch angle and prevalence of profilometry scanning error. Discussed within this section are both a qualitative and quantitative analysis, each performed respectively prior to and after the development of the scan data analysis script detailed in chapter 4 of this thesis report.

Chapter 6 of this report discusses an experiment performed to examine the effect of thermoset material's long-term exposure to ambient conditions on profilometry scanning noise. In this experiment, two identical groups of layup samples were exposed to varying storage conditions, allowing half of the samples to cure at room temperature. A subsection of these material samples was constructed to simulate common layup errors. All samples were scanned daily, and scan data was processed using the analysis script described in chapter 4 of this report. Results of these scans are plotted over time, with trends discussed.

Chapter 7 of this report discusses the third and final experimental investigation to determine the effects of scanner settings on profilometry scanning error. This includes four distinct paths. The first presented is an analysis of scanning variables in which an

iterative investigation was performed into the effects of various combinations of scanner settings with the goal of determining a set of ideal settings. The ideal settings presented in this section are settings which when utilized do not present profilometry scanning noise in the resulting scan data. The second path presented in this chapter is an investigation into the setting of peak selection as it pertains to scanning error isolation. The next section presented in this chapter is the experimental investigation into the effect of scanning laser intensity. This section explores this variable in depth, presenting generated images of scans performed at varying intensity and pitch angle as well as plots of the calculated scanning error present and discussing trends thereof. Lastly, the combined effects of scanner settings and pitch angle are presented to determine if there exists a positive cumulative effect of these proposed solutions. Finally, chapter 8 presents conclusions and final remarks drawn from the preparation of this thesis report.

# CHAPTER 2

# LITERATURE REVIEW

The goal of this section is to provide an adequate exploration into previously established research performed on a broad selection of related topics. Relevance is determined by suitability in addressing research topics as stated herein. Addressed are the fundamental justifications for automated inspections systems (section 2.1) along with their history and the varying methods by which they are designed and employed (section 2.2). Additionally, material considerations such as surface quality and reflectivity characteristics are addressed (section 2.3).

## 2.1 EFFECTS OF LAYUP DEFECTS IN A LAMINAR COMPOSITE PART MANUFACTURED THROUGH AUTOMATED FIBER PLACEMENT

The manufacturing process of automated fiber placement (AFP) has existed since the 1970's and has been commercially available since the 1990's [4]. The AFP process was introduced as an advancement of automated tape laying (ATL) to tackle the challenges of laying up tape onto a curved surface. This automated process of delivering multiple tows/tapes of material at variable speeds to create composite laminates with custom geometries, reduces manufacturing waste and improves both manufacturing accuracy and efficiency compared to traditional hand-lamination techniques [4]. This led to the ability to create more light weight aircraft structures, cutting down on fuel consumption requirements. These benefits are further evident in the rapid adoption of composite manufacturing in the aerospace industry. For instance, the Boeing 787 has an

aircraft structure fraction of 50% composite material [4]. However still today there exists a manufacturing issue in layup errors. Layup defects occur sporadically, often correlating with part geometry and material characteristics. More importantly, as both shown through finite element analysis (FEA) simulations and determined experimentally, undermine the performance of the part as well as the ability to accurately replicate results [2,4–10]. This report subsection addresses varying defect characterization, causes of defects during AFP, and effects of defects on part performance.

### 2.1.1 COMMON DEFECT GEOMETRY AND FORMATION

Within the context of this report "defect" will refer to any deviance in a manufactured structure from the as-designed structure. These defects of interest herein occur as part of the on-line AFP consolidation process (Figure 2.1) [11]. Historically, many efforts have been made into identification, sourcing, and characterization of these defects [4,12,13].

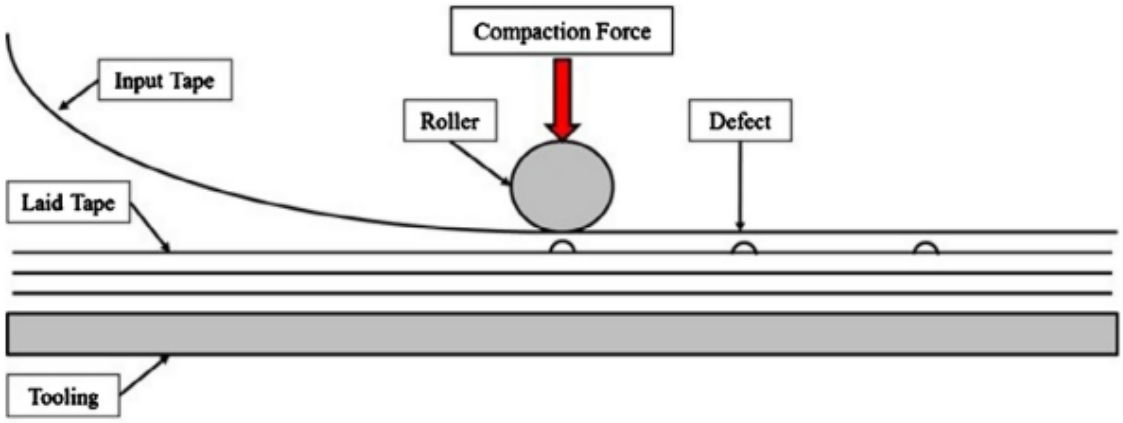


*Figure 2.1: On-line Consolidation Process* [11]

For the purpose of neural network based automated defect detection Sacco at al. identify 15 unique types of defects. These defect types include twists, gaps, and unintentional overlaps of material tows [14]. These defect classifications are far from

novel to their work, however. Shadmehri et al. explores common defect characteristics such gap size (Figure 2.2), angle deviation (Figure 2.3), ply location, and twisted tows (Figure 2.4) in their introduction of a new inspection technique [15].

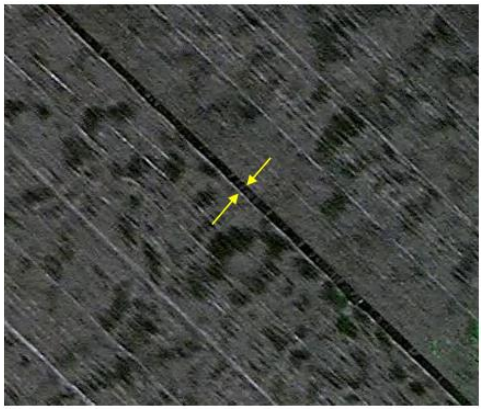

*Figure 2.2: Gap Defect Example* [15]

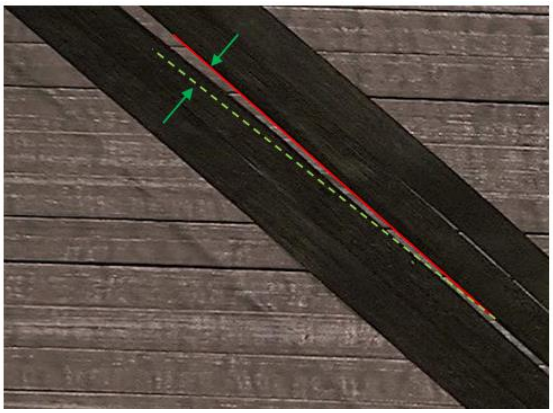

*Figure 2.3: Angle Deviation Defect* [15]

*Figure 2.4: Tow Twist Defect* [15]

Similarly, Lukaszewicz, Ward, and Potter [4] identify three distict principal tow steering defects; tow buckling, tow pull-up, and tow misalignment, where buckling and pull-up are a result of compressive and tensile forces respectively and misalinement describes any result of variability in the layup system. Their paper identified additional steering defects similar to other reference liturature; including tow gaps, unintentional overlaps, twists, and gaps [4]. That is to say that they attribute the presence of these defects to the specific fiber steering implemented during the AFP process. During layup,

the prominance of defect areas has been additionally proven to corrolate to both the number or tows and the width of the course (band of tows) inversely and directly respectively. This was proven through MATLAB simulations by Nik et al. [12].

Bakshi and Hojjati explore this further in their experimental and simulative study into AFP defects. Much of their work explores the correlation between fiber steering and defect occurance, although other process parameters are addressed. One such parameter is tack, which plays a significant roll in reducing the occurance of wrinkles during layup [13,16]. Bakshi and Hojjati address that increasing temperature during compaction, the resin viscosity is decreased. This increases the "intimate contact" made thus achieving higher tack. Through their work they were able to make correlations between sets of varying temeperatures, layup speeds, and compaction forces to the formation on two defect types; wrickle and blister (Table 2.1). [13].

*Table 2.1: AFP Parameters and Defect Correlations* [13]

| Process Parameters and resulting Layup quality | | | | | | |
|---|---|---|---|---|---|---|
| # | Radius (mm) | Nitrogen Gas | | Speed (mm/s) | Force (N) | Defect Type |
| | | Temp (C) | Flow Rate ($s^{-1}$) | | | |
| 1 | 889 | 250 | 75 | 114 | 222.4 | No defect |
| 2 | 635 | 220 | 100 | 88 | 266.9 | Waviness |
| 3 | 635 | 220 | 100 | 76 | 266.9 | Sheared fiber |
| 4 | 558.8 | 250 | 75 | 114 | 311.4 | Tow pull up |
| 5 | 558.8 | 250 | 75 | 114 | 222.4 | Wrinkle/blister |
| 6 | 558.8 | 260 | 85 | 140 | 222.4 | |
| 7 | 558.8 | 250 | 75 | 114 | 111.2 | Did not stick |

### 2.1.2 EFFECTS OF DEFECTS ON PART PERFORMANCE

Defect types each effect the strength of the composite to varying degrees. Significant literature exists supporting both FEA [8,17] and experimental investigations into defect effect on performance. Discussed in this section are results from these investigations as reported by the literature. Croft et al. report the results of tension, and

compression tests, quantifying the effects of both gap defects and overlap defects. These results show that gap defect impact on performance in both tension and compression is negligible (± 3%), however when changing the gap size this can vary to up to a 13% decrease in performance under tension. Similarly reported, overlap defect impact on performance in negligible in tension (± 3%). In compression this overlap defect has a positive effect, increasing performance up to 13% [2].

Fayazbakhsh et al. explores further the premise that defects are not always detrimental to the performance of a part. Specifically, they show that the presence of overlaps in a laminate configuration can improve the in-plane stiffness by 11% and bucking load by 71%. The effects of gap defects is also reported. Gaps, they show, can increase the bucking load by 15% over the baseline samples, although the in-plane stiffness is increased by 14% [9].

Blom et al. calculate the performance impacts of tow drop areas through FEA. Tow-drop areas are describes as small triangular resin heavy areas without any fiber present. They are caused by multiple passes of the layup head overlapping, cutting tows at the course boundary to avoid inconsistancies in part thickness. They find that the reduction in stiffness is proportional to the amount of tow-drop area and is dependent on the fiber angle distribution. The reduction in stength, they report, can be upwards of 29%. Additionally, they conclude that wide tows lead to larger tow-drop areas, and therefore more significant reductions in laminate strength [17].

Experiments conducted by Lan et al. explore the variations of in-plane shear and compression properties of laminates formed with intentional embedded gaps and overlaps of varying size. Overall, both apparent in-plane stress and compression stress is dreduced

as gap distance increases. They report that overlap length does not effect in-plane stress, and that overlap strenth decreases compression strength, but only when a caul plate is not used during autoclave curing of the AFP part. It is noteworthy that these relationships are reported for varying stacking sequences [10].

In a short series of papers, Mukhopadhyay et al. performs and reports experiments into the compressive and tensile failure of laminates containing intentional wrinkle defects, in an effort to confirm their approach to FEA modeling of wrinkle defects. Wrinkles were embedded by changing the tow direction within specified locations in the layup process. Once the laminate cured, the wringle angle was then measured by analyzing the sample's cross section (Figure 2.5). FEA models were dependant on this variable and compared to experimental results, ultimately proving the usefulness of their models. For the pupose of this literature review, the experimental results are of interest. Four samples were tested; a baseline sample and three samples with increasing wrinkle severity. Experimental results show that as wrinkle severity increases, both tensile strength and compressive strength decreased by  up to 22% and 32% below baseline figures respectively [5,6].

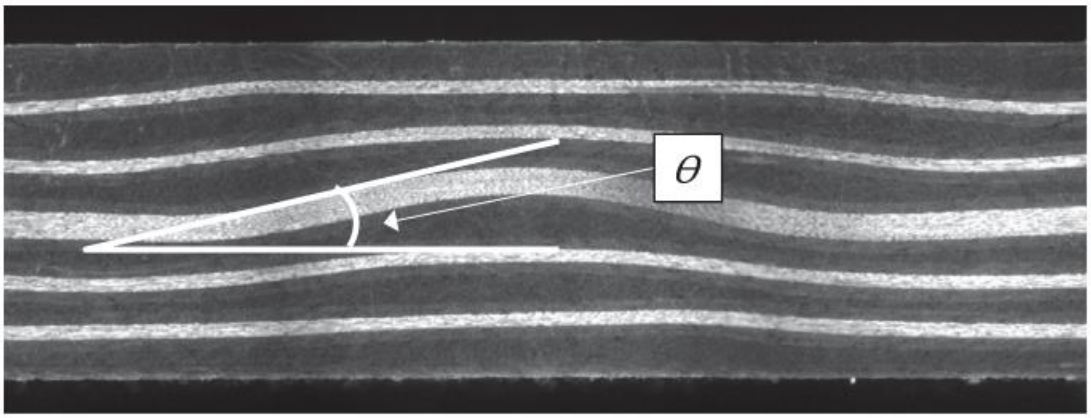


*Figure 2.5: Wrinkle Angle Measurement* [5,6]

## 2.2 PROCESS AND BENEFITS OF AN AUTOMATED INSPECTION SYSTEM

Noncontact inspection systems, whether automated, semi-automated, or manual, have been generally regarded as essential within the context of composite manufacturing, as layup errors, the presence of foreign objects, or any deviation from the as-designed structure can limit the performance of a part [2,4,14]. Because of this, the topic has been broadly explored, yielding multiple methods for profilometry and inspection. Within this section, common methods of in-process inspection are explored, along with benefits these provide to operators and overall production efficiency.

### 2.2.1 AUTOMATION, BENEFITS, AND HISTORY

To minimize the occurrence of undetected layup defects within the process of AFP manufacturing, in-process or onboard automated inspection systems have been developed and improved upon over time. Automated inspection systems can spare a manufacturing process costly rework time and reduce variability and intervention of operators. In many instances, inspection and rework can account for over 60% of total manufacturing time without automation [18]. In their current generation, and within the context of AFP manufacturing, automated inspection systems, as described by Cemensaka, Rudberg, and Henscheid of Electroimpact Inc, consist of a series of laser line emitting profilometers which scan the surface of the ply, this creating a 3D profile of the surface. The data from these scanners is then processed to detect unintentional overlaps, gaps, and other layup defects through semi-automatic inspection, in which a UI operator is provided images to inspect, or fully-automatic, in which defects can be detected, often improving these results with the use of a neural network algorithms [19][14].

Prior to this design, inspection systems were manual, however intelligent in their own regards. This process involved a laser outline projected onto the surface of the tow.

An operator would then manually inspect the tow end geometry of the layup against the projection to confirm compliance about the perimeter. Gaps, unintentional overlaps, foreign objects, and other defects within this boundary were manually inspected by sight [18]. This process was improved marginally with the introduction of a laser-vision process. In this system, a laser system was again projected over the ply, aligning with the intended, as-designed geometry of the layer in various specific locations. After which, a vision system creates images of the ply with the projected lines present, providing an operator with this digital image for inspection. It is then determined whether or not the ply is within compliance of the as-designed geometry [15].

Another example of alternative method of topography analysis is the development of Fourier transform profilometry (FTP). The precursor to this, presented by Meadows, et al. in the early 1970's, moiré contouring is a well-known method of assessing the 3D profile of objects [20][21]. This method, part of the "fringe-contour-generation" of topography techniques [22], uses a physical grid (fringe-pattern) to project its shadows onto the surface of an object [20]. The patterns of the shadows projected shadows correspond to the physical contours of the body on which they are projected through mathematical analysis and consideration of the observation position. For better understanding, pictures of the experimental setup can be seen Figure 2.6 and Figure 2.7, in which both the projection of the grid's shadows as well as the projection onto the target object are shown. This usable depth field of this setup is limited to within 20 cm. This is a limitation of the projections washing out past this depth due to diffraction. In this introduction, the overall resolution limit was experimentally determined to be 25 μm [20].

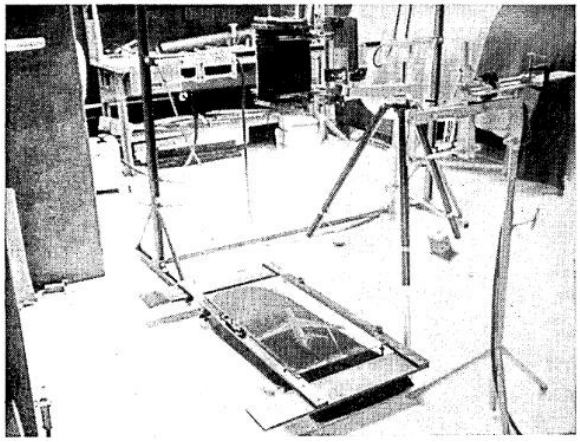

*Figure 2.6: Experimental Setup of Moiré Contouring* [20]

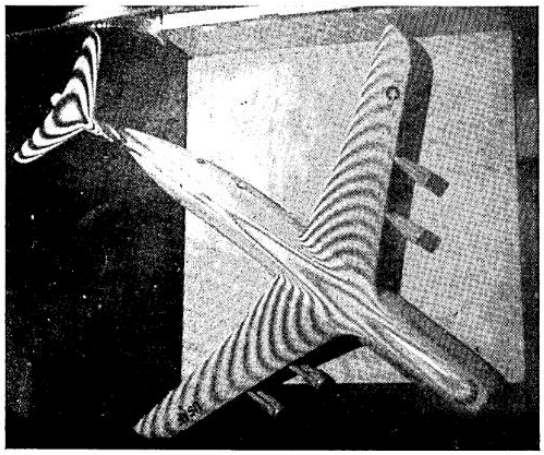

*Figure 2.7: Projected Shadows on Target Object* [20]

Moiré contouring, although prominent for much time, was improved upon a decade later with the introduction of Fourier-transform profilometry (FTP). Introduced by Takeda et al. [22] and expanded upon in 1983 [21], FTP's main improvement is that it resolves an issue in moiré contouring by solving automatic discrimination between peaks and valleys of the surface topography through computer-based fringe-pattern analysis [22]. In FTP, a fringe pattern is projected onto the surface of a target object. This deformed fringe pattern is then Fourier transformed and processed in the spatial frequency domain [21–23]. Additionally, it allows for fully automated analysis, without operator input [22]. An example of a grating pattern deformed by a target object can be seen in Figure 2.9. FTP introduced a much higher resolution for 3D shape measurement, although in its introductory version, was limited in its ability to contour steep surfaces. The maximum slope of a contoured target object, as shown in Equation 2.1 and Figure 2.8, was dependent on the distance between the camera and the object ($l_0$) and the distance between camera and the projector ($d$), [21].

$$Slope_{max} = l_0/3d$$

*Equation 2.1: Maximum Slope of Fourier-transform Profilometry*

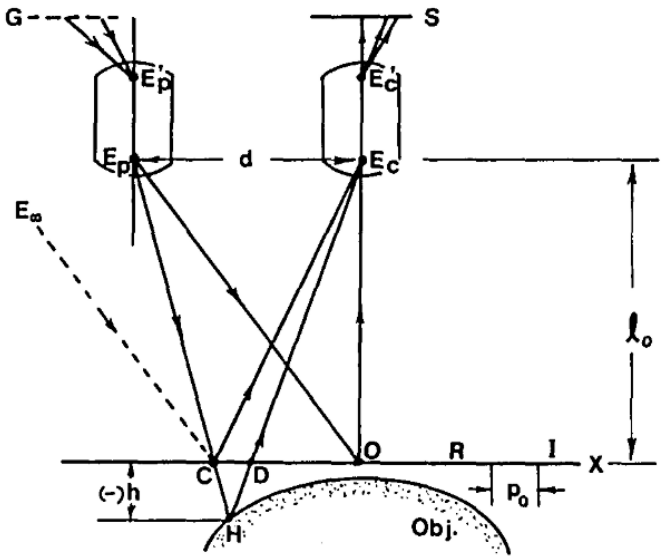


*Figure 2.8: Optical Geometry, Fourier-transform Profilometry* [21]

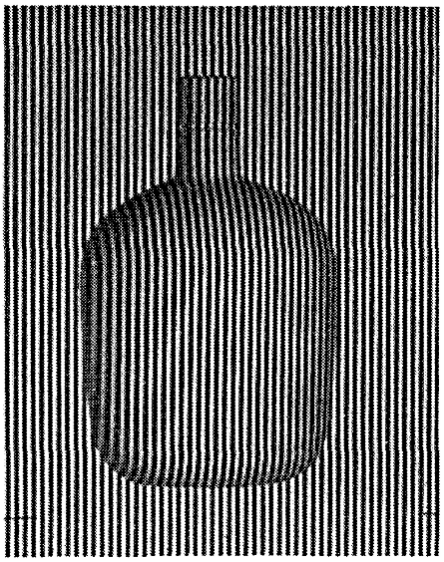

*Figure 2.9: Deformed Grating Pattern, Fourier-transform Profilometry* [21]

The slope limitation of Fourier-transform profilometry was improved upon much later by Li et al. in their introduction of improved Fourier-transform profilometry (IFTP). By introducing a grating phase shift technique, the slope limiting factor was almost tripled, allowing for FTP to be performed for objects with greater high variations [24]. The method was improved again by Yi and Huang in their introduction of modified Fourier-transform profilometry (MFTP). Their work makes a successful mathematical effort to eliminate the randomly occurring "phase-shift error" introduced by IFTP [25]. Further improvements were made to FTP by Tang and Hung in their introduction of a "fast" FTP method, doubling the processing speed by processing images in the real-signal domain instead of the frequency domain [26]. More recently, Yue et al. improve upon IFTP by utilizing a singular fringe pattern created by modulating two distinct fringe

patterns with a phase shift between them, as opposed to a utilizing two separate fringe patterns. This new method is coined “composite Fourier-transform profilometry” (CFTP). Experimentally, they prove that CFTP is an improvement in that it requires one less fringe pattern, however more processing steps are required [23].

Ultimately, within the context of AFP inspection, these methods gave way to digital topography measurement methods in the form of laser based profilometers. For the scope of this report the methods discussed in this section serve ultimately as a foundation for profilometry science.

### 2.2.2 PROFILOMETER SCANNING AND PROCESSING

Modern inspection systems, such as the ACSIS developed by IMT shown in Figure 1.3, rely on processing profilometry data to automatically detect layup errors in AFP laminates. These profilometers, mounted on a KUKA robotic arm and traversing the surface of the laminate ply, each project a laser line onto the ply surface, measuring the height along that line. Scanning along the surface of the ply, an area can be automatically investigated [19]. The laser light is both emitted and received by the profilometer, relying on the targets ability to diffusely reflect light [3]. Scanning data, reported numerically as heights, can be analyzed by a compute algorithmically to find sudden changes in topography. Further algorithms can be implemented to automatically identify defect types and locations and alert an operator [19][14].

## 2.3 MATERIAL CONSIDERATIONS MADE WHEN UTILIZING LASER SCANNING FOR INSPECTION

Scanning inspection systems have been studied extensively due to the subject’s applicability to multiple industries. The automotive industry for example pays much attention to surface quality analysis capabilities for composite parts [27]. Properties like

surface appearance, roughness, fiber strike through are such surface characteristics of interest in the study of surface reflection regardless of industry application [15,27–30]. Within this section literature is reviewed that shows practical considerations in the correlation between surface characteristics and reflection.

### 2.3.1 REFLECTIVE PROPERTIES OF COMPOSITE TOWS

As the model of profilometers employed in the current generation of automated inspection systems rely on the target object's ability to diffusely reflect light [3], reflective properties of a composite material can present challenges in imaging [15]. Although not directly addressing profilometry scanning, Shadmehri et al. address this consideration in the form of a rule for image capturing. In discussing the technical challenges of inspection of AFP plies, they acknowledge that the "wet shiny black look" causes both laser projection and imaging difficulties. With no more explanation, a "projection rule" is introduced, in which the laser incident ray is not to exceed a 30° angle with the normal to the surface, as shown in Figure 2.10. In this use case, following this rule allows for precise projection onto highly contoured composite parts. [15].

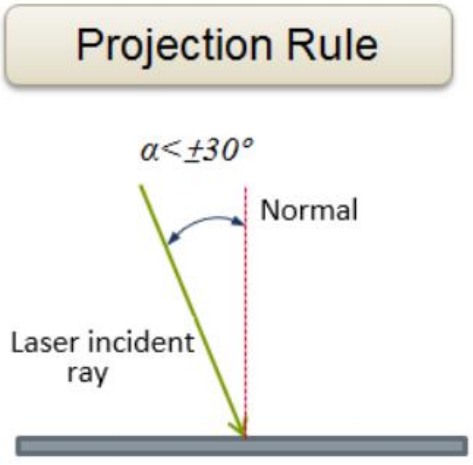


*Figure 2.10: Projection Rule* [15]

### 2.3.2 EFFECTS OF SURFACE ROUGHNESS AND FIBER PRESENCE

Material characteristics' impact on scanning errors has been explored further and continuously assessed alongside the development and prominence of laser based profilometry. In addition to appearance caused reflective qualities, i.e. color, Schubel, et al. discuss the relationship between light reflectivity and physical surface characteristics of composite parts. The information presented in their paper is discussed as it pertains to the automotive industry, and specifically as it influences the cosmetic appearance of automotive parts. However, they present an interesting correlation between increased surface roughness and the part's improved ability to diffuse light (although the predominant investigation regards painted surfaces) [27].

A surface feature of composite parts, as defined by Schubel et al., is fiber "strike-through"—defined as a periodic topography variation in the surface corresponding to the fiber geometry. It is explained that fiber strike-through occurs in composite parts because during curing, matrix rich regions will shrink more than fiber rich regions, as shown in Figure 2.11. This surface feature can lead to surface inconsistency or roughness—assuming that the laminate is not coated in anyway [27].

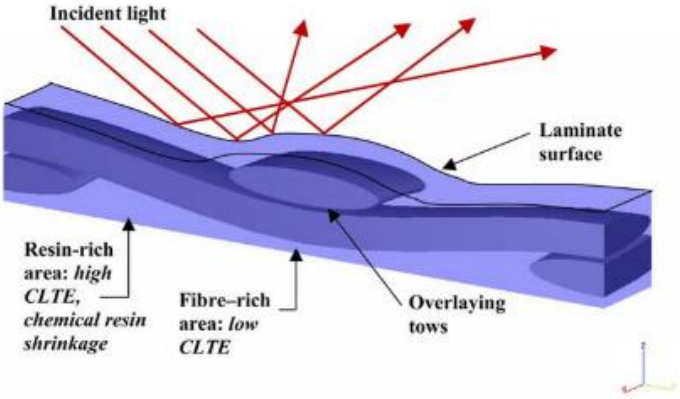


*Figure 2.11: Fiber Strike-Through* [27]

Along with visual inspection, there are three methods of surface characterization employed within in the context of this report. These are stylus profiling, in which the surface is physically traversed and finely measured, optical microscopy, in which the transverse section is imaged for inspection, and utilizing a BYK Gardner Wavescan DOI, which records a measurement of surface waviness by simulating the visual perception of waviness based on the distance of an observer [27][31]. In the later method, a wave-scan device optically scans the topography of a surface similar to a profilometer. The instrument directs a laser at the surface at an incident angle 60° to the normal and measures the reflected light intensity at an equal angle opposite to the incident about the normal. Again, as with a profilometer, the device is traversed along an area of interest and the optical profile data is recorded for the length travelled. This signal is then separated into ranges to simulate varying observation distances, and it is then plotted on a normalized rating scale. This can be shown in Figure 2.12 and Figure 2.13 [31].

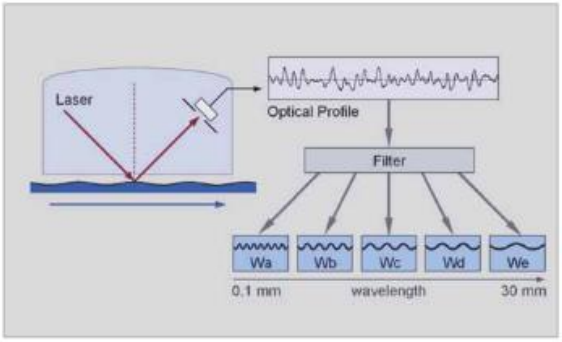


*Figure 2.12: Surface Characterization Signal Separation Method* [31]

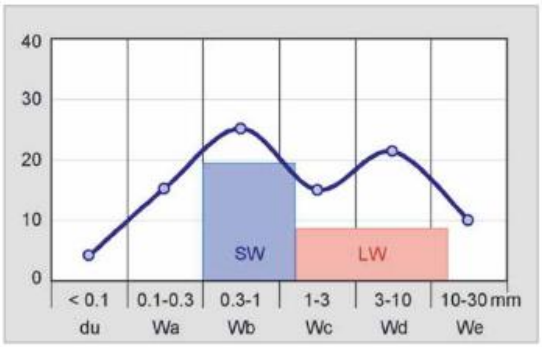


*Figure 2.13: Surface Characterization Signal Analysis Example* [31]

In their investigation, which exhibited prominent visible strike through regions were consistently deemed “unacceptable” laminates by the instrumented waviness detection. These fiber rich samples were determined to be “easily detected” by this surface characterization technique based on specular reflectivity [27]. This should be

compared to previous assessments of scanning composites, in which techniques based on diffuse reflectivity, such as the ones utilized in AFP manufacturing, underperform when inspecting composite parts [15][3].

## 2.4 CONCLUSION

The review of the supporting literature shows the breadth of the topic of AFP layup defects. Defects are shown to occur in a variety of geometries and categories—each experimentally proven to effect performance of the laminate structure to varying degrees based often on defect type, severity of layup deviation from the as-designed geometry, and the direction of force exerted on the structure during its intended use. In the ideal performance of current generation of inspection systems, these layup defects can be automatically detected and identified as each ply of the layup is scanned during the manufacturing process. The core principle upon which modern laser scanning based profilometers rely is a target material's surface's ability to diffusely reflect light. However, as one can ascertain from the preceding sections, material characteristics can greatly influence the success of scanning technology. Furthermore, refining the focus of this report, for some select thermoset materials reliable profilometry cannot be reported.

Although investigations into surface characteristics' influence on profilometry scanning results have been performed and published, such as surface roughness and material appearance as explored through this section, there exists a lack of focus on the application of AFP manufacturing. To further justify the application of automated scanning systems within AFP manufacturing, the technology must be reliable for a broader selection of materials. It is the author's hope that the narrative introduced in this section can be furthered through the presented investigation into material feasibility.

# CHAPTER 3

# DATA COLLECTION

Detailed herein are the steps taken in preparation of the execution of experiments and the method in which data was to be acquired. This includes material selection and the physical experimental setup. To accurately and fairly compare experimental data of profilometry scans, consistency between these scans must be established, ideally designing for an automated system in which human error can be mitigated to a degree. Additionally, the design for material sample preparation must be established. The storage, mounting, and scanning of these sample "layups"—mounted thermoset tows on metal tooling in a prespecified geometry—is discussed throughout this section.

## 3.1 MATERIAL SELECTION

Scanning a selection of thermoset materials, "noisy" results were consistently able to be replicated using default settings of the Keyence LJ-V7060 profilometry scanner. The materials of interest to be studied in this research were selected based on this preliminary scan data. Three materials were selected, each displaying varying levels of scan error: "Very Noisy", "Noisy", and "Good". At the beginning of this research, these levels were completely qualitative, as there was not yet a way to quantify a materials noise level. The three materials were selected from prominent composite manufacturers and are referred to simply as material A, B, and C. The results of the initial scan test, which informed this material selection, can be seen in Figure 3.1.

Material A

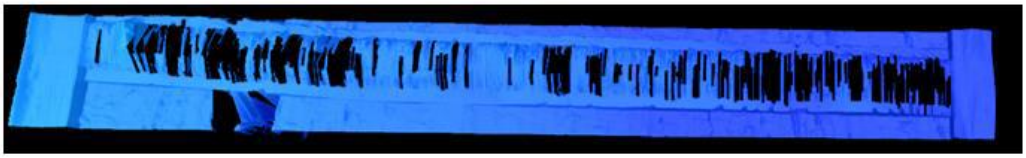

Material B

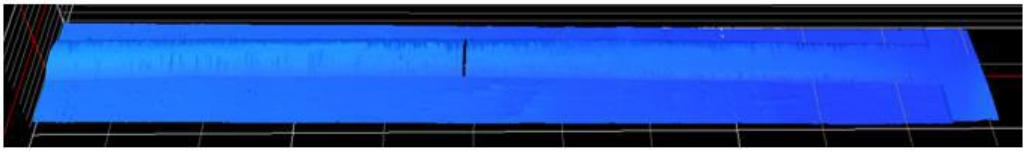

Material C

*Figure 3.1: Initial Profilometry Scans of Thermoset Composite Tows*

In addition to being scanned with the profilometer device, images were taken of these material tow's transverse cross section. These images, represented in Figure 3.2, 3.3, and 3.4 display the fiber cross section and additionally indicate information regarding each material's fiber volume fraction, i.e. the percentage of the material's volume represented by carbon fiber. As shown in these microscopy images and noteworthy, material C displays prominent areas in which there is a void of fibers and the material's polymer dominates. These areas occur throughout the material as well as on the surface of the tow, both on the exposed surface (top of image) and the surface in contact with the sample mount (bottom of image). The other two materials, material A and material B have their material's polymer distributed more evenly throughout the surface of the tow and do not exhibit any fiber void areas.

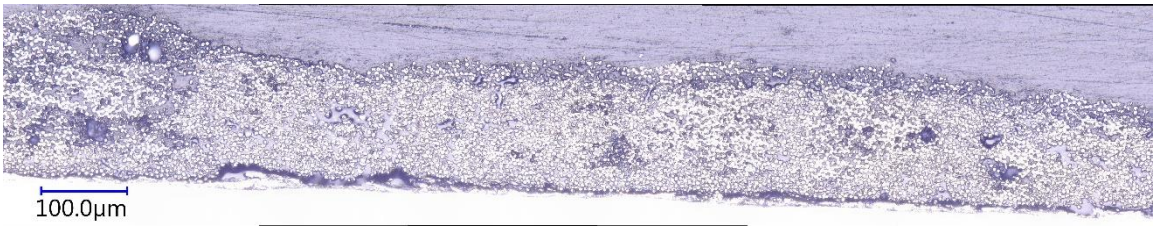


*Figure 3.2: Microscopy Generated Image of Material A Transverse Cross Section*

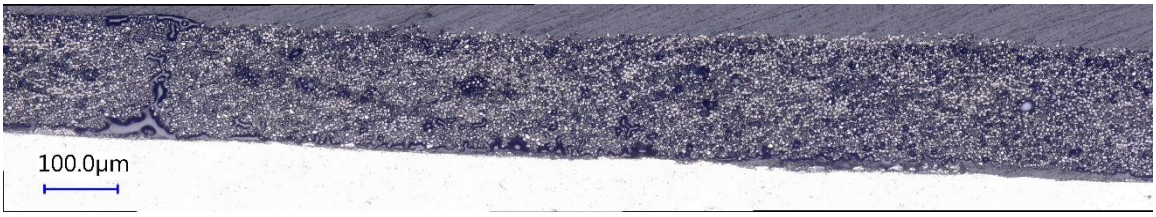


*Figure 3.3: Microscopy Generated Image of Material B Transverse Cross Section*

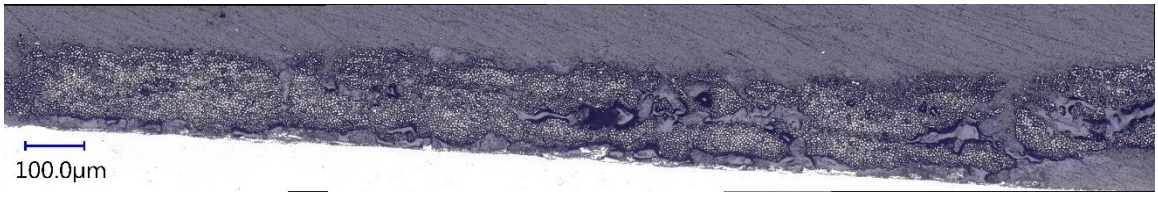


*Figure 3.4: Microscopy Generated Image of Material C Transverse Cross Section*

## 3.2 EXPERIMENTAL SETUP

Several steps were taken to appropriately prepare for experimentation. A gantry system was designed to allow for consistent automated scans. To investigate the effects of scanning at various pitch angles, a modular scanner mount was added to this system. Additionally, guidance lasers were mounted to ensure as little alignment variation as possible between scans. A sample mount was also designed which allowed for height adjustability as well as easily swapping out samples without disrupting experimental setup. These samples were made using hand lay-up on aluminum stages, representing single tow examples as well as simulated common layup errors. It is important to note that IMT's ACSIS employs a Keyence model profilometer, LJ-V7080. These

investigations were made utilizing Keyence LJ-V7060, which was found to be identical to the LJ-V7080 apart from housing geometry, ideal scan distance, and resulting scan resolution.

### 3.2.1 PROFILOMETRY SETUP AND DATA ACQUISITION

Shown in Figure 3.5 is the developed gantry system, which allowed the operational scanner to be mounted at an adjustable height above the target and to traverse a horizontal path, scanning the length of the target. This automated approach provided a high level of consistency between scans. Operational instructions for this gantry system are presented in Appendix C.

Data files from each scan were exported in CSV format using the Keyence Navigator Software. The matrix in the default exported CSV is 400 columns wide, representing the number of points in the width of a scan. The length of the CSV is defined by the physical distance scanned by the gantry system, with one row per trigger. Trigger pitch (the distance between triggers) was calculated to be 14.15 triggers per mm or 0.0707 mm between each trigger and was defined by the gantry system's step motor's pulses per rotation. The traversing of the profilometer was controlled by manual start and stop triggers (the impact of which is discussed further in section 4.2.3). The analysis program was designed to accept any size CSV, and thus any scan width and length.

The files were named following a consistent convention which allowed for all variables to be obvious and saved in the appropriate folder of a file management setup (Section 6.1, Figure 6.1). The naming convention was for each file name to list in order the sample material type, storage condition, and the date on which that scan was performed.

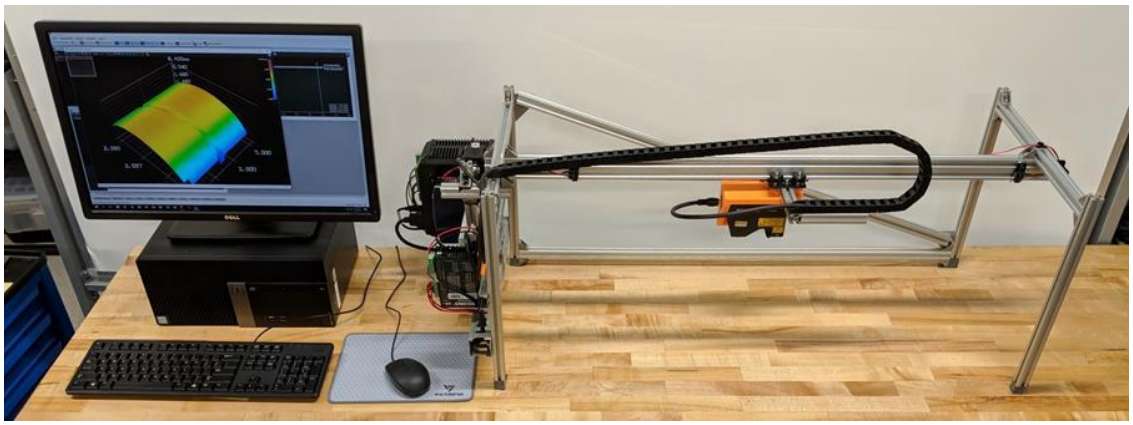

*Figure 3.5: Gantry System*

### 3.2.2 SCANNER MOUNT FOR VARYING PITCH

A new scanner mount was designed with the ability to position the scanner such that target objects could be scanned at various pitch angles. The printed and installed mount can be seen in Figure 3.6 and Figure 3.7. This mount allowed for precise angles to be held while investigating the effects of scanning pitch angle on sample noise. Additionally, a digital angle finder was used to confirm angle measurements against this mount (not pictured).

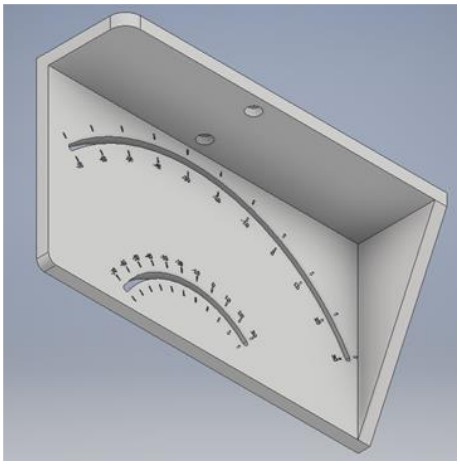

*Figure 3.6: Variable Pitch Mount CAD Model*


*Figure 3.7: Variable Pitch Mount Installed on the Gantry*

Guiding line lasers were added to the gantry system to aid in generating consistently aligned scans (Figure 3.8). These were attached by a printed mount, such that they show the path of the scan. The addition of the lasers prevented having to perform multiple passes to align scans correctly, saving setup time and allowing for more data to be collected. The lasers were switched off prior to scanning to prevent interference from the lasers with the Keyence equipment.


*Figure 3.8: Mounted Guidance Lasers*

### 3.2.3 SAMPLE STAGE

To analyze the same samples over time, a modular sample mount was designed with removable stages. This allowed for sample layups to be easily swapped out between scanning trials. Layups would be performed on these removable stages, made from .067" thick, brushed 5052-H32 Aluminum sheets. These stages were tested and scanned to confirm that they did not produce noise or error. The mount was constructed using Aluminum T-Slot rail and four identical printed corner brackets, as shown in Figure 3.9 and Figure 3.10. The stage mount was adjustable by design in both height and stage size. Initial scans displayed possible vibration noise. A solution to eliminate the printed corner braces was implemented and the stages were instead clamped directly to the T-Slot rail

on either side of contact, as shown in Figure 3.11. This had the desired effect of lessening vibration influences significantly.

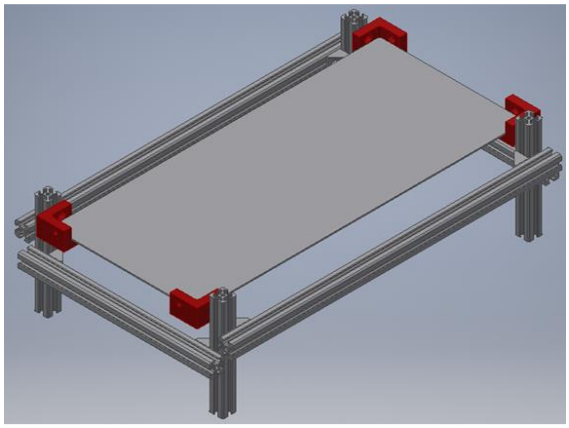

*Figure 3.9: CAD Model of the First Iteration Stage with Corner Brackets*

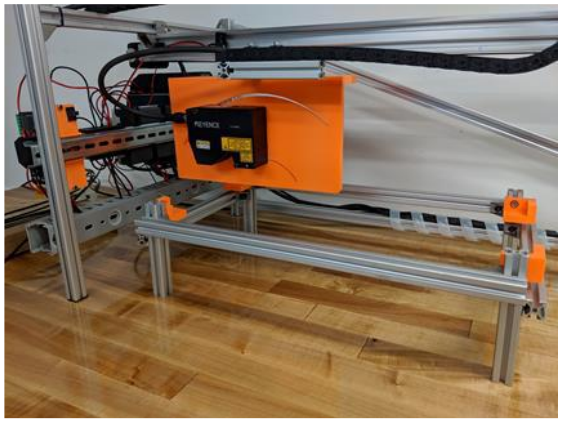

*Figure 3.10: Initial Sample Stage Mount*

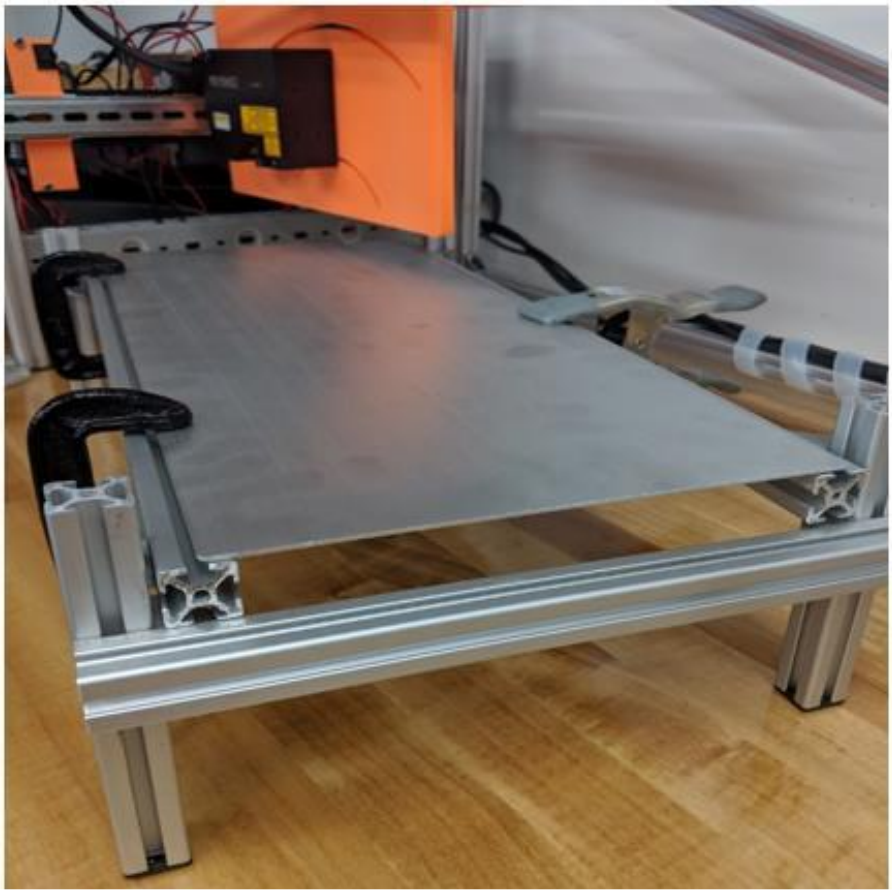

*Figure 3.11: Sample Stage Mount with Improved Clamping to Reduce Scan Vibration*

### 3.2.4 MATERIAL STORAGE & SAMPLE PREPARATION

Multiple layup geometries were investigated during the scanning tests, each representing respective common real-life configurations of tows and common geometries of layup errors. For this, each layup stage consists of several individual tows as well as a simulated missing tow layup error placed over a base ply of both 45° and 90° tows. The stage layout design is shown in Figure 3.12.

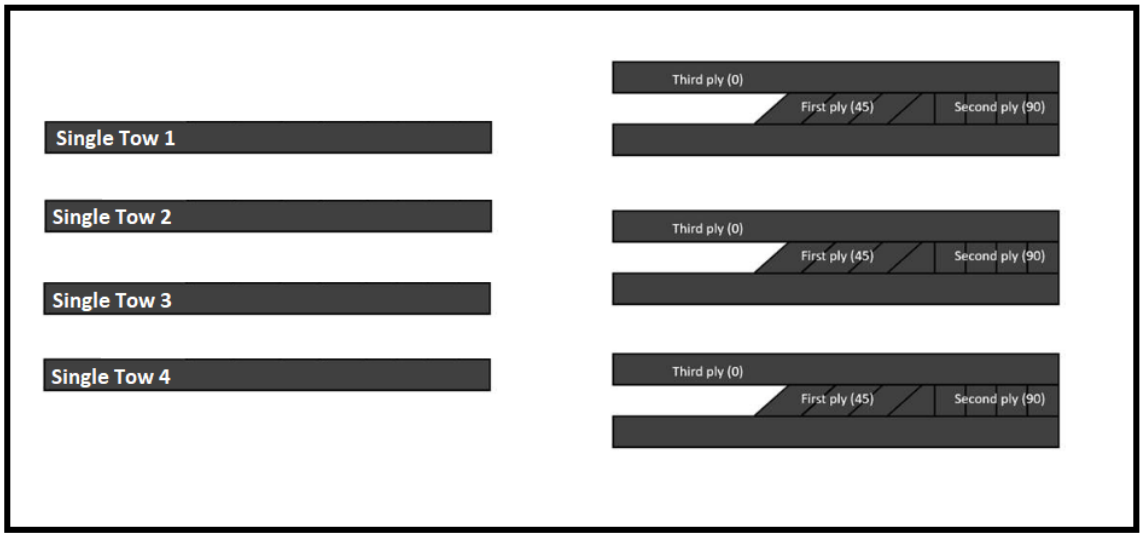


*Figure 3.12: Sample Stage Layout Design*

The layup of each of the three materials of interest, as preplanned, included two stages, onto which four samples of single tows as well as multiple arrangements of simulated layup errors (typically between four and seven depending on the working ease of material) were placed (refer to Figure 3.13).

The layup of each stage was done in an identical manner. Special care was taken to maintain a clean environment. The setup area was thoroughly cleaned and cleared of all foreign debris. Researchers wore gloves at all times and the material only came into contact with the cleaned shears, roller, and tooling. Each aluminum stage was first prepared by cleaning it with Acetone and was then set aside until the acetone dried

completely. Thermoset materials were removed from a storage freezer for the duration of the setup yet were not left in room temperature conditions for longer than twenty minutes at a time. Tows were cut to length using clean stainless-steel shears and were then placed on the aluminum stage. During this step, care was taken to limit contact between the surface of the tows and any foreign object. Once placed, the tows were compacted by using a soft roller held with a firm grip to secure the tows onto the aluminum plate. The number of passes of the roller was kept at a minimum and the process was completed when the tow had fully secured in its layup geometry. A similar method was followed for each material, however material C had initial difficulty adhering. This difficulty could be due to the uneven disbursement of the material's polymer as shown in Figure 3.4 and discussed in section 3.1. To compensate, prior to tow placement a heat gun was used on the plate for roughly three seconds or until the tooling was warm to the touch. These steps are directly comparable to compaction steps taken in the AFP process. Once the two stages were completed for each material, both were scanned for day one results. Following this, one stage was placed in the freezer and the other in ambient conditions.

The industrial freezer used, held at a set temperature of 0° Fahrenheit, was the same freezer used for bulk material storage. Therefore, these samples would be subjected to the same conditions as prior to use on AFP machines. Samples in ambient conditions were subjected to the lab environment with an air conditioning system set at 70° F. However, on select unrecorded dates, loading dock cargo doors in adjacent lab spaces were open due to daily lab operation. Humidity fluctuated day to day, as discussed in chapter 6 of this report. The experiments related to these ambient samples were performed in Columbia, South Carolina between May 9$^{th}$ and June 10$^{th}$ of 2019.

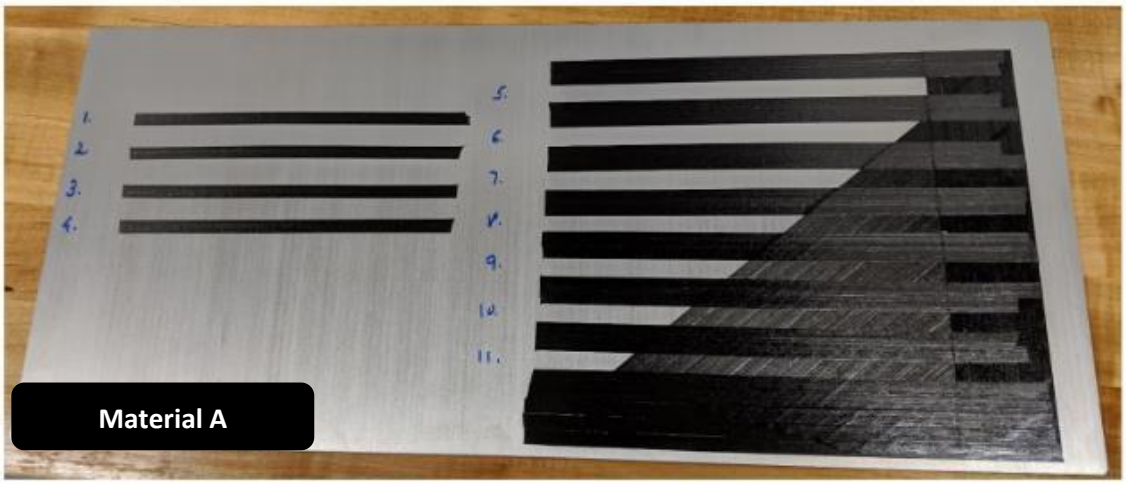


*Figure 3.13: Sample Stage Layup*

## 3.3 CONCLUSION AND REMARKS

An idealized case for the series of experiments presented in this thesis report is performing all profilometry scanning on the actual ACSIS itself. Additionally, material sample layups with imbedded intentional defects would ideally be manufactured by the AFP machine. This would improve repeatability and control of the scanning process and remove potential human errors such as sample contamination and inconsistency in the by-hand layup procedure. However, as detailed in this chapter, a significant effort was made to replicate an automated layup by hand and to create an experimental setup which most authentically replicated the ACSIS system. Utilizing the resource of an AFP machine and ACSIS system would have been time preventative and ultimately limiting to the investigative process. The benchtop system detailed here allowed for small scale experiments to be ran without the risk of significant resource waste or expensive machine time.

# CHAPTER 4

# DATA ANALYSIS METHOD

To produce meaningful experimental results, profilometry scan data error needs to be quantified in a consistent way. This allows for direct comparison of proposed solution and noise mitigation techniques. To this end, a data analysis script was developed for use in this research project. The steps and considerations of this program development are discussed herein. Additionally presented, is a numerical definition of profilometry scanning error as well as a base level of expected variation in scanning noise between scans with identical experimental setups. In short, this chapter presents the tools with which upcoming experiments were analyzed.

## 4.1 SCAN NOISE DEFINITION

It is important to note that throughout this document, two types of noise error signatures are referred to. As discussed within this section, scanning noise error manifests as both “Voids”, or “Lower Noise”, and “Spikes”, or “Upper Noise”. Examples of each of these can be seen in Figure 4.1 and Figure 4.2. In an analytical sense, within the exported profilometry data each type of noise displays itself in the data as a sudden decrease or increase in value compared to the local average or neighboring values. Furthermore, voids appear as sudden decreases in value, trending towards negative infinity, and spikes appear as sudden increases in value, trending towards positive infinity. On Keyence’s built in 3D data visualization tool, spikes appear as one would

expect; sharp and sudden increases, maxing out at a point. In contrast, voids appear as missing data.

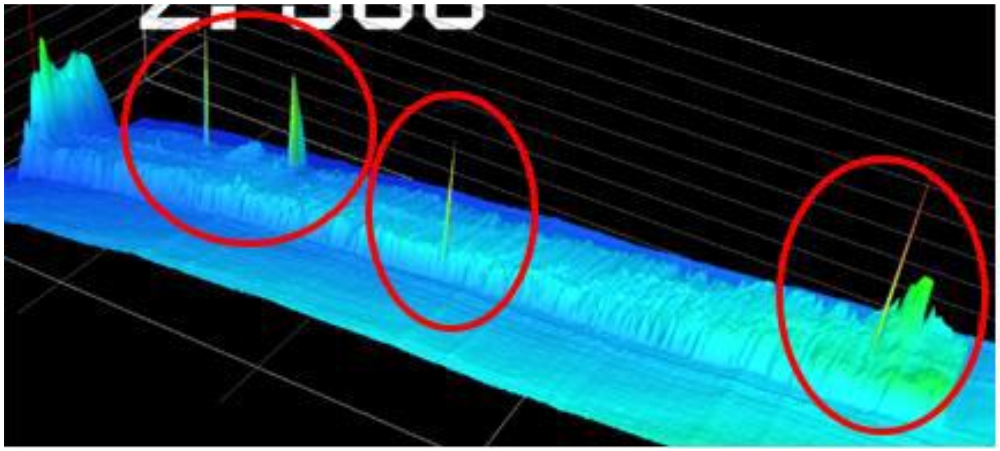

*Figure 4.1: Prominent Spike Noise Example*

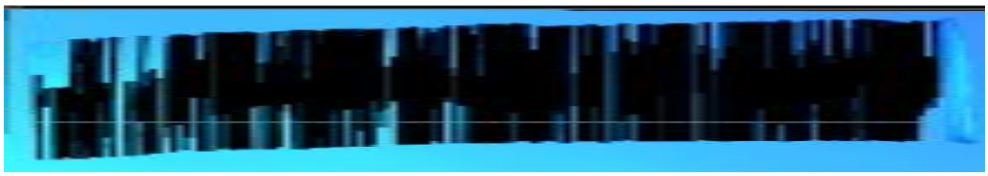

*Figure 4.2: Prominent Void Noise Example*

## 4.2 NOISE ANALYSIS SCRIPT

In an effort to quantify noise data from scans of these samples, a processing script was developed. This script accepts raw profilometry scan data (in the form of CSV input files) and returns meaningful information about noise represented within the scan such as noise levels, along with a generated image of the scan. This script was used and continuously developed throughout the project to create fair comparisons between possible solution approaches. It was also utilized in establishing what was determined "standard noise deviation". This was done by comparing noise levels between scans in which the target object was reset between trials versus scans in which the target was unmoved between trials. This allowed for a better understanding of what constitutes a significant change in noise level. The program, written in Python 3.7 and using the

development environment Spyder 3.3.3, was designed to accept the exported profilometry data and search for voids and spikes in the data, recording each as noise and returning computational information regarding how "noisy" a sample is. A flowchart of the final program design can be seen in Figure 4.3. The details of the script are elaborated on in the following subsections. The final script is presented in its entirety in Appendix A, with operational instructions presented in Appendix B.

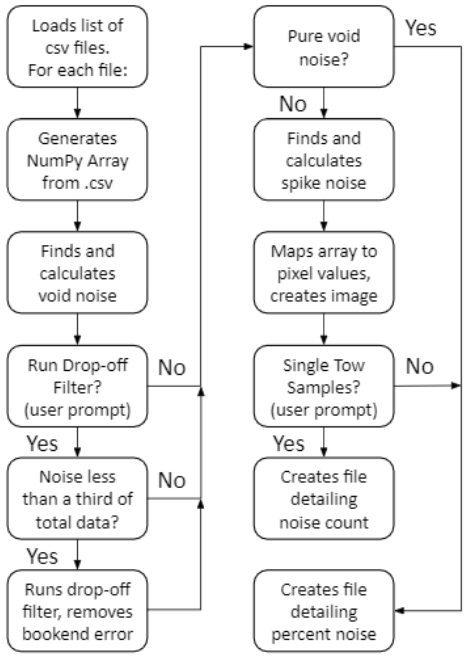


*Figure 4.3: Flow Chart of Final Design of Developed Scan Analysis Program*

### 4.2.1 INITIAL ALGORITHM DESIGN

The script is capable of analyzing the scan data imported in CSV form. These CSV files are the default output format of Keyence's controller software and store topographical data collected by the scan. At the first stage of development, the script first accepted an individual CSV file and converts it into an array. The script then generates an image of the scan by mapping the data point values to pixel values. Since void noise manifests as a value of approximately negative ninety-nine, these values are counted as a

percentage of total data points and mapped to a pixel value of zero. Similarly, the largest data value (in many cases a spike noise) is mapped to a pixel value of two hundred fifty-five. Because of this method, two potential issues arose in image generation—a key troubleshooting tool in the development of the script.

In the first case, if the average value of "non-void" data (data which does represent lower noise values) is close to the maximum value, then the resulting image would appear very bright. This case would occur when there are no spikes present in the data set and there exists a small standard deviation. The second case follows a similar logic. If the average value of non-void data is much less than the max value (typically in a case where spikes are present), then the data tends to appear very dark and with little gradient variance. This case is the large standard deviation case. To resolve this, a redefined image filter was developed.

### 4.2.2 REFINED FILTER

This filter was implemented to more accurately define which selection of the data is determined to be spikes and to allow for a refined image to be generated for every data set. This filter utilized the average and standard deviation values to determine a range of data in which a large majority of non-void values existed (97%) and then mapped that range to pixel values. This was done by first defining a step size of one eight of the standard deviation. Centered about the average, the starting range is two step sizes. The program then checks to determine if the range contains ninety-seven percent of the data not defined as voids. If so, all values above this range are defined as spikes, and mapped to a value of two hundred fifty-five for image generation. The amount of data points in this set is recorded as a percentage of all data and defined as "Percent Upper Noise". If the range does not contain the set percentage of non-void values, then the range in

increased by one step size in either direction of the average. The check is then performed again. An example result of this refined filter can be seen in Figure 4.4, where the same scan is presented with and without the filter applied. The image generated by the filtered array allows for much more detail to be observed, as well as a calculation of the percentage of data representing spikes, or “Upper Noise”.

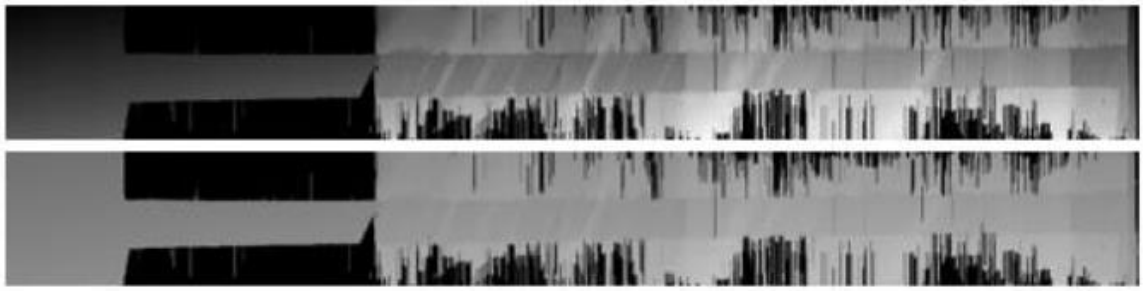

*Figure 4.4: Sample of Material B Processed without (bottom) and with (top) Refined Filter Applied*

Note, that this investigation was not purely an effort in developing better images, but a trouble shooting tool in determining which selection of the data was noise and which yielded relevant information. This application of the script allowed a better understanding of that nuance.

### 4.2.3 EDGE DETECTION

To more accurately compare daily scans of single tow samples, the data points which were to be analyzed needed to be better specified. Potential issues arise when scans are not the same length, which was typical for the data due to a manual start and stop trigger on the automated gantry scanning system. For this reason, an effort was began investigating the implementation of a Canny Edge Detection (CED), where the values describing the continuous edge of the single tow sample would be determined, yielding a region in which to analyze data. This would allow the calculated noise results

to be percentages of data only representing the tow surface, validating comparisons between scan samples. However, pursuing this would potentially be a significantly time intensive effort. A display of the results of a short investigation can be seen in Figure 4.5. An alternative option to CED was to find the rows within the array which represented each the beginning and end of tow surface. Then, the script could remove all data from the array which precedes or follows these rows. However, due to time limitations and input from industry partners this was not explored further.

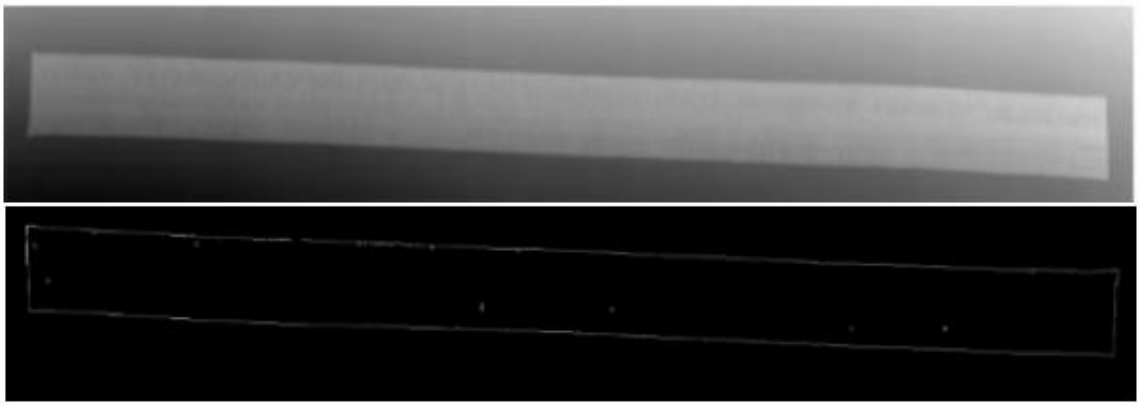

*Figure 4.5: CED Implemented on Scan File (top: original, bottom: edge detection) MATERIAL_A_AMBIENT_NOVACUUM_17-5_SCAN_3_5-10-19.csv*

### 4.2.4 DROP OFF FILTER

Due to physical placement of the sample on the stage and the scanning path during operation, many scans of simulated layup errors had invalid data appearing at the end of the scan. These samples were starting, ending, or in some cases “bookended” with rows of pure noise. This was due to the scanner path extending beyond the edge of the stage on which the sample was laid up. This caused data from that portion of the scan to register as void noise due to the detection range of the scanner. This anomaly, unknowingly caused by a human error, influenced the results. These few samples were

measured erroneously to have a higher percentage of noise due. To fix this, the noise analysis script needed to be modified.

To resolve this, a method was developed to catch and filter out and data due to this “drop off” error. Once implemented, the result eliminated this error, removing rows of pure noise occurring only at the ends of the scan. Additionally, the program operator has the choice of applying this filter or not—ideally implementing it only after an initial run displays the need for it.

The method works by implementing a simple count of noise data points within each row while the program checks the scan row by row for total voids. Once the noise count in a row equals the total number of elements in a row, that row’s position in the array is recorded and the number of data points in a row subtracted from the total void noise count at that instant. Once all rows have been checked, the program checks to see if the number of pure noise rows represents less than a third of total rows. If it does, then the filter continues. The list of rows containing pure noise is then sorted into two separate lists, one list containing rows at the beginning of the scan and one comprised of rows at the end of the scan. Any other rows (in the middle) are ignored, as they represent valid noise data. The rows from these two lists are then removed from the scan.

The check was implemented as a way to allow pure noise samples to pass the filter. Otherwise, the entire data set would be selected for removal and no meaningful results returned. If the number of pure noise rows represents an amount more than or equal to a third of all rows, the filter doesn’t continue running. Additionally, the count of data points subtracted from the total void noise count is added back to that count by

multiplying the width of the scan (total number of elements in a row) by the length of the list of pure noise rows and adding it back.

Results of this filter can be seen in the resultant image, Figure 4.6, as well as the resultant noise analysis, Figure 4.7. In this scan of material A, the erroneous data occurred at the end of the array. As shown, the noise levels calculated before and after applying the filter vary significantly.

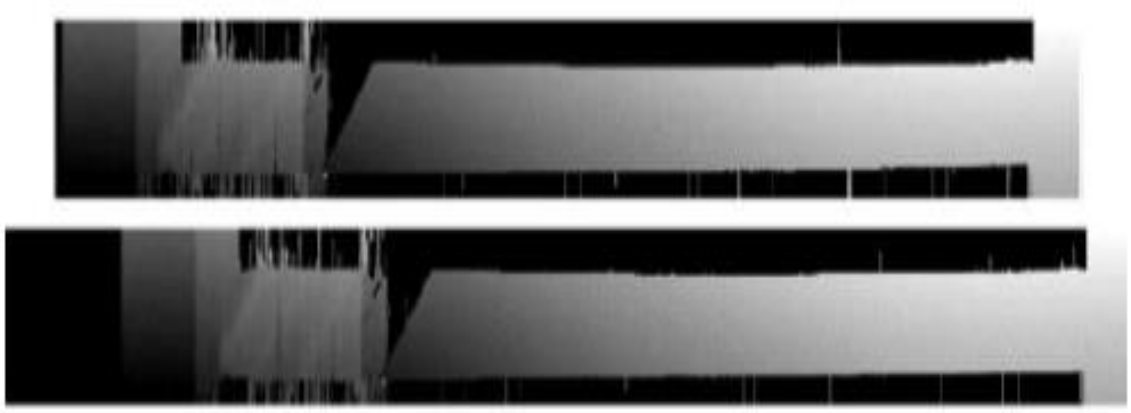

*Figure 4.6: Drop Off Filter applied to Scan image (top: original, bottom: drop-off filtered) MATERIAL_A_AMBIENT_NOVACUUM_SCAN_6_5-9-19*

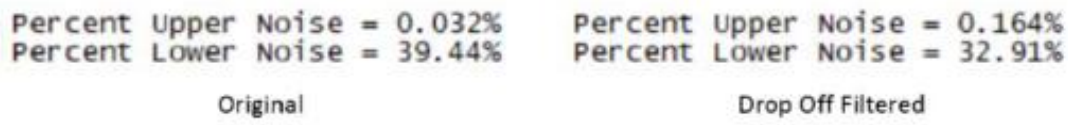


*Figure 4.7: Analysis File Generated by Applying Drop Off Filter to Scan File MATERIAL_A_AMBIENT_NOVACUUM_SCAN_6_5-9-19_Analysis*

## 4.3 BASELINE VARIABILITY ANALYSIS

Before analyzing any scan results, it was important to understand the effect in variations of the stage location on the results of the analysis script. This influence occurs during swapping out of samples on the stage or moving the stage to focus on another target area for scanning. An investigation into standard noise deviation was performed. For this, scans were performed for each material at 0° pitch under two cases. Firstly, with

no stage movement between each scan, and secondly, while resetting the target between each scan. The goal was to determine what constitutes a significant change in noise levels, through observing base levels of fluctuation between identically setup scans. The results of this short experiment can be seen plotted as percent noise in Figure 4.9 through Figure 4.12, where the graph legend is presented in Figure 4.8.

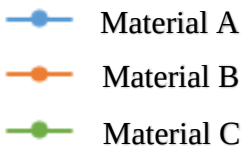


*Figure 4.8: Graph Legend*

**No Stage Movement**

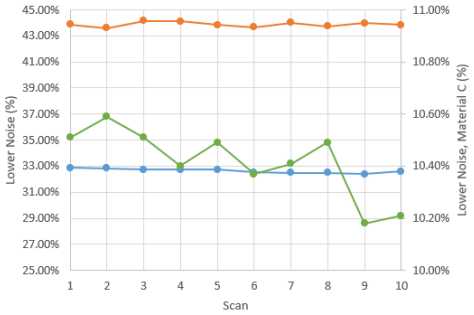


*Figure 4.9: Standard Deviation of Void Noise across Identical Scans*

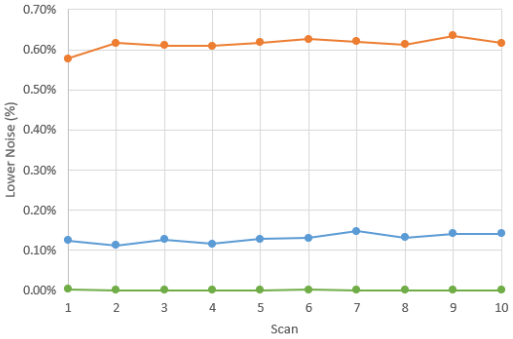


*Figure 4.10: Standard Deviation of Spike Noise across Identical Scans*

**Stage Movement**

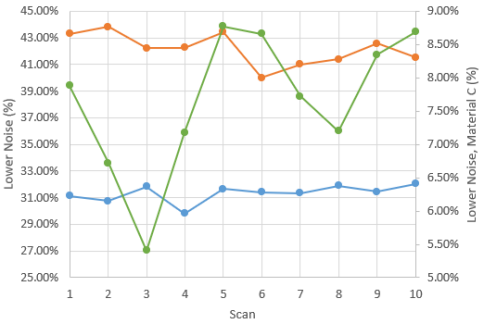


*Figure 4.11: Standard Deviation of Void Noise across Identical Scans*

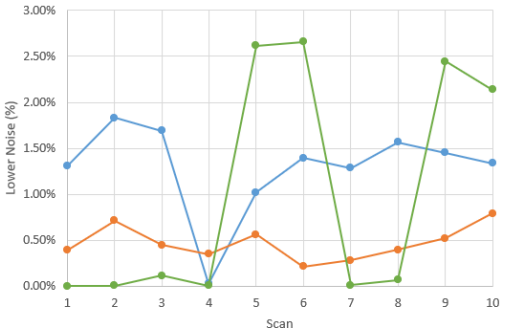


*Figure 4.12: Standard Deviation of Spike Noise across Identical Scans*

Results from the stage movement experiment display minimal deviation between samples in the case of no base movement between scans. This is true for all material types and for each void and spike noise types. Specifically, for the case of no base movement, void noise standard deviation was all within 0.2%. Spike noise was even lower, with standard deviations between scans all within 0.015% for all materials.

*Table 4.1: Standard Deviation of Noise per Material and Base Movement*

| | **No Base Movement** | | **With Base Movement** | |
|---|---|---|---|---|
| **Material** | **Void Noise SD** | **Spike Noise SD** | **Void Noise SD** | **Spike Noise SD** |
| A | 0.17% | 0.01% | 0.65% | 0.50% |
| B | 0.19% | 0.01% | 1.20% | 0.18% |
| C | 0.13% | 0.00% | 1.07% | 1.26% |

In the practical case—with stage movement between scans to replicate a typical scan setup—a marginal increase in standard noise can be seen. For void noise, the standard deviation between scans was calculated to be less than 1.2% for all material types, where spike noise standard deviation was similarly less than 1.3% across all materials. The detailed conclusions can be seen in Table 4.1. These results can inform the conclusions drawn from other experiments and display what this report considers a base-level expected acceptable standard for noise. Any results with noise variance within these thresholds can be regarded as insignificant.

## 4.4 CONCLUSION

The final version of the developed analysis script was rigorous enough to return meaningful data with consideration and built in solutions for corner cases such as scans which run off the edge of the sample stage and scan data sets which are represented by pure noise. Additionally, regardless of the average height of a scanned object, the final version of the script was able to return clear black and white images, allowing the

program operator a valuable troubleshooting tool. The key result of this script development, however, is the program's ability to output quantitative data measuring profilometry scanning data error i.e. noise. This allows for meaningful comparison of varying scans and allows for conclusions to be drawn regarding experiment and proposed mitigation methods, as shown in the following chapters. Lastly, the result of the final tool presented in this chapter is a better understanding of what constitutes a significant variation in profilometry scanning noise. Shown in section 4.3, standard deviation between scans of identical setup is less than 1.3% regardless of whether the stage is reset between scans. This informs all experimental results and contextualizes what is determined a significant change in profilometry scanning error.

# CHAPTER 5

# EFFECT OF SCANNER PITCH ANGLE

Presented in this section are results from investigations into profilometry scanner pitch angle. The effects of scanner pitch angle are displayed in both qualitative descriptions and quantified noise level, the latter of which was determined by utilization of the analysis script developed. The trends of and conclusions drawn from each are discussed. The goal of this chapter is to experimentally and definitively determine whether there is a benefit to performing profilometry scans at a varied pitch with regard to scan data error mitigation. If there is a clear benefit of introducing a pitch angle, then an idealized pitch angle should be determinable based on scanner geometry.

## 5.1 THEORY AND CONFIRMATION

The predominant cause of noise observed was shininess, or the high, mirror-like quality of the material's surface. This surface characteristic, reflectivity (high specular reflectivity), prevents scattering (diffuse reflectivity) of light into the sensor (see Figure 1.5). Specular reflection refers to the reflection of waves in which the reflection angle is equal to the incident angle. It is this specular reflection that was theorized to be responsible for the emitted laser light to not reach the scanner's receiver. This was also in part due to the specific incidence angle of the emitted laser to the surface. A short experiment was devised to observe the effects of pitching the "shiny" target object to direct reflected light towards the scanner's receiver.

For this initial test, the target object was the same mirror used to replicate scan noise results. The mirror was scanned initially without a tilt, and then scanned again at varying degrees of pitch. Measurable readings were expected when the mirror was pitched in the direction of the scanner, allowing the scanner to receive some of the reflected light (Figure 5.1).

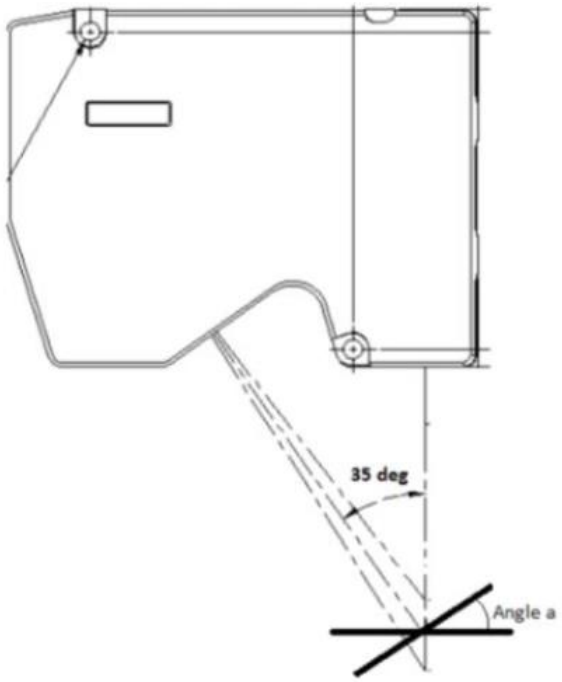


*Figure 5.1: Early Pitch Test Scanning Mirror Surface Setup*

Results were consistent with theory. For angles away from the sensor ($a < 0°$), no data was captured. These readings were consistent with void noise present on thermoset tows. For shallow angles towards the sensor ($0° < a < \approx 45°$), there was a measurable reading with little to no void noise present. For larger angles ($a > \approx 45°$), no data was captured as most light is reflected away from the sensor.

Considering these results, it was theorized that there is likely an optimum pitch angle that can be applied when scanning objects with highly reflective surfaces, when

modifying the target object is not an option. Based on the scanner's geometry, observing the ideal 35° incident angle, a bisecting angle of 17.5° would be expected to be optimal for reading highly reflective surfaces. This was to be confirmed through the following experiments.

## 5.2 QUALITATIVE ANALYSIS

Prior to the development of the analysis script, which was developed to produce a numerical analysis of scan noise, a pitch test was performed with the goal of investigating the noise reduction effects of introducing a pitch angle while scanning using the LJ-V7060 Keyence scanner. Three single tow samples of material A were selected for study. Tows were scanned at each 0° and 12° and analyzed visually for the presence of spikes and voids. The setup for this test can be seen in Figure 5.2 and the image results for this test generated by Keyence software are shown in Figure 5.3.

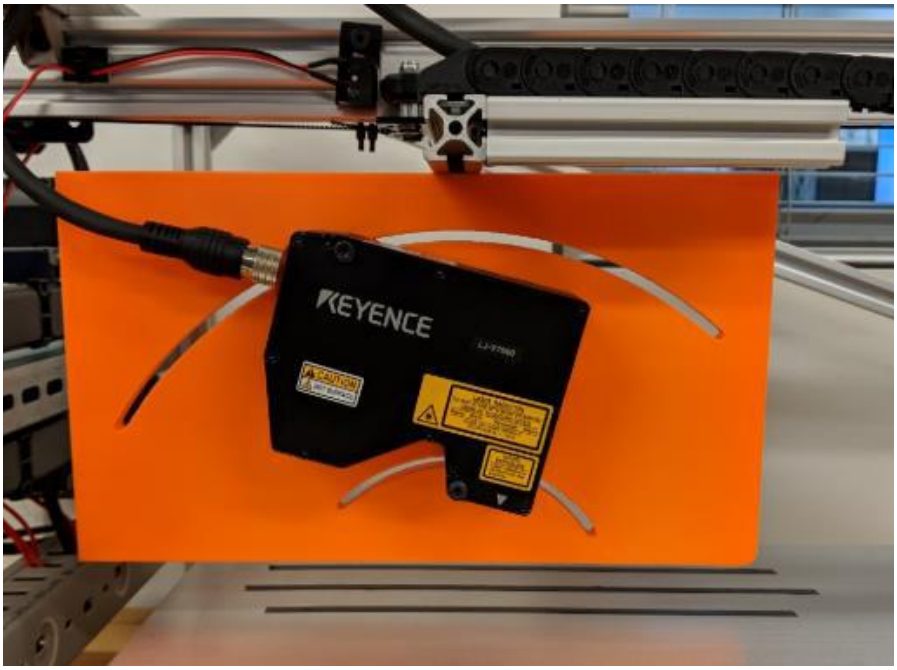


*Figure 5.2: Pitch Test Experimental Setup*

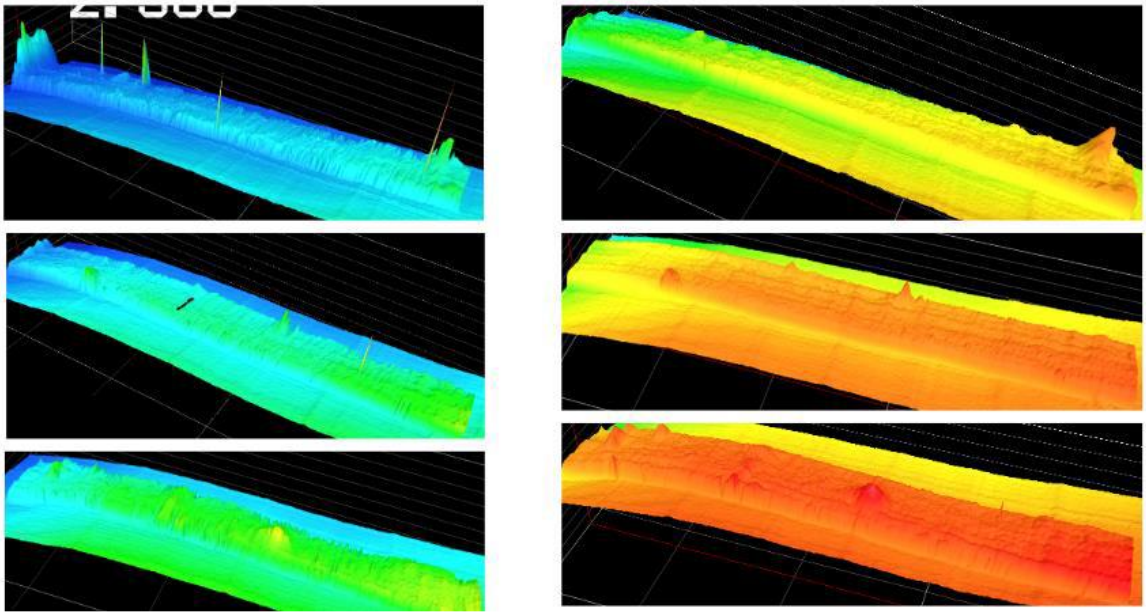

*Figure 5.3: Pitch Test Results (0° on Left, 12° on Right)*

As shown in the pitch test results in Figure 5.3, for which the scales were unfortunately not recorded, the images generated when scanning at a pitch of 0° display both erroneous spikes and voids throughout the sample. These noise signatures do not seem to be as prominent in the images from scans performed at a pitch of 12°. This lends some support to the proposed solution that pitching the scanner or target object in the direction of the scanner's receiver has a positive effect on decreasing noise present in a sample.

An additional experiment was performed to investigate the difference between scanning the same material A tow at two different pitch angles, to determine whether varying pitches had varying results in terms of noise mitigation. The experiment was performed on a single tow sample of material A. The two scans were performed at each 10° and 17.5° consecutively, pausing in-between for only enough time to reset the pitch

angle of the scanner. As one can observe in Figure 5.4, scanning the sample 17.5° seems to almost eliminate noise in this instance when compared to the pitch angle of only 10°.

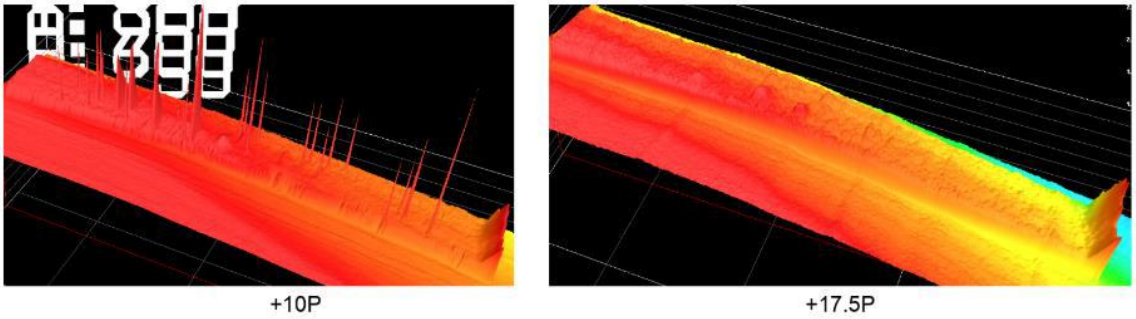


*Figure 5.4: Experimental Results of Varying Pitch Angle*

## 5.3 QUANTITATIVE ANALYSIS

Once the development of the analysis program was complete, a quantitative pitch test was performed by scanning simulated layup error samples of each material of interest at incremental angles between -30° and 30°. The results of these scans were processed and plotted for each Upper and Lower Noise. The results of these analyses are summarized in Figure 5.5 and Figure 5.6, where the legend for each graph is presented in Figure 4.8.

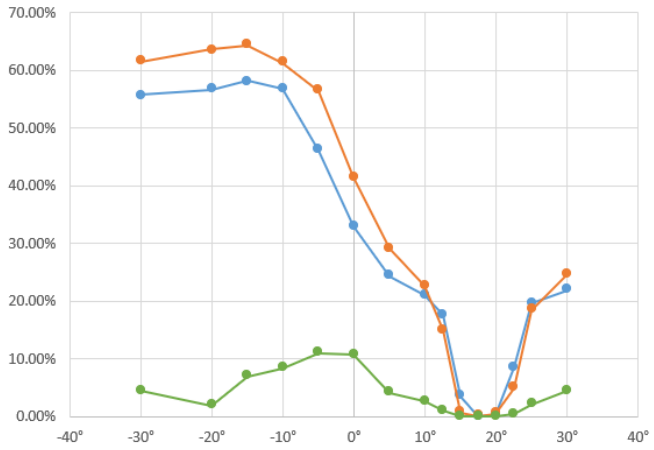


*Figure 5.5: Void Noise by Percent of Total Data as a Function of Pitch Angles*

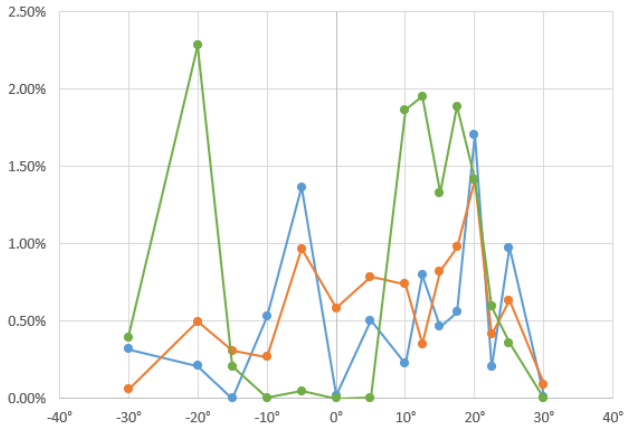


*Figure 5.6: Spike Noise by Percent of Total Data as a Function of Pitch Angles*

## 5.4 CONCLUSION

Results of the pitch tests clearly display a benefit of scanning at the bisecting angle of 17.5°. For all materials and samples studied, the void noise results fall to their lowest calculated values when scanning at this pitch (refer to Figure 5.5). The change in calculated noise presence is significant when compared to the baseline anticipated noise deviation determined in section 4.3, Table 4.1. Standard deviation is determined in this section to be 1.3% of the total data set. As shown in Figure 5.5, there exists an error reduction of over 40% for the noisiest material scanned. Spike noise does not display a similar trend, however as shown throughout this report, is not the dominating factor in profilometry scanning error analysis. The conclusion drawn is that a pitch benefits profilometry scanning error, and when possible, introducing a pitch angle of the bisecting angle, in this case 17.5°, is the preferred angle to resolve scanning noise when scanning highly reflecting materials.

# CHAPTER 6

# EFFECT OF ENVIRONMENTAL EXPOSURE

One of the variables that can affect scan results is time. As thermoset composites cure at room temperature, the chemical and physical properties change as they are exposed over time. There was an interest to evaluate how scan results of the composites can vary over time, as the thermoset tows were stored. Material handling, storage, and out time considerations are an integral aspect of AFP manufacturing, and these practices impacting the feasibility of layup error detection would be significant. It is therefore important to evaluate this effect. For this purpose, an environmental exposure test was designed, where a material's scanning error levels as calculated by the analysis script would be tracked over time. The details of this program are presented in chapter 4.

As mentioned in chapter 3, samples were stored in freezer conditions prior to use. For a more detailed explanation of these varied storage conditions, refer so section 3.2.4 regarding material storage and sample preparation. Once the samples had been prepared, the effect of various storage conditions on scan data noise levels could be measured. This chapter summarizes the scanning and data processing, the collection, and the results of these experiments.

## 6.1 SCANNING AND DATA PROCESSING

To examine the effect of exposure, two daily scans of each sample were performed, one at each pitch of interest, 0° and 17.5°, until there were no noticeable

changes in results for a significant time. All scans were performed with the LJ-V7060 Keyence scanner. Data files from each scan were exported in CSV format using the Keyence Navigator Software, named following a consistent convention which allowed for all variables to be obvious, and saved in the appropriate folder (Figure 6.1).

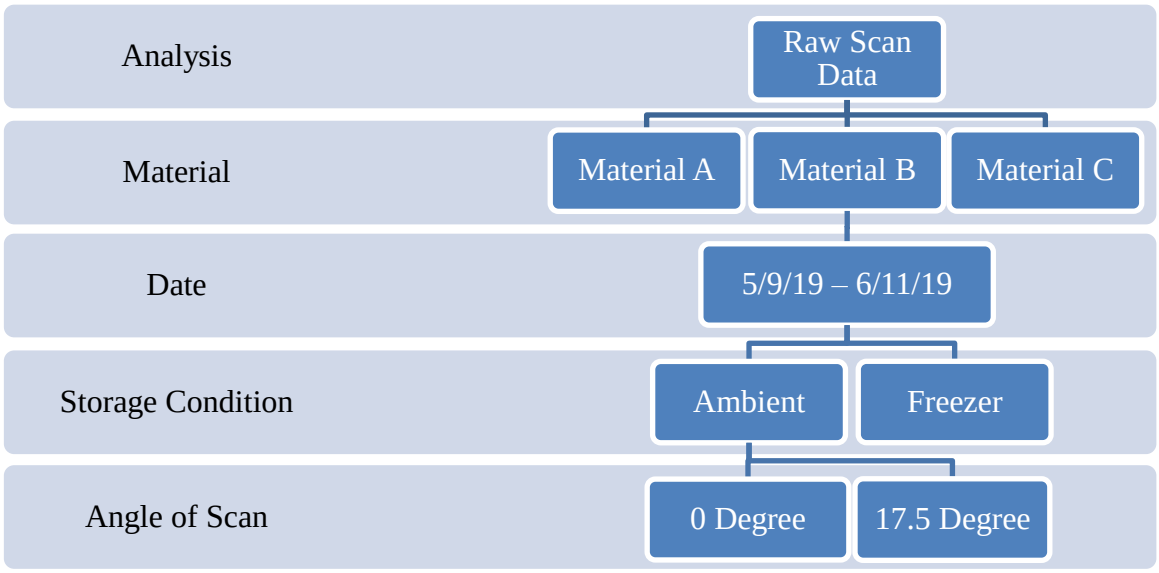


*Figure 6.1: Folder Hierarchy of Raw Scan Data*

Scan data was processed utilizing the analysis script developed. The script generated and saved an image from a single CSV file. Noise was then calculated as a strict percentage of the total data present for each voids (as "Percent Lower Noise") and spikes (as "Percent Upper Noise"). A summary of this information was saved by the program as a text file. An example of this can be seen in Figure 6.2.

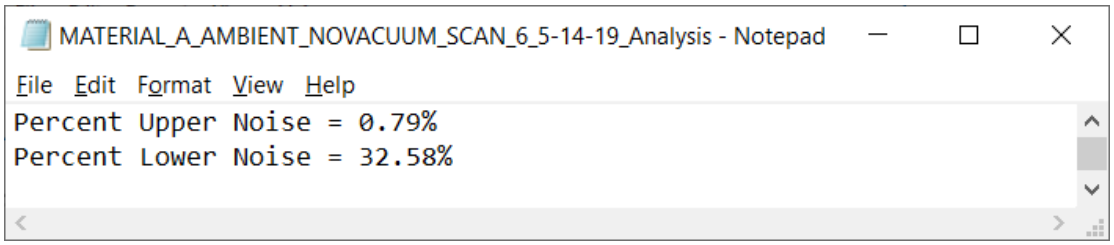


*Figure 6.2: Example of Analysis File Generated for Each Scan Data File (csv)*

These analytical tools allowed information to be presented in two ways. Firstly, visual inspections of scan quality and observations of changes in this quality can be made over the life of the experiment. Secondly, the noise quantifications could be presented in such a way that one can spectate on the effects that exposure time has on noise by plotting these quantitative results. Throughout this time, all scan data was processed and resulting images and noise quantifications saved.

During the initial phase of processing scan data, two potential issues were noticed:

Firstly, it was observed that for single tow samples the scans varied in length. This meant, that if two scans of different lengths had identical noise levels, the results (measured by a percentage of total data present) would be recorded as different values. It was decided that there needed to be a tool implemented to better select the portion of scan data to be analyzed, validating a direct comparison of percent noise.

After processing all data, a second issue was observed. Some samples were starting, ending, or in some cases “bookended” with rows of pure noise. This was due to the scanner path extending beyond the edge of the stage on which the sample was laid up. This caused data from that portion of the scan to register as void noise due to the detection range of the scanner. This anomaly, unknowingly caused by a human error, influenced the results. These few samples were measured erroneously to have a higher percentage of noise due. To fix this, the noise analysis script needed to be modified. For a detailed explanation of the solution to these problems, see Section 4.2.4.

## 6.2 DATA COLLECTION

Starting on day 25 of the scanning, scans of samples in each freezer and ambient conditions were completed on alternating days, as there were no significant observable day-today changes and the daily scanning was time-intensive.

Data collection was stopped on day 40, as no observable differences were seen in the last two weeks of data collection. The observation was that scans did not begin to display the effects of the materials' ambient curing and that the noise reduction over out-time that was expected was could not be obviously observed. In addition, over a month of scanning had taken place at this point, and the amount of data collected was substantial.

Once the drop off issue was resolved (Section 4.2.4 and Section 6.1), all data of each simulated layup errors and single tow samples were processed utilizing the developed script. The noise levels were plotted over time for each individual sample. Additionally, sample results were plotted alongside one another, grouped by combinations of material type, storage condition (ambient versus freezer), and pitch angle of scanning (0° versus 17.5°) and noise type (Lower Noise/Voids versus Upper Noise/Spikes). A selection of these plots can be seen in the following section.

## 6.3 RESULTS FROM ENVIRONMENTAL EXPOSURE EXPERIMENT

Plotted in this section are a selection noise results of samples plotted over the life of the exposure test. The noise is presented as a percentage of total scan data within a sample for simulated layup samples, and a simple count of occurrences for single tow samples. The goal is to observe the noise quality as a function of time for sets of similar scanning and storage conditions for each material of interest.

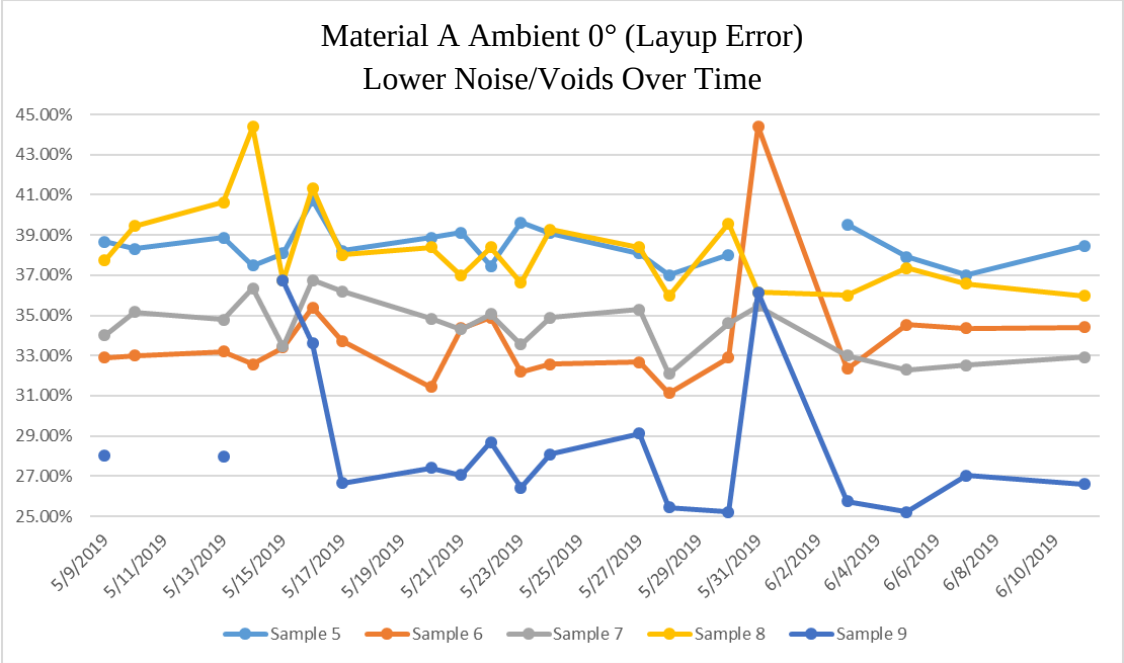


*Figure 6.3: Void Noise for Material A Ambient Layup Error Samples Scanned at 0°*

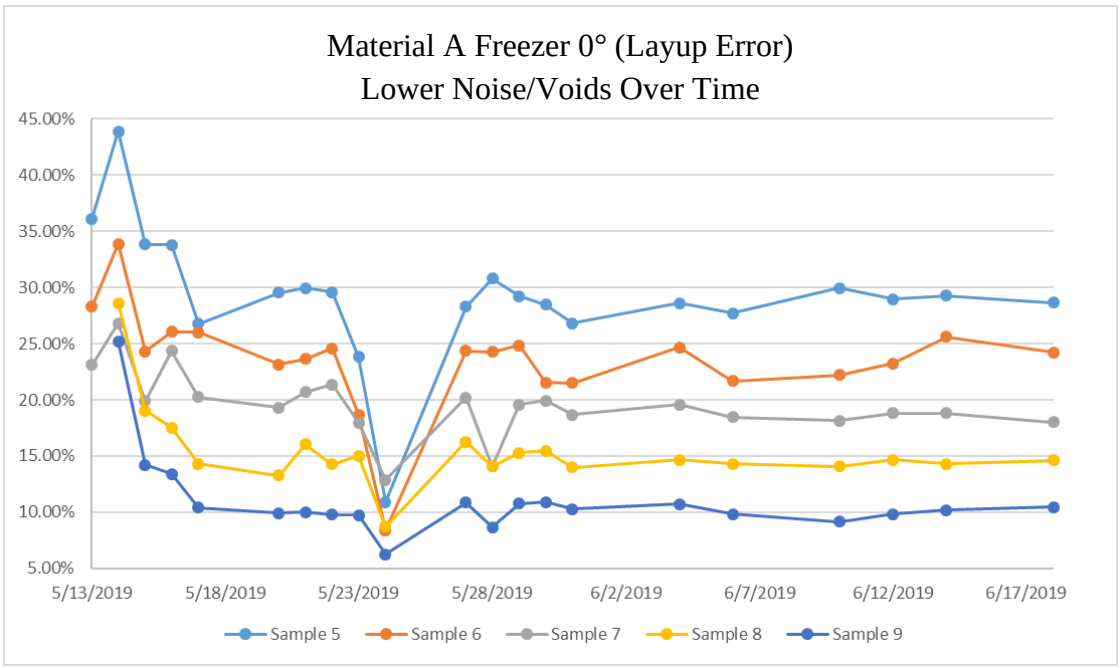


*Figure 6.4: Void Noise for Material A Freezer Layup Error Samples Scanned at 0°*

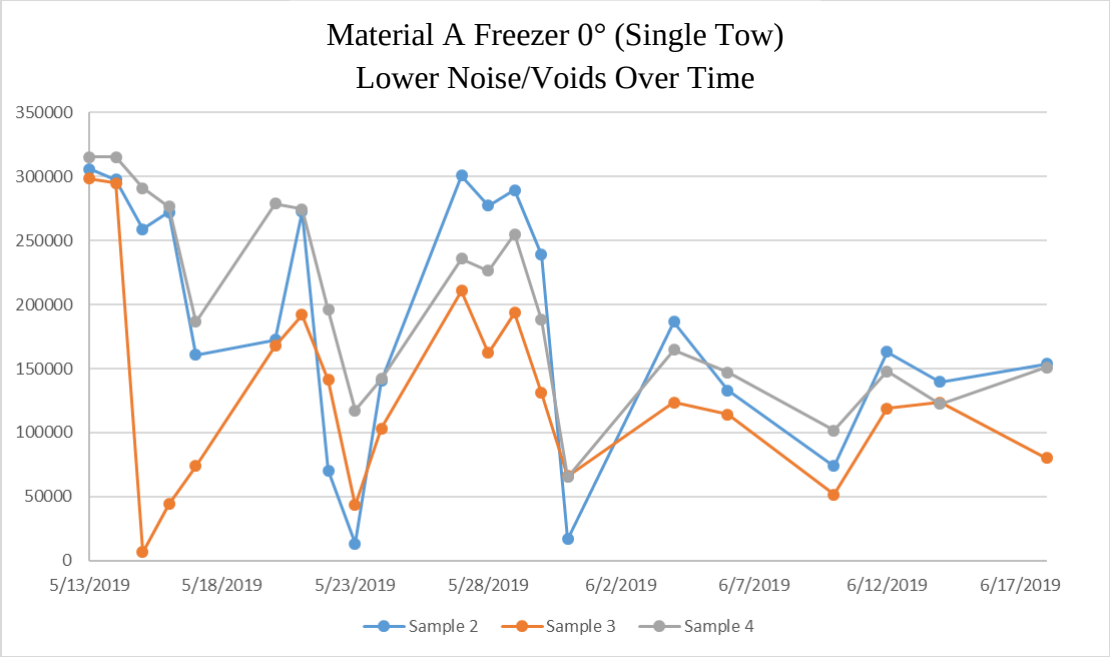


*Figure 6.5: Void Noise for Material A Freezer Single Tow Samples Scanned at 0°*

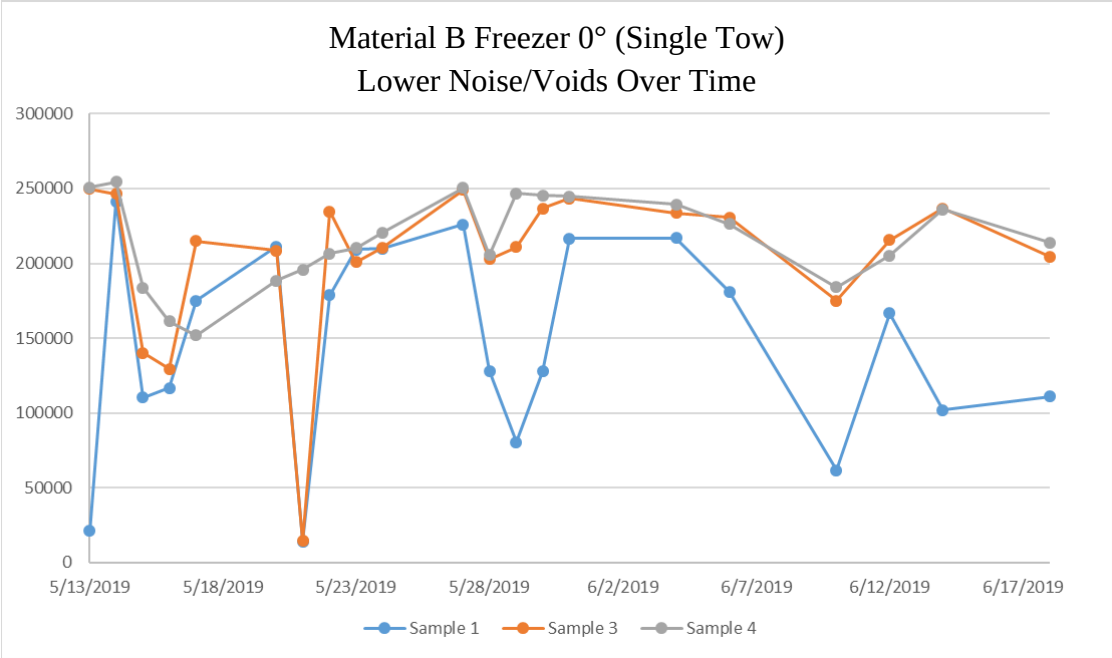


*Figure 6.6: Void Noise for Material B Freezer Single Tow Samples Scanned at 0°*

When daily scan data is plotted based on samples' shared material type, storage condition, scanning pitch angle, and noise type, there is an obvious consistency in results. We can define each possible combination of these variable as a "set" of samples. For many sets there exist days on which all samples either dramatically spike or drop in noise levels. Plots displaying such occurrences can be seen in Figure 6.3 through Figure 6.6. These plots show dramatic changes in noise values which align for most or all samples within the set. However, these occurrences do not necessarily display an overall trend. In fact, the expected result of noise levels dropping due to the samples' ambient curing over the life of the experiment was, in most cases, not observed.

## 6.4 CONCLUSION

It is deduced that ambient air effects may have an impact of noise levels. Comparing between sets shows that specific dates (or small ranges of dates) appear to have increased or decreased noise across most samples. This can be attributed to factors outside of the setup's control, such as ambient humidity temperature. This effect seems to override any one variable's effect, including storage condition. This indicates that the impact of ambient air effects seems to effect material rapidly, as samples were only removed from storage for the duration of the scans. These ambient effects could have also been responsible for the potential presence of condensation on the surface of freezer samples, impacting scanning errors. A comparison was made to correlate scanning noise levels as computed by the analysis script with local weather data reported by the National Oceanic and Atmospheric Administration (NOAA), but with no clear conclusions. Additionally, a definite relationship cannot be drawn as the internal ambient conditions were not recorded during the life of the experiment.

# CHAPTER 7

# EFFECT OF SCANNER SETTINGS

Presented in this chapter is a series of studies which were performed to determine the effects of scanner settings on reading material prone to noise error. This includes a development a set of common “ideal settings” which could be implemented to improve the scan quality of any material (Section 7.4.2). Scanner parameter settings are also investigated individually. The intensity range and peak selection are each studied individually for a series of materials, the former of which was studied intensively at varying pitch angles. Finally, a combined variable analysis is presented in which the effects of applying the ideal settings and introducing a pitch angle is studied.

## 7.1 VARIABLE ANALYSIS

An investigation into the effects of the software’s scanner settings on resultant noise while scanning at 0° was conducted. This was done for each material through an iterative trial and error process. Various combinations of settings were changed throughout the experiment, until visual results of the scan data improved (as generated by the Keyence software). This was performed until some user-identified “Ideal Settings” were realized. The default settings are presented in Figure 7.1, with the corresponding scan images shown in Figure 7.2.

- **Trigger Settings.**
  Trigger Mode : Encoder
  Input Mode : 2- phase 2 times
  Sample Frequency : 1 kHz
  Pitch : 0.075.
  Pitch between triggers : Set at 0.075.
  Batch Points : 9383.

- **Common Measure Settings.**
  Operation Mode : High Speed.
  TRG : 100 µs.
  Encoder : 500 ns.
  Control Terminal : 250 µs.

- **Imaging Settings.**
  Common head Binning : On.
  CMOS Sensitivity : High Dynamics range 3
  Exposure time : 960 µs.
  Control light setting : Auto.
  Peak Detec. Sensitivity : 5(High).
  Intrpol pts inval data : 75 points.
  Peak selection : Standard (Max Peak)
  Imaging Mode : Multi Emission.
  Emission Times : (2 times).

*Figure 7.1 Default Profilometry Scanner Settings*

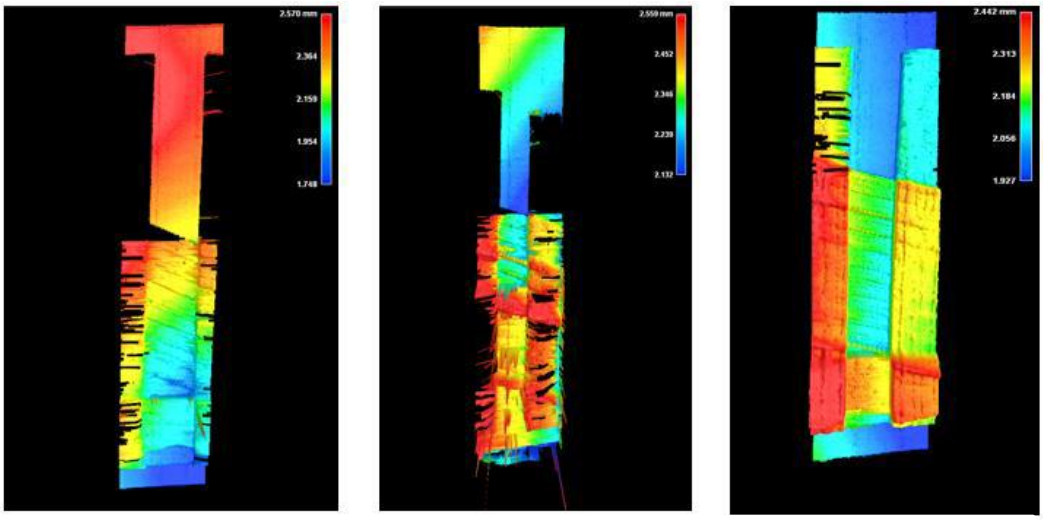

Material A
0 Degree

Material B
0 Degree

Material C
0 Degree

*Figure 7.2: Keyence Software 3D Images Generated by Scanning with Default Settings*

7.1.1 Conclusion

The experiment into scanner settings yielded consistent results across all material types investigated. For each material, in both simulated layup error and single tow samples, the default settings yielded noisy results. As shown in Figure 7.4, although the iterative investigation was run for each material in the study, it was observed that these

"Ideal Settings" converged to a common set, i.e. for each material, investigated while scanning at 0°, ideal setting was determined to be the same. These ideal settings can be seen in Figure 7.3. The settings not listed were held at values informed by the scanning software's default settings. An example of how a scan can be improved by varying the settings can be seen in Figure 7.5.

**Imaging Settings.**
CMOS sensitivity : High Precision.
Exposure Time : 1920µs.
Control Light Intensity : 99-99.
Peak selection : Invalidate data.
Intrpol pts Inval data : 65 points.

*Figure 7.3: Experimentally Determined Ideal Settings*

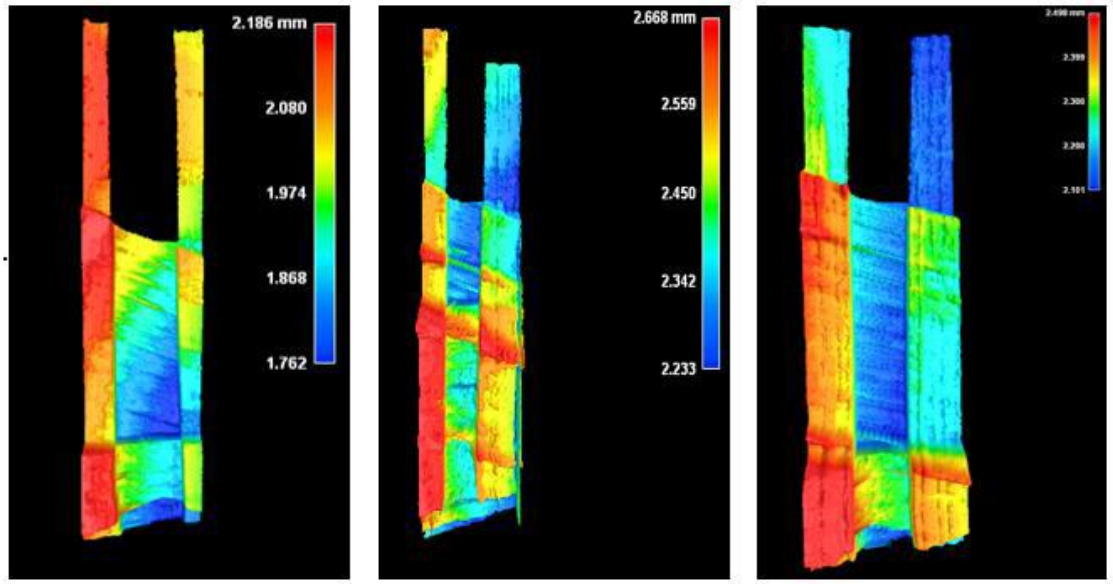


Material A
0 Degree

Material B
0 Degree

Material C
0 Degree

*Figure 7.4: Keyence Software 3D Images Generated by Scanning with Ideal Settings*

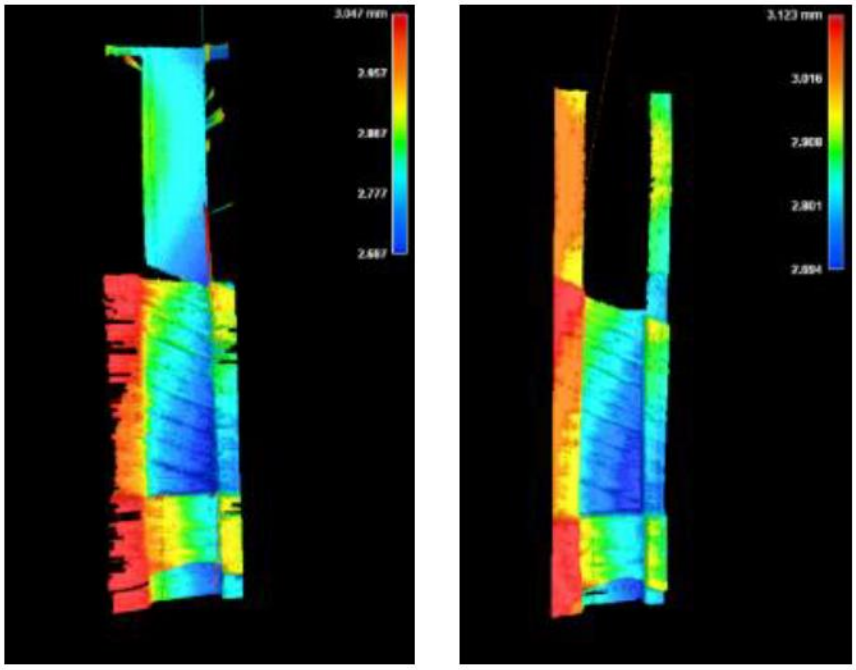

*Figure 7.5: Results of Setting Optimization on Scanner Results (Left: Default Settings, Right: Ideal Settings) Material A*

## 7.2 PEAK SELECTION

Peak Selection was one setting investigated to isolate its effects of noise. All scans were performed on simulated layup error samples. Samples were scanned at 0° while selecting each option for this variable; Far, Invalidate Data, Near, Remove X Multiple Reflection, Remove Y Multiple Reflection, Standard (Maximum Peak).

### 7.2.1 Conclusion

As can be seen from the results in Figure 7.6 and Figure 7.7 (legend presented by Figure 4.8), the investigation into the peak selection setting does not yield very strong results. However, shown in the graphed results, each “Remove X Multiple Reflection” and “Remove Y Multiple Reflection” settings produce more void noise within samples. When focusing on void noise, the remaining options for the peak selection setting; “Far”, “Invalidate Data”, “Near”, and “Standard”; all appear to have comparable results—none

of which display a preference. The results of spike noise analysis are similar, although "Remove Y Multiple Reflection" and "Standard" yield the lowest amount of noise. Overall, improvements in scanning error is marginal. From the results of this experiment, the scanner's peak selection setting is concluded to not have a significant impact on profilometry scanning error mitigation.

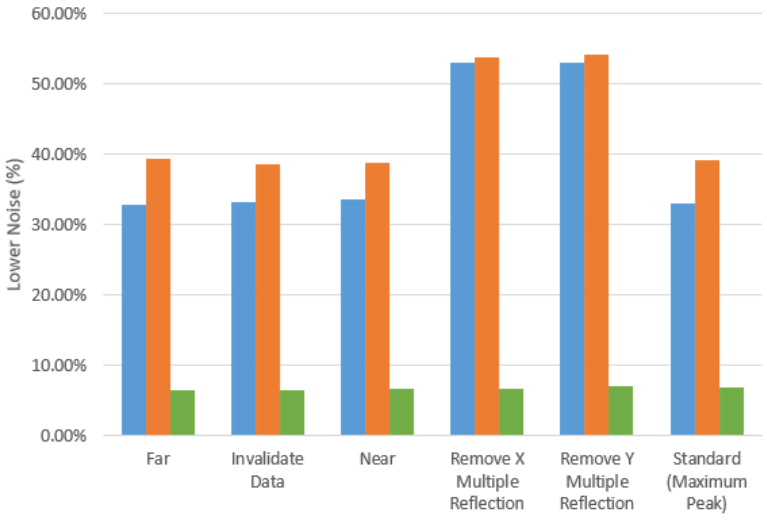


*Figure 7.6: Void Noise as a Function of Peak Selection*

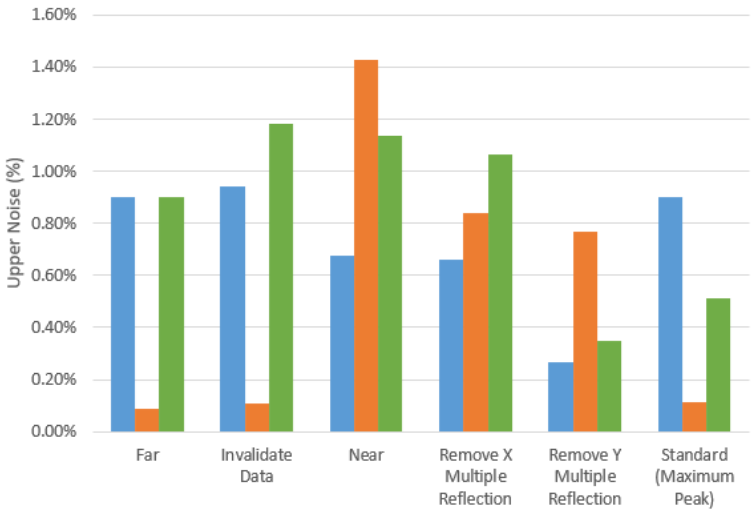


*Figure 7.7: Void Noise as a Function of Peak Selection*

## 7.3 INTENSITY RANGE

Experiments were performed to determine the effects of the laser's intensity range scanner setting on profilometry noise error. This was performed by scanning a simulated layup error sample for each material at incremental Intensity Ranges and additionally studying the effects intensively at varying pitch angles. First, scans were performed at 0° at Intensity Range settings between 80 and 99 in increments of 1. Then, scans were performed at 17.5° at Intensity Range settings between 11 and 99 in increments of 11.

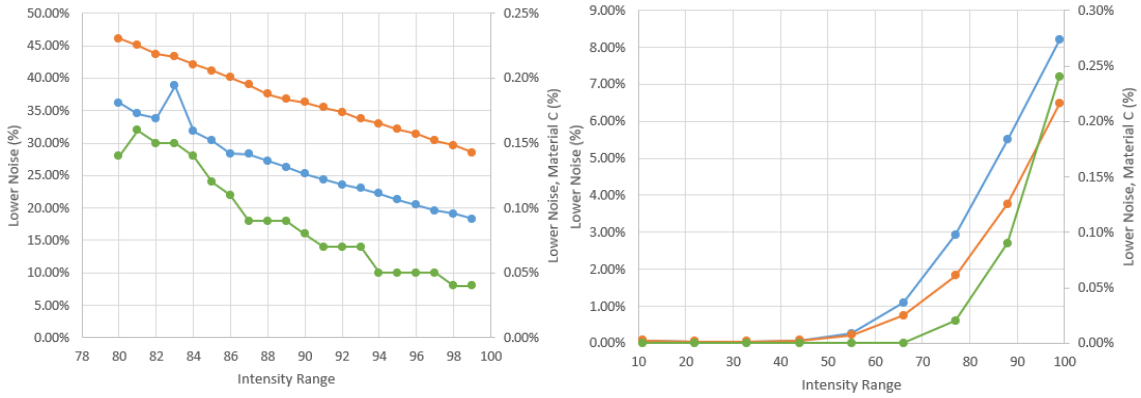


*Figure 7.8: Void Noise Plotted as a Function of Intensity Range (Left: 0° Pitch, Right: 17.5° Pitch)*

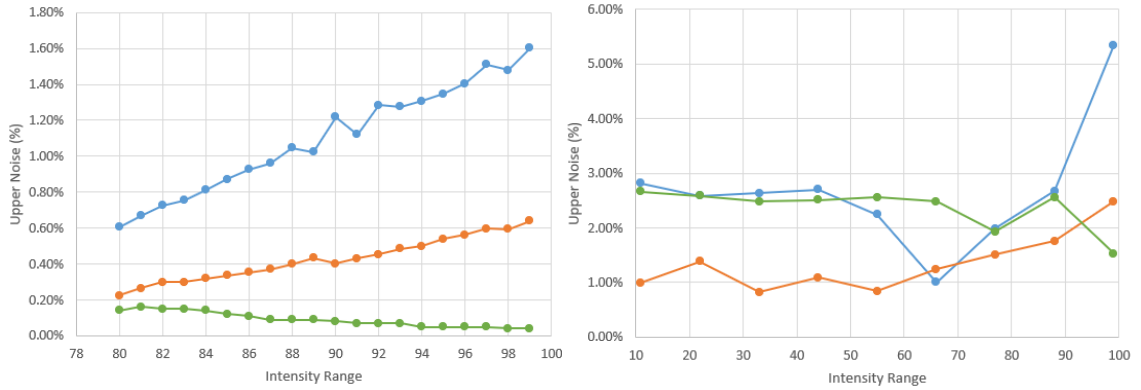


*Figure 7.9: Spike Noise as a Function of Intensity Range (Left: 0° Pitch, Right: 17.5° Pitch)*

### 7.3.1 Conclusion

The conclusion of this experiment is that modifying the Intensity Range setting had varied results depending on pitch angle, as presented in Figure 7.8 and Figure 7.9 (legend presented in Figure 4.8). Additionally, void noise and spike noise had opposite results in each trial. While scanning with a pitch angle of 0°, increasing the intensity range decreased void noise significantly, while increasing spike noise marginally. Conversely, while scanning with a pitch angle of 17.5°, increasing intensity range increased void noise yet seemed to have no consistent effect on spike noise. These results are presented in Table 7.1. The following subsections show the resulting plotted images from this experiment. The following subsections show the resulting plotted images from this experiment; Figure 7.10 through Figure 7.15.

*Table 7.1: Noise Level Effects of Increasing Intensity Range per Pitch Angle*

| Pitch Angle | Effect on Void Noise | Effect on Spike Noise |
|---|---|---|
| 0° | Decreased | Increased |
| 17.5° | Increased | Inconsistent |

### 7.3.2 Intensity Range Pitched at 0°

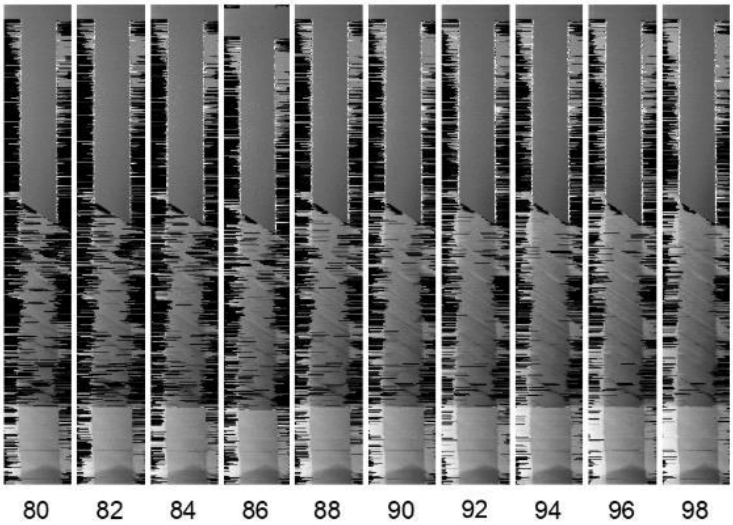


*Figure 7.10: Images Generated at Various Intensity Ranges Material A – Scanned at 0°*

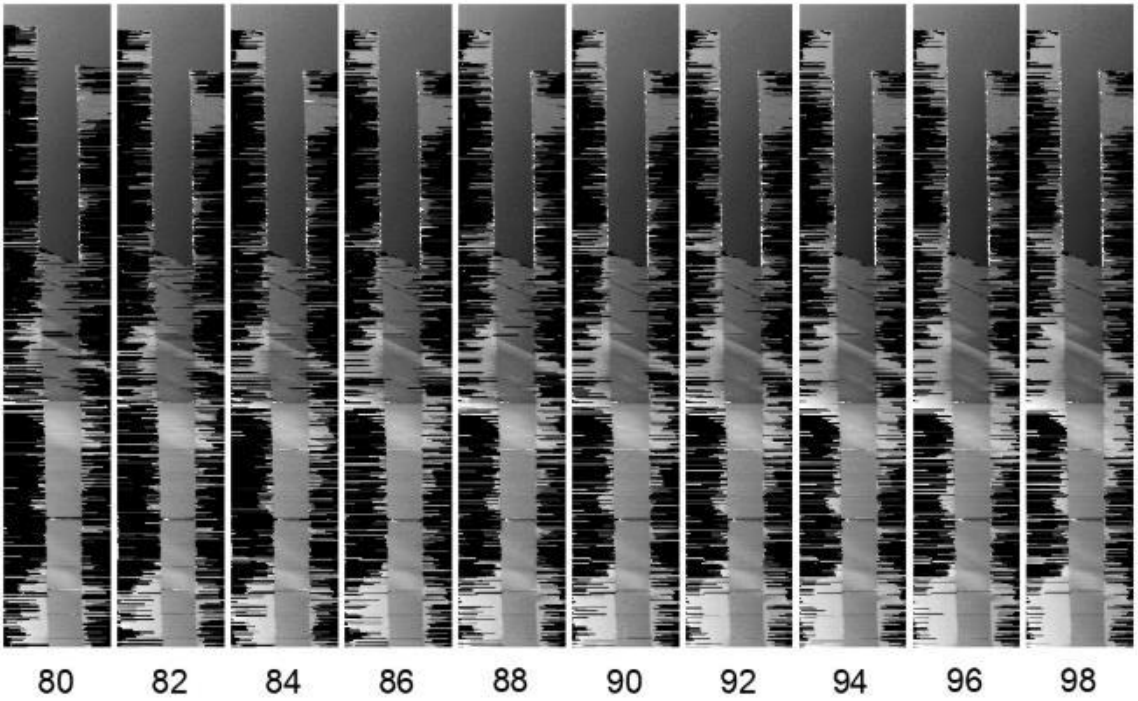


*Figure 7.11: Images Generated at Various Intensity Ranges Material B – Scanned at 0°*

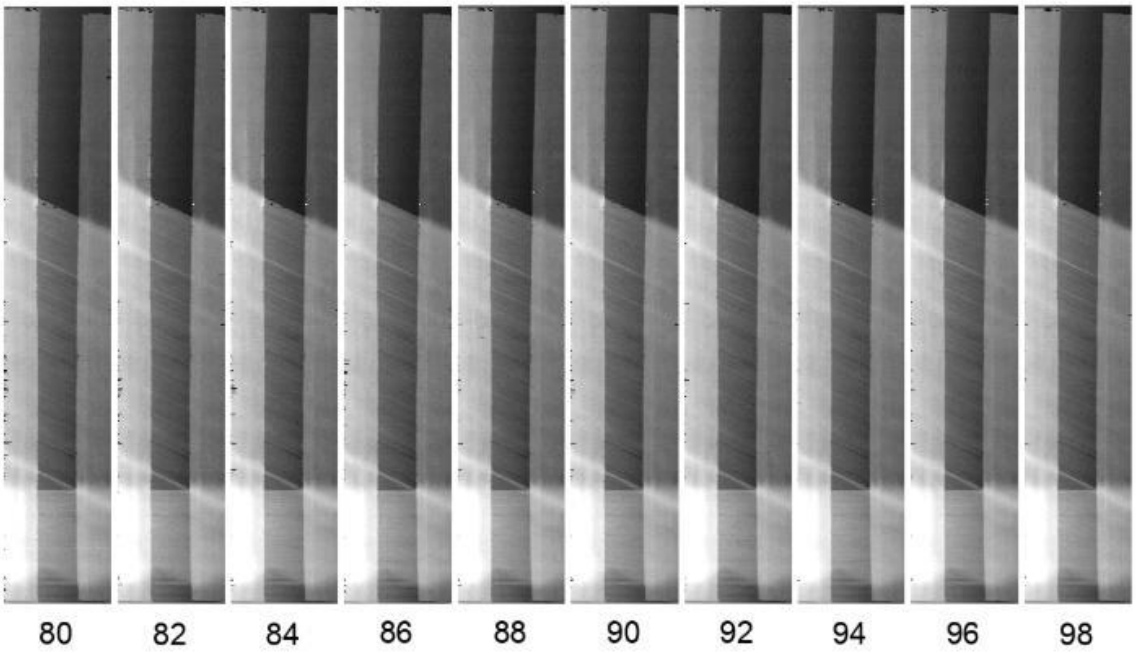


*Figure 7.12: Images Generated at Various Intensity Ranges Material C – Scanned at 0°*

7.3.3 Intensity Range Pitched at 17.5°

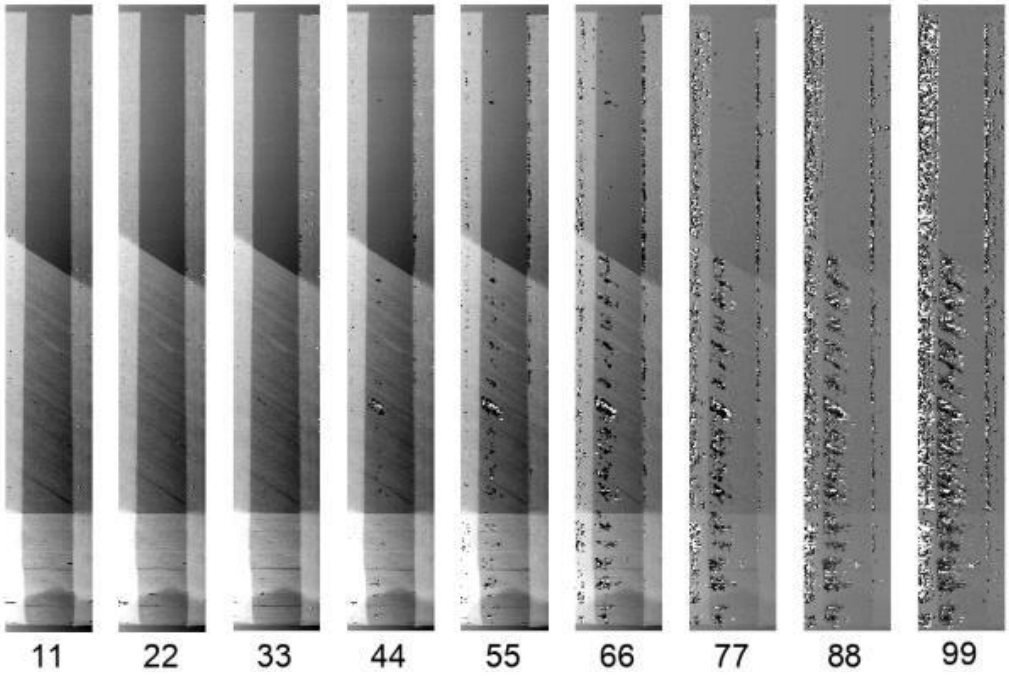


*Figure 7.13: Images Generated at Various Intensity Ranges Material A – Scanned at 17.5°*

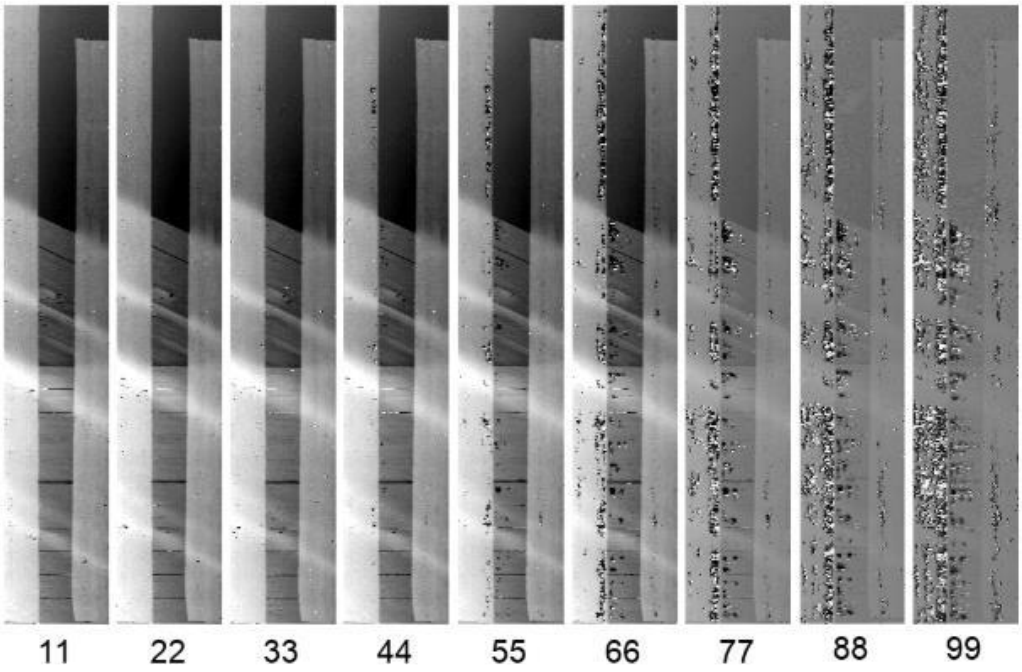


*Figure 7.14: Images Generated at Various Intensity Ranges Material B – Scanned at 17.5°*

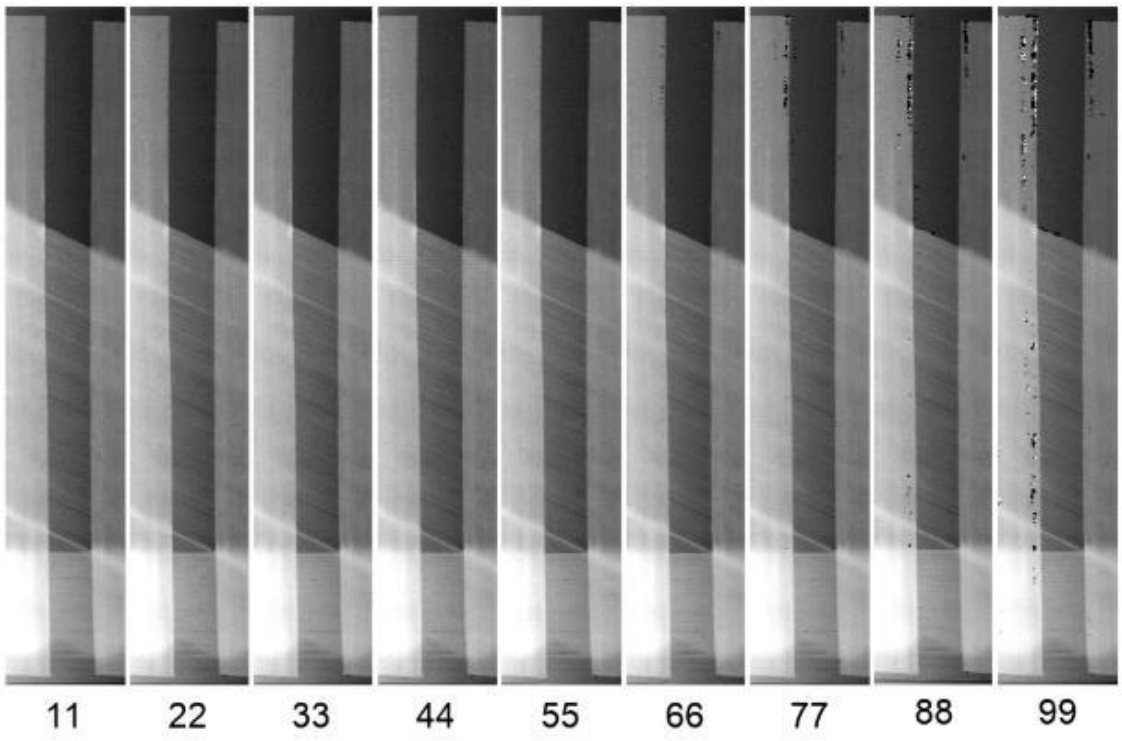


*Figure 7.15: Images Generated at Various Intensity Ranges Material C – Scanned at 17.5°*

## 7.4 COMBINED VARIABLE ANALYSIS AND SCANNER PITCH

An experiment to determine the combined effects of variables was performed, this includes both scanner settings and pitch angle. In this approach, the experimentally determined "Ideal Settings" were tested while scanning at a pitch angle of 17.5°. The results of each study (one scanning while pitched at 0° and the other at 17.5°) could then be compared to determine if pitching the scanner and implementing the ideal settings has a combined effect. Additionally, multiple geometries of each material type were investigated. Scans were performed for each single tow as well as simulated layup error samples. For each material in this final comparison, eight groups were analyzed (see Table 7.2). The default and ideal settings along with the results from this investigation are presented and discussed in the following subsections.

*Table 7.2: Combinations of Variables to be Analyzed*

1. Layup Error - Default Settings 0°
2. Layup Error - Default Settings 17.5°
3. Layup Error - Ideal Settings 0°
4. Layup Error - Ideal Settings 17.5°
5. Single Tow - Default Settings 0°
6. Single Tow - Default Settings 17.5°
7. Single Tow - Ideal Settings 0°
8. Single Tow - Ideal Settings 17.5°

7.4.1 Conclusion

When samples were scanned with default settings at 0°, void noise dominated the scan, due to the reflectivity of the material. In comparison, when scans were performed with default settings and a pitch of 17.5° was introduced, the void noise was mitigated significantly, however in many cases not entirely. Additionally, spike noise was increased in many cases (typically this increase in spike noise due to an introduction of pitch angle can be observed in simulated layup error samples).

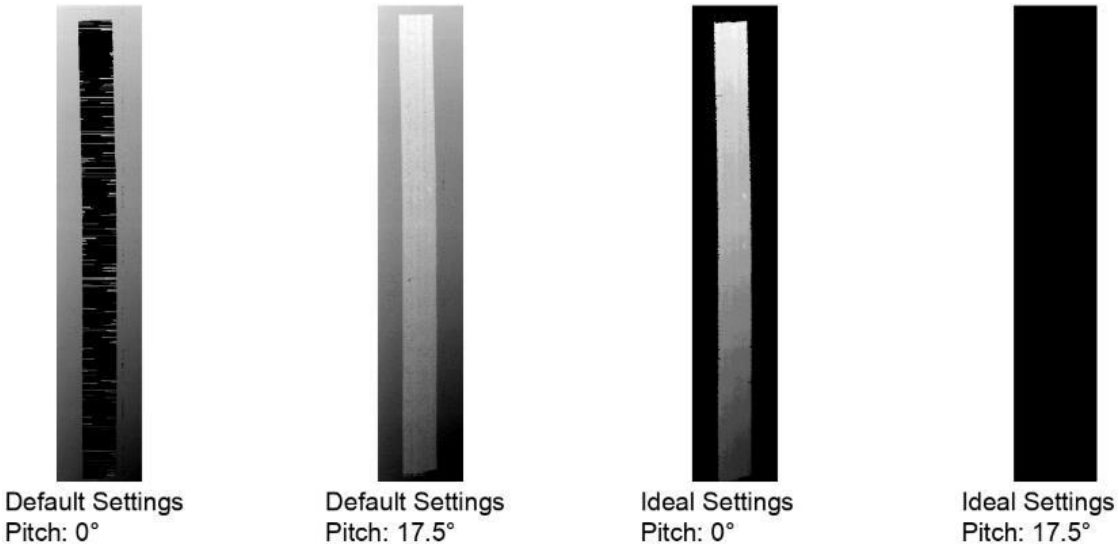


*Figure 7.16: Script Created Images Generated by Scanning with Combinations of Default/Ideal Settings and 0°/17.5° Pitch – Material A Single Tow Samples*

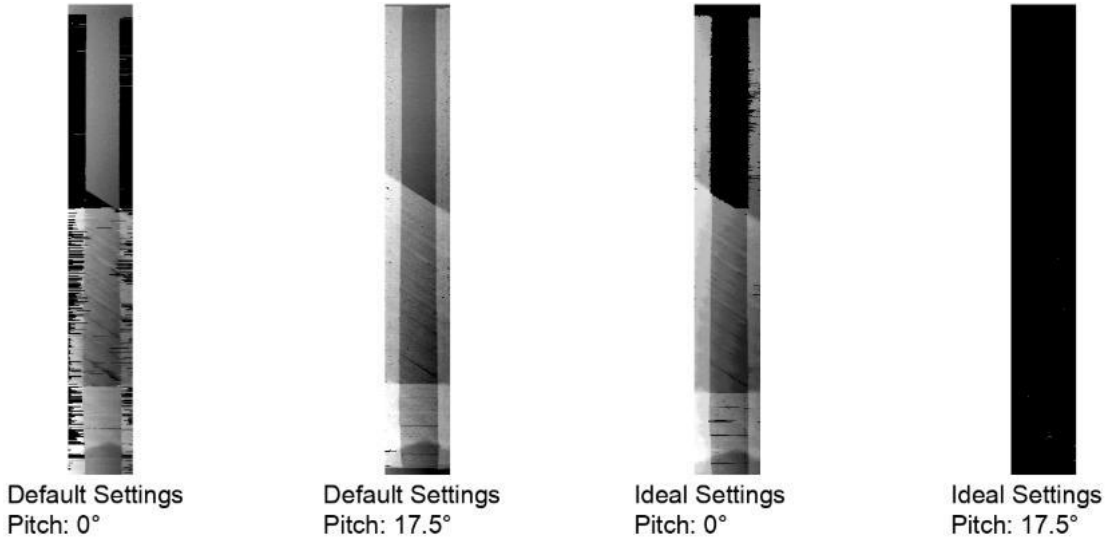


*Figure 7.17: Script Created Images Generated by Scanning with Combinations of Default/Ideal Settings and 0°/17.5° Pitch – Material A Simulated Layup Error Samples*

Scanning at the ideal settings had a significant improvement over default settings when scanning at 0°. Visually, all noise on the target object's surface appears to be completely mitigated for all material types (both void noise and spike noise). Select results are presented in Figure 7.16 and Figure 7.17, comparing each default and ideal settings investigated at each 0° and a pitch angle of 17.5° for one material of interest. The script generated images of all scans analyzed are presented in their entirety in Appendix D. Results are similar for all three materials inspected. However, introducing the pitch angle while scanning with "ideal" settings does not have a positive cumulative effect. In fact, utilizing the defined "ideal" settings in conjunction with a pitch of 17.5° results in unreadable scan data. This is consistent for all materials and for each single tow and simulated layup error samples.

Additionally, scanning with ideal settings at 0°, while resulting in material legibility, introduces a unique effect on scan data. When analyzing these results, it was observed that the brushed 5052-H32 Aluminum backing plate does not register in the

scan data. The regions that otherwise would manifest as relatively consistent values—measuring effectively the flatness of the backing plate—instead appear similarly to pure void noise, recorded as values of approximately negative one hundred. This anomaly could not be resolved by the developed analysis script. For this reason, only a visual analysis is presented in this report.

The final observation on this topic is that utilizing the ideal settings while scanning at 0° are only a marginal improvement to scanning with default settings at 17.5°. Additionally, the previously mentioned issue of the backing plate introducing simulated noise suggests that this method of noise reduction may introduce secondary erroneous noise sources which cannot be predicted at this time. Scanning at 17.5° while utilizing the described default settings is preferred to scanning at 0° with ideal settings. However, since the two are comparable, the use of them shall likely be situationally determined (part geometry, collision prevention, feasibility, etc.).

# CHAPTER 8

# CONCLUSION

Conclusions made from this thesis report are presented in this chapter. As drawn from the previous discussions, performance of profilometry scanning is predominately dependent on light diffuse reflection (section 1.2, section 2.2, chapter 5, section 6.4, & section 7.4). Because of this, mitigation techniques are expected to improve to varying degrees of success a target objects ability to reflect light into the receiver of the profilometry scanner. This, in some cases, is dependent purely on geometry of the scanning setup (section 1.2 & chapter 5), and in other cases, some combination of settings of the profilometry equipment (chapter 7). These, as explicitly stated below, form the set of equipment configuration-based solutions for profilometry scanning error mitigation (section 8.2). Additionally, material selection impact the success of laser topography scanning (sections 1.2, 2.3, & 3.1). Furthermore, the degree to which material characteristics impact scanning error is determined by the environmental conditions that the material is exposed to and the duration of that exposure (chapter 6). These impacts of material characteristics inform what is the second set of considerations in the mitigation of profilometry scanning error (section 8.1). The development of the data analysis tool (chapter 4) and gantry scanning system (chapter 3) was a vital part of drawing these conclusions. Simply stated, observations of scans are insignificant without quantifiable data to allow for meaningful comparisons between consistently performed scans.

## 8.1 MATERIAL CHARACTERISTICS

Prior to experimental investigations, observations were made on the performance of select materials. These observations of inherent scanning error and how that error varies between materials is presented herein. Additionally discussed, are the conclusions of the experimental investigation of ambient conditions effect on material scanning performance. These ambient conditions—and the exposure duration to these conditions—has an established impact of the physical and chemical properties of the thermoset material (chapter 6, section 3.2.4). The effect these ambient conditions have on measurable profilometry scanning error can speak directly to the relationship between these properties and the scanning error produced.

### 8.1.1 Material Variability

Initial selection of thermoset composite materials, although not based on a quantitative analysis via the later developed script, yielded results that highlight the variations in unmitigated profilometry noise. The three materials initially selected performed significantly different under identical equipment configurations. As shown in Figure 3.1 (section 3.1), each of the materials had a varied impact on profilometry data, highlighting that material characteristics influenced performance. Specifically noteworthy, is that material C scanned with the least amount of initial scanning and was the most challenging to layup by hand (section 3.2.4). Additionally, as seen in Figure 3.4 (section 3.1) this material displayed an uneven disbursement of the material's polymer, likely contributing to this reduced tackiness. Additionally, this impacts reflective properties due to potential fiber strike through, as supported by the literature in section 2.3.2. The conclusion drawn here is that the tackiness of the material which allows

thermoset composite tows to adhere to tooling is the same characteristic which prevents successful topography measurement via modern profilometry scanners. Furthermore, analysis of this material characteristic may allow for the prediction of profilometry scanning performance prior to the layup process.

### 8.1.2 Ambient Conditions

Environmental properties are shown definitively to impact thermoset samples performance in profilometry scanning in the information presented in chapter 6. This impact is due to the environmental exposure affecting the physical and chemical properties of the thermoset composite samples. Although not measured directly day to day, the environmental impact is determined to be on a material's tackiness. This is in line with common practices in AFP manufacturing in which material out time is restricted prior to laying up due to its impact of the material's ability to adhere to tooling [4]. The plots in chapter 6 are presented by grouping samples by similar scanning and storage conditions for each material of interest (section 6.3). When comparing scanning error measurements from different dates for a particular set of samples, it is clear that levels of scanning error rise and all due to conditions specific to that date (Figure 6.4 most dramatically displays this). As experimental setup is consistent day to day, this can only be attributed to environmental factors outside the scope of this setup. Additionally, the impact these conditions have on the thermoset composite tows occurs rapidly, as samples were only removed from the freezer for the duration of scanning.

## 8.2 EQUIPMENT CONFIGURATION

The success of profilometry scanning is greatly dependent on both physical equipment configuration and scanner settings. As show in chapter 5, the geometry of

equipment during scanning, as expressed by scanning pitch angle, has a significant impact on error levels. Additionally, both isolated and combined adjustments of scanner settings can improve or worsen scanning results, as shown in chapter 7.

### 8.2.1 Pitch Angle

Pitch angle is definitively shown to have a significant effect of profilometry scanning error mitigation. Comparing the performance of scans at varying pitch angles presented in chapter 5, Figure 5.5, and the angle between the emitted laser signal and the direction of the receiver as defined by the geometry of the profilometer housing shown in Figure 5.1, it is clear that the bisecting angle of 17.5° is the pitch angle which gives the best scanning results in terms of signal error mitigation. The reduction in calculated error far surpasses the anticipated noise variance between scans of identical setup, as presented by Table 4.1 (section 4.3).

### 8.2.2 Laser Signal Intensity

The effect of laser intensity range, as investigated in section 7.3, resulted in varied effects dependent on whether or not a pitch was introduced during scanning. The conclusions are drawn with regards to void noise, as it was consistently determined to be the dominating scanning error. When scans are performed with no pitch, i.e. a pitch angle of 0°, intensity and profilometry scanning error has an inverse relationship. When scans are performed with some pitch present, in the case of this experiment, 17.5°, intensity and scanning data error have a direct relationship. This is expressed visually in Figure 7.8, as well as tabulated in Table 7.1. Additionally, images generated by the analysis script, presented in Figure 7.10 through Figure 7.15, display this trend.

### 8.2.3 Scanner Settings

Intensity of laser signal was not the only scanning parameter experimentally investigated. Combinations of scanner settings were iteratively tested and a user-defined set of “ideal settings” was determined. These settings can be seen in Figure 7.3, with scanning performance (as generated by the Keyence software) shown in Figure 7.4. Default scanning settings are displayed in Figure 7.1, with default scanning performance (again, Keyence software) shown in Figure 7.2.

Finally, these “ideal” scanner settings are proven to only benefit without the presence of pitch, i.e. a pitch angle of 0°. As discussed in section 7.4.1 and shown in images generated by the analysis script from experimentally collected scan data, Figure 7.16 and Figure 7.17, the default settings at a 0° performed similar to ideal settings at a pitch of 17.5° with regard to scanning the surface of the thermoset tow sample. However, utilizing the “ideal settings” at 0° results in the backing plate returning meaningless data. Further investigations would need to be performed to determine the cause of this effect, which falls out of the scope of research presented in this report. Additionally, further work would need performed to determine how the removal of the tooling from meaningful scan data would impact the performance of the ACSIS system’s ability to automatically detect or categorize layup defects. Lastly, when scanning with these “ideal settings” at a pitch angle of 17.5°—the pitch angle determined to perform the best utilizing default settings—the data collected was meaningless and resulted in pure signal error. Combining the ideal settings with the ideal pitch angle ultimately has a negative effect of the presence of profilometry scanning error.

## 8.3 REMARKS AND FUTURE WORK

The work presented in this thesis report, although thorough, leaves avenues of explorations open for future work on this subject and hopefully serves as a jumping off point for further advancements in this field. The determination and clear evidence presented of the relationship between material characteristics and equipment configuration on laser light diffuse reflection successfully explain the anomaly of profilometry scanning error and support the experimentally determined, viable solution methods for mitigation of this scanning noise. The next development of this topic would be to quantify the relationship between a composite material's tackiness and that sample's measurement of specular reflection. This would develop a determination of a material's layup performance and the ACSIS' ability to detect layup errors in the AFP process for said material. Additionally, research directed at quantifying the relationship between ambient conditions and material profilometry feasibility would suitably further the investigation presented in Chapter 6. An additional step not presented within this work would be to determine why the "ideal settings" presented in section 7.1 perform with varied success between scanning a thermoset tow and scanning the metal tooling. Specifically, when they are utilized at a pitch angle, the scan data presents meaningless data for the tooling's surface.

Finally, the development of a predictive model would be paramount in determining material's overall feasibility for profilometry scanning measurement and utilization in layup defect detection systems driven by this form of inspection. It is clearly shown through this work that a material's physical characteristics—such as the distribution of polymer and carbon fiber along the surface of the tow (section 3.1)—

determine the material's tackiness, reflective quality, and therefore scanning performance. This leads to the possibility of expanding upon this correlation in the form of a predictive model possibly relying on prediction methods such as bidirectional reflectance distribution functions [28,29].

# REFERENCES


[1] Astrom, 1997, *Manufacturing of Polymer Composites*, Chapman & Hall, London, UK.

[2] Croft, K., Lessard, L., Pasini, D., Hojjati, M., Chen, J., and Yousefpour, A., 2011, "Experimental Study of the Effect of Automated Fiber Placement Induced Defects on Performance of Composite Laminates," Compos. Part A Appl. Sci. Manuf., **42**(5), pp. 484–491.

[3] Keyence Corporation, 2013, "High-Speed 2D/3D Laser Scanner LJ-V7000 Series."

[4] Lukaszewicz, D. H. J. A., Ward, C., and Potter, K. D., 2012, "The Engineering Aspects of Automated Prepreg Layup: History, Present and Future," Compos. Part B Eng., **43**(3), pp. 997–1009.

[5] Mukhopadhyay, S., Jones, M. I., and Hallett, S. R., 2015, "Tensile Failure of Laminates Containing an Embedded Wrinkle; Numerical and Experimental Study," Compos. Part A Appl. Sci. Manuf., **77**, pp. 219–228.

[6] Mukhopadhyay, S., Jones, M. I., and Hallett, S. R., 2015, "Compressive Failure of Laminates Containing an Embedded Wrinkle; Experimental and Numerical Study," Compos. Part A Appl. Sci. Manuf., **73**, pp. 132–142.

[7] Elsherbini, Y. M., and Hoa, S. V., 2017, "Experimental and Numerical Investigation of the Effect of Gaps on Fatigue Behavior of Unidirectional Carbon/Epoxy Automated Fiber Placement Laminates," J. Compos. Mater., **51**(6), pp. 759–772.

[8] Li, X., Hallett, S. R., and Wisnom, M. R., 2015, "Modelling the Effect of Gaps and Overlaps in Automated Fibre Placement (AFP)-Manufactured Laminates," Sci. Eng. Compos. Mater., **22**(2), pp. 115–129.

[9] Fayazbakhsh, K., Arian Nik, M., Pasini, D., and Lessard, L., 2013, "Defect Layer Method to Capture Effect of Gaps and Overlaps in Variable Stiffness Laminates Made by Automated Fiber Placement," Compos. Struct., **97**, pp. 245–251.

[10] Lan, M., Cartié, D., Davies, P., and Baley, C., 2016, "Influence of Embedded Gap and Overlap Fiber Placement Defects on the Microstructure and Shear and Compression Properties of Carbon-Epoxy Laminates," Compos. Part A Appl. Sci. Manuf., **82**, pp. 198–207.

[11] Gangloff, J. J., Simacek, P., Sinha, S., and Advani, S. G., 2014, "A Process Model for the Compaction and Saturation of Partially Impregnated Thermoset Prepreg Tapes," Compos. Part A Appl. Sci. Manuf., **64**, pp. 234–244.

[12] Arian Nik, M., Fayazbakhsh, K., Pasini, D., and Lessard, L., 2014, "Optimization of Variable Stiffness Composites with Embedded Defects Induced by Automated Fiber Placement," Compos. Struct., **107**(1), pp. 160–166.

[13] Bakhshi, N., and Hojjati, M., 2018, “An Experimental and Simulative Study on the Defects Appeared during Tow Steering in Automated Fiber Placement,” Compos. Part A Appl. Sci. Manuf., **113**(March), pp. 122–131.
[14] Sacco, C., Radwan, A. B., Harik, R., and Van Tooren, M., 2018, “Automated Fiber Placement Defects: Automated Inspection and Characterization,” Int. SAMPE Tech. Conf., **2018**-**May**.
[15] Shadmehri, F., Ioachim, O., Pahud, O., Brunel, J. E., Landry, A., Hoa, S. V., and Hojjati, M., 2015, “Laser-Vision Inspection System for Automated Fiber Placement (AFP) Process,” *ICCM International Conferences on Composite Materials*, Copenhagen.
[16] Wohl, C., Palmieri, F. L., Forghani, A., Hickmott, C., Bedayat, H., Coxon, B., Poursartip, A., and Grimsley, B., 2017, “Tack Measurements of Prepreg Tape at Variable Temperature and Humidity,” CAMX 2017 - Compos. Adv. Mater. Expo, **2017**-**Decem**.
[17] Blom, A. W., Lopes, C. S., Kromwijk, P. J., Gürdal, Z., and Camanho, P. P., 2009, “A Theoretical Model to Study the Influence of Tow-Drop Areas on the Stiffness and Strength of Variable-Stiffness Laminates,” J. Compos. Mater., **43**(5), pp. 403–425.
[18] Black, S., 2018, “Improving Composites Processing with Automated Inspection,” Compos. World.
[19] Cemenska, J., Rudberg, T., and Henscheid, M., 2015, “Automated In-Process Inspection System for AFP Machines,” SAE Int. J. Aerosp., **8**(2).
[20] Meadows, D. M., Johnson, W. O., and Allen, J. B., 1970, “Generation of Surface Contours by Moiré Patterns,” Appl. Opt., **9**(4), p. 942.
[21] Takeda, M., and Mutoh, K., 1983, “Fourier Transform Profilometry for the Automatic Measurement of 3-D Object Shapes,” Appl. Opt., **22**(24), p. 3977.
[22] Takeda, M., Ina, H., and Kobayashi, S., 1982, “Fourier-Transform Method of Fringe-Pattern Analysis for Computer-Based Topography and Inteferometry.,” J. Opt. Soc. Am., **72**(1), pp. 156–160.
[23] Yue, H. M., Su, X. Y., and Liu, Y. Z., 2007, “Fourier Transform Profilometry Based on Composite Structured Light Pattern,” Opt. Laser Technol., **39**(6), pp. 1170–1175.
[24] Guo, L., 1990, “Improved Fourier Transform Profilometry for the Automatic Measurement of 3D Object Shapes,” Opt. Eng., **29**(12), p. 1439.
[25] Yi, J., and Huang, S., 1997, “Modified Fourier Transform Profilometry for the Measurement of 3-D Steep Shapes,” Opt. Lasers Eng., **27**(5), pp. 493–505.
[26] Tang, S., and Hung, Y. Y., 1990, “Fast Profilometer for the Automatic Measurement of 3-D Object Shapes,” Appl. Opt., **29**(20), pp. 3012–3018.
[27] Schubel, P. J., Warrior, N. A., Kendall, K. N., and Rudd, C. D., 2006, “Characterisation of Thermoset Laminates for Cosmetic Automotive Applications: Part I - Surface Characterisation,” Compos. Part A Appl. Sci. Manuf., **37**(10), pp. 1734–1746.
[28] Koenderink, J. J., Van Doorn, A. J., Dana, K. J., and Nayar, S., 1999, “Bidirectional Reflection Distribution Function of Thoroughly Pitted Surfaces,” Int. J. Comput. Vis., **31**(2), pp. 129–144.

[29] Westin, S. H., Arvo, J. R., and Torrance, K. E., 1992, “Predicting Reflectance Functions From Complex Surfaces,” Comput. Graph., **26**(2), pp. 255–264.
[30] Neitzel, M., Blinzler, M., Edelmann, K., and Hoecker, F., 2000, “Surface Quality Characterization of Textile-Reinforced Thermoplastics,” Polym. Compos., **21**(4), pp. 630–635.
[31] BYK-Gardner GmbH, “Visual Evaluation and Instrumental Measurement of Orange Peel and DOI,” pp. 33–36.

# APPENDIX A

# DATA ANALYSIS SCRIPT

Presented here is the data analysis script, which was developed for the analysis of profilometry scan data, in its entirety. The functionality and justifications of the code are presented throughout section 4.2.

```
'''''---CSV Scan Plotter Final Version---
Jacob Ondeck, 2019'''

from PIL import Image
import numpy as np
import time
from numpy import genfromtxt
import os

def main():
    directories = ['C:\\FilePath\\'] #List of folder names to be analysed (Operator input)

    RunFilter = ask_user() #Prompts user to filter leading and trailing rows of pure noise ("Drop-off Filter")
    SingleTow = ask_single_tow() #Asks user if samples are Single Tow samples, in which case the noise is simply counted and not calculated as a percentage
    for i in range(len(directories)): #Iterate through list of folder names manually input by operator
        directory = directories[i]
        print(directory)
        ScanNames = os.listdir(directory) #Create list of file names within folder "directory"
        for i in range(len(ScanNames)): #Iterate through list of file names

            filename = directory + ScanNames[i]

            if filename.endswith('.csv'):
                dot = filename.rfind('.')
                filename = filename[:dot]
                a, NoiseNom, PercentLowerNoise, RealValAvg, RealValCount, AllNoise = GenerateArray(filename, RunFilter) #Generates a Numpy Array from CSV File, and Simply Counts Noise Elements

                if AllNoise == True: #If csv is completely invalid, an error message is printed and the loop moves onto the next file
                    print("Data file completely noise, no valid data: ", ScanNames[i])
                    writedoc(100, 0, filename, 9999999, 0, SingleTow)
                    GenerateImage(a, filename)
```

```
                    continue

                Refineda, PercentUpperNoise, UpperNoiseNom = ScaleRefined(a, RealVa
lAvg, RealValCount) #Runs the array through the Refined Scale
                Pixela = PixelVal(Refineda) #Maps array to pixel values
                GenerateImage(Pixela, filename) #Creates and saves image from pixel
 numpy array
                writedoc(PercentLowerNoise, PercentUpperNoise, filename, NoiseNom,
UpperNoiseNom, SingleTow) #Creates and saves document detailing two types of noise
present in sample, either as percentage or simple count

            else:
                pass

def ask_single_tow():
    #Asks user if samples are Single Tow samples, in which case the noise is simply
 counted and not calculated as a percentage
    check = str(input("Are these samples scans of a single tow? (Y/N): ")).lower().
strip()
    try:
        if check[:1] == 'y':
            return True
        elif check[:1] == 'n':
            return False
        else:
            print('Invalid Input')
            return ask_user()
    except:
        print("Please enter valid inputs")
        return ask_user()

def ask_user():
    #Prompts user to filter leading and trailing rows of pure noise ("Drop-
off Filter")
    check = str(input("Would you like to apply a 'Drop-
off Filter' on these samples? Note, the filter will not be ran for samples in which
 more than a third of their rows are pure noise. (Y/N): ")).lower().strip()
    try:
        if check[:1] == 'y':
            return True
        elif check[:1] == 'n':
            return False
        else:
            print('Invalid Input')
            return ask_user()
    except:
        print("Please enter valid inputs")
        return ask_user()

def writedoc(PercentLowerNoise, PercentUpperNoise, filename, NoiseNom, UpperNoiseNo
m, SingleTow):
    #Creates and saves document detailing two types of noise present in sample
    #If sample is a single tow, records information as a simple count
    #If sample is a simulated layup error, records information as a percentage

    f= open(filename + '_Analysis.txt',"w+")
    if SingleTow == False:
        f.write("Percent Upper Noise = %s%%\n" % str(round(PercentUpperNoise, 3)))

        f.write("Percent Lower Noise = %s%%\n" % str(round(PercentLowerNoise, 2)))
```

```
    else:
        f.write("Quantity of Upper Noise Signals = %s\n" % str(round(UpperNoiseNom)
))
        f.write("Quantity of Lower Noise Signals = %s\n" % str(round(NoiseNom)))
    f.close()

def DropOffFilter(array, CrossNoiseRows, NoiseNom):
    #This filter is most applicable when the tow is at the end of a stage or table
and the end of the scan reads a drop-off.
    #The filter only runs if the number of pure noise rows represents less than a t
hird of the total number of rows in the scan (called out in GenerateArray function)

    rarray = np.copy(array) #Create copy of array to use in this function. (NumPy A
rray mutability)
    StartVoidRows, EndVoidRows = CheckVoidArray(CrossNoiseRows) #Separate list of p
ure noise rows into lists of continuous rows at each start and end of sample

    g = 0
    darray = np.empty([np.shape(rarray)[0] - len(StartVoidRows) -
 len(EndVoidRows), np.shape(rarray)[1]]) #Initialize empty array. Size is equal to
length of origional array minus amount of both continuous start and end pure noise
rows

    for k in range (np.shape(rarray)[0]):
        if (k  in StartVoidRows) or (k in EndVoidRows): #Is this row a pure noise r
ow
            pass
        else:
                for z in range(np.shape(rarray)[1]): #If this row is not a pure nois
e row add the row in the next available spot in the new array
                    darray[g,z] = rarray[k, z]
                g = g + 1

        return(darray, NoiseNom)

   def GenerateArray(fileName, RunFilter):
        #Generates a Numpy Array from CSV File, and Simply Counts Noise Elements
        #Reads File, adjusts lower out of bounds errors to zero, Calculates Noise Pe
rcentage, performs a noise count, and returns 2D numpy array along with noise data

        NoiseNom = 0 #Simple Count for instances of values around -99
        RealValTotal = 0 #Used in calculating average value of real points
        array = genfromtxt(fileName + ".csv", delimiter=',', dtype=np.float) #Genera
tes numpy array from csv file
        array = np.squeeze(array) #Resizes Numpy Array from a 3D Matrix to a 2D Matr
ix

        CrossNoiseRows = [] #List which stores pure noise rows by their row number

        #This for Loop filds lower out of bounds errors, sets them to 0 and counts t
hem as variable Noise Num
        # This loop also records all pure noise rows
        for i in range(np.shape(array)[0]): #Length of scan row by row
            CrossNoiseCount = 0 #Used to determine if row is pure noise
            for j in range(np.shape(array)[1]): #Width of scan, zero to four hundred

                if array[i,j] < -
20: #Negative values are errors, typically all are around -99
```

```
123.                    array[i,j] = 0 #Lowest actual value on unscaled scan, backing pl
    ate is typically equal to zero
124.                    NoiseNom = NoiseNom + 1 #Count each instance as a noise element
    in the overall array
125.                    CrossNoiseCount = CrossNoiseCount + 1 #Records an instance of no
    ise in the row
126.                    #if (j == np.shape(array)[1]-
    1) and (CrossNoiseCount >= 0.75*np.shape(array)[1]):
127.                    if CrossNoiseCount == np.shape(array)[1]:   #Switch to above if
    statement if goal is to eliminate drop off errors while backing plate visible
128.                        CrossNoiseRows.append(i) #Add this row number to list of pur
    e noise rows
129.                        NoiseNom = NoiseNom -
     np.shape(array)[1] #Removes count of drop-
    off row from NoiseNom (Correcting this value since the row is to be removed)
130.                else:
131.                    RealValTotal = RealValTotal + array[i,j] #If value is not noise,
     the value is added to later determine average of real values
132.
133.        if RunFilter == True and len(CrossNoiseRows) < 0.33*(np.shape(array)[0]) and
     len(CrossNoiseRows) > 0: #Only perform if commanded to and if pure noise is less t
    han a third of total rows
134.            barray, NoiseNom = DropOffFilter(array, CrossNoiseRows, NoiseNom) #Remov
    e pure noise rows from start and end of array
135.
136.        else: #If not running filter to remove pure noise rows from start and end of
     array
137.            NoiseNom = NoiseNom + np.shape(array)[1]*len(CrossNoiseRows) #Add back c
    ount of noise points previously removed due to pure noise rows
138.            barray = np.copy(array) #Rename array to match name moving forward
139.
140.        RealValCount = np.size(barray) - NoiseNom
141.        PureNoise = False
142.
143.        if len(CrossNoiseRows) == len(array): #If array is entirely noise values, ev
    ery row is pure noise
144.            #Set some values in the case of pure noise.
145.            #Doing this also solves divide by zero errors
146.            PureNoise = True
147.            RealValAvg = 0
148.            RealValCount = 0
149.            PercentNoise = 100
150.        else: #Array is not entirely noise
151.            RealValAvg = RealValTotal/RealValCount
152.            PercentNoise = 100*NoiseNom/np.size(barray)
153.
154.        return (barray, NoiseNom, PercentNoise, RealValAvg, RealValCount, PureNoise)

155.
156.    def CheckVoidArray(CrossNoiseRows):
157.        #This function sorts the list of rows appearing as pure noise into lists 'St
    art' and 'End' to confirm they are caused by drop off.
158.        #This function will be called out within DropOffFilter function, which is ca
    lled out within GenerateArray function.
159.
160.        #Initialize empty arrays and boolean
161.        StartVoidRows = []
162.        EndVoidRows = []
163.        IsStart = False
164.
```

```
        if(CrossNoiseRows[0] == 0): #If first pure noise row is first row of main array
            IsStart = True
        else: #First row of array contains some meaningful data
            IsStart = False

        if(IsStart == True):
            for q in range(len(CrossNoiseRows)):
                if(CrossNoiseRows[q] == 0): #Add first value to Start row list
                    StartVoidRows.append(CrossNoiseRows[q])
                else:
                    if (CrossNoiseRows[q] == CrossNoiseRows[q-1]+1): #Check if row count is continuous 0,1,2,3...
                        StartVoidRows.append(CrossNoiseRows[q]) #If continuous, add row number to Start row list
                    else: #If not continuous, no longer at start and break for loop

                        IsStart = False
                        break

        if(IsStart == False):
            for w in range(len(CrossNoiseRows)-1, 0, -1): #Start at end and move backwards (Increment of negative one)
                if(w == len(CrossNoiseRows)-1): #Add last value to End row list
                    EndVoidRows.append(CrossNoiseRows[w])
                else:
                    if (CrossNoiseRows[w] == CrossNoiseRows[w+1]-1): #Check if row count is continuous w, w-1, w-2, w-3...
                        EndVoidRows.append(CrossNoiseRows[w]) #If continuous, add row number to End row list
                    else: #If now continuous, break for loop
                        break

        return (StartVoidRows, EndVoidRows)

    def GenerateImage(G, filename):
        #Generates an Image from a NumPy array using PIL.Image

        Garray = np.copy(G)
        if (np.amax(Garray != 0)): #Check for valid values
            if round(np.amax(Garray)) != 255: #Check if values are already mapped to pixel values
                Garray = (Garray-np.amin(Garray)) #Shift all values down by minimum value, down if min is positive, up if min is negative
                Garray = (Garray)*255/np.amax(Garray) #Scale max value to 255 for greyscale
                Garray = np.ceil(Garray) #Round to integer values for image generation
        else:
            pass

        img = Image.fromarray(Garray) #Create Image
        img = img.convert("L")
        img.save(filename + ".bmp") #Save Image
        return img

    def PixelVal(P):
        #This function maps a NumPy array to pixel values

        Parray = np.copy(P)
```

```
214.        Parray = (Parray-
    np.amin(Parray)) #Shift all values down by minimum value, down if min is positive,
    up if min is negative
215.        if (np.amax(Parray != 0)):
216.            Parray = Parray*255/(np.amax(Parray)) #Scale max value to 255 for greysc
    ale
217.        else:
218.            pass
219.        Parray = np.ceil(Parray) #Round to integer values for image generation
220.        return Parray
221.
222.    def ScaleRefined(S, RealValAvg, RealValCount):
223.        #This function refines an array for generating images by determining range,
    symetric about the average, in which 97% of valid (non-
    void) data falls (including spikes).
224.        #This function also calculates the count and percentage of non-
    void data represented by spikes.
225.        #All Lower Out of Bounds values are mapped to lower limit of range, all Uppe
    r Out of Bounds values mapped to upper limit of range
226.
227.        ScalingArray = np.copy(S)
228.        step = 0.125*np.std(ScalingArray) #Defines step size for while loop
229.        if (step != 0 and step != 'nan'):
230.            i = 0 #Count of number of loops. Not used in this version
231.            while ((((RealValAvg -
     step) < ScalingArray) & (ScalingArray < (RealValAvg + step))).sum() < (0.97*RealVa
    lCount)): #Check if range centered about the average value encompases 97% of valid
    (non-void) data
232.                step = step + 0.125*np.std(ScalingArray) #Increase step size by one
    eighth of the standard deviation of the subject array
233.                i = i+1 #Count loops
234.
235.            UpperBound= RealValAvg+step #Define Upper Bound of valid data
236.            LowerBound = RealValAvg-step #Define Lower Bound of valid data
237.
238.        else: #If errors occur when defining step size, just set max and min and upp
    er and lower bounds respectively
239.            UpperBound= np.amax(S)
240.            LowerBound = np.amin(S)
241.
242.        UpperNoiseNom = 0 #Initialize value for simple count of Upper Noise values
243.
244.        for i in range(np.shape(ScalingArray)[0]): #Length of scan row by row
245.            for j in range(np.shape(ScalingArray)[1]): #Width of scan, zero to four
    hundred
246.                if ScalingArray[i,j] < LowerBound: #Value is Void Noise
247.                    ScalingArray[i,j] = LowerBound #Set this noise value to lower bo
    und value for image creation
248.                elif ScalingArray[i,j] > UpperBound: #Value is Spike Noise
249.                    UpperNoiseNom = UpperNoiseNom + 1 #Count instance of Spike Noise

250.                    ScalingArray[i,j] = UpperBound #Set this noise value to upper bo
    und value for image creation
251.
252.        PercentUpperNoise = 100*UpperNoiseNom/np.size(ScalingArray) #Calculate Perce
    ntage of array represented as spike noise using count of upper noise values and siz
    e of input array
253.
254.        return (ScalingArray, PercentUpperNoise, UpperNoiseNom)
255.
256.    if __name__ == '__main__': #good practice
```

```
257.        tStart = time.time()
258.        print('--
    Program started at ' + time.strftime("%H:%M:%S", time.localtime()) + ' --')
259.        main() #run
260.        print('-- Program completed in %s seconds --' %round((time.time() -
    tStart)))
```

# APPENDIX B

# DATA ANALYSIS SCRIPT INSTRUCTIONS AND INFORMATION

**Prerequirements**

Development and execution of the code was performed in version 3.3.3 of the development environment Spyder. The code is written in Python version 3.7.

**Running the Code**

Coded in Python 3.7, the program accepts manual input of a directory path (or list of directories to iterate through) in line 11. From this directory, a list of folders is generated to be iterated over. For each folder, a list of files contained within the folder is created. During each loop, the program confirms that the file is of the file type ".csv" and processes the data.

Two user prompts appear during execution of the script. The first asks whether or not to apply a drop-off filter to samples. This filter was implemented to avoid erroneous noise presented when information is scanned past the boundary of the tow, resulting in noise "bookending" a sample. This filter is further detailed in Section 3.5.4, "Drop Off Filter". The second prompt asks if all samples are single tow samples.

The result of running the script is the generation of two new files for each .csv input file. A text file is generated reporting the sample's noise quantified (percentage for layup error samples and simple count for single tow samples). Additionally, an image file is generated from the data.

**Sample Type**

All samples must be similar layup type to appropriately quantify noise. Noise for single tow samples, for this report, was reported as a simple count for direct comparison between scans. Compare that to simulated layup error samples, in which noise data is reported as a percentage of overall data present.

**Features**

- The option to run or not run the drop off filter
- The ability to specify single tow samples or simulated layup error samples

**Known Bugs**

- If a simulated layup error sample is represented by pure noise, it is intentionally reported as having 100% noise and “9999999” data points of noise. This is to avoid a division by zero.

# APPENDIX C

## GANTRY SYSTEM OPERATIONAL INSTRUCTIONS

Presented here the steps in operation of the gantry system used to collect profilometry scan data. The system utilizes the LVJ Keyence software to collect and export scan data and custom Arduino code to move the gantry as desired.

Step 1: Check that the Keyence sensor is plugged in and the green led on the Keyence power supply and controller is turned on.

Step 2: Open the Arduino software on the desktop and then open the LVJ Keyence software.

Step 3: Open the Serial Monitor through Arduino by clicking tools or by pressing CLRT +SHIFT+M.

Step 4: Check the settings on the Keyence software based on the experimental requirements.

Step 5: Set up the material samples. Standard setup is such that they are parallel with the gantry system motion. The lasers mounted on the gantry can be used for reference, but the lasers are to be switched off prior to scanning.

Step 6: Begin data collection by clicking “start scan” from within the Keyence software.

Step 7: Begin the gantry motion by inputting capital “F” in the serial monitor of Arduino.

Step 8: Stop data collection by clicking “stop scan” from within the Keyence software.

Step 9: Stop the gantry motion by inputting capital “S” in the serial monitor of Arduino. Alternatively, or if needed, reverse the gantry motion by inputting capital “B”.

Step 10: To save the CSV click “export data” from within the Keyence software and select the desired file location.

# APPENDIX D

## WEATHER DATA

Presented here is weather data as reported by the National Oceanic and Atmospheric Administration (NOAA). The data is representative of daily average temperatures and humidity levels during the life of the experiment into the effect of environmental exposure on profilometry scanning error prominence, conducted in Columbia, South Carolina from May 9th, 2019 through June 11th, 2019.

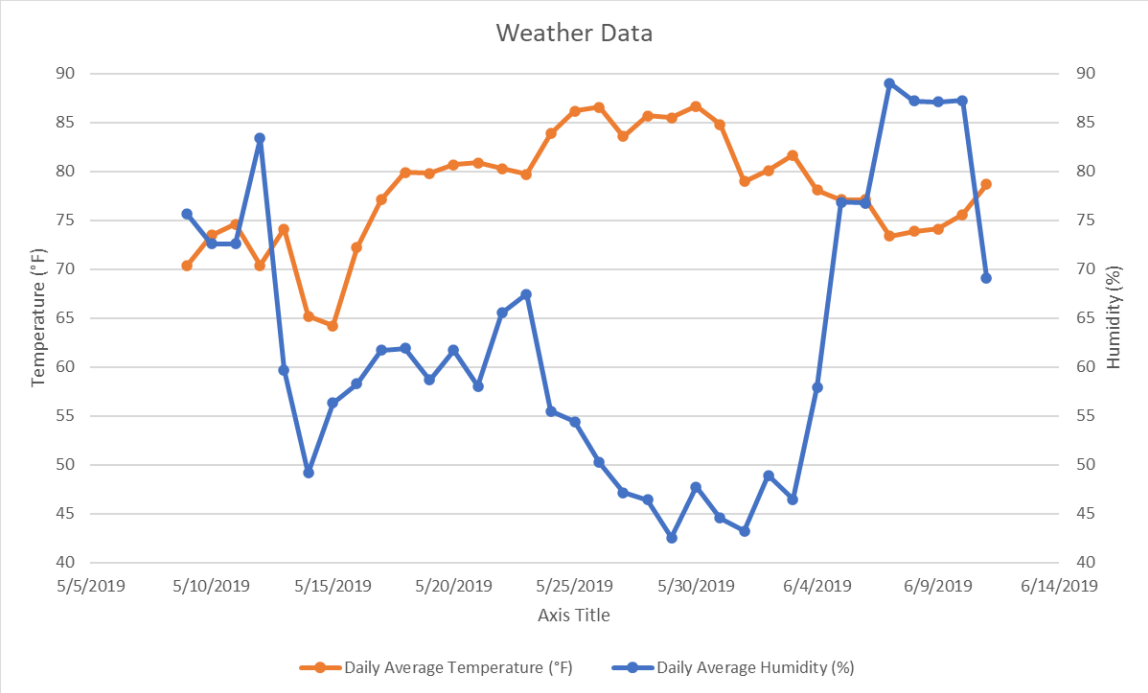


*Figure D.1: Weather Data Columbia, SC Summer 2019*

# APPENDIX E

# COMBINED VARIABLE ANALYSIS RESULT PLOTS

Presented here are the experimental findings from the analysis of combining variable manipulations to improve scanning result quality. The results are presented per material type. Each simulated layup errors and single tow samples were investigated.

## E.1 MATERIAL A

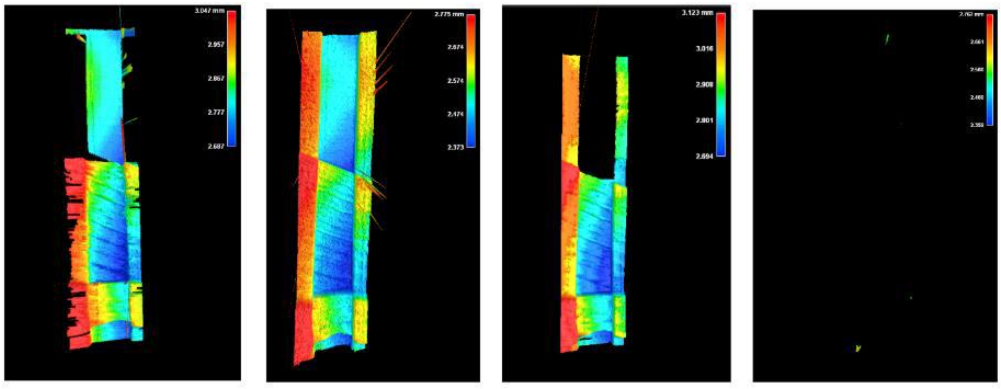


*Figure E.1: Keyence Software 3D Images Generated by Scanning with Combinations of Default/Ideal Settings and 0°/17.5° Pitch – Material A Simulated Layup Error Samples*

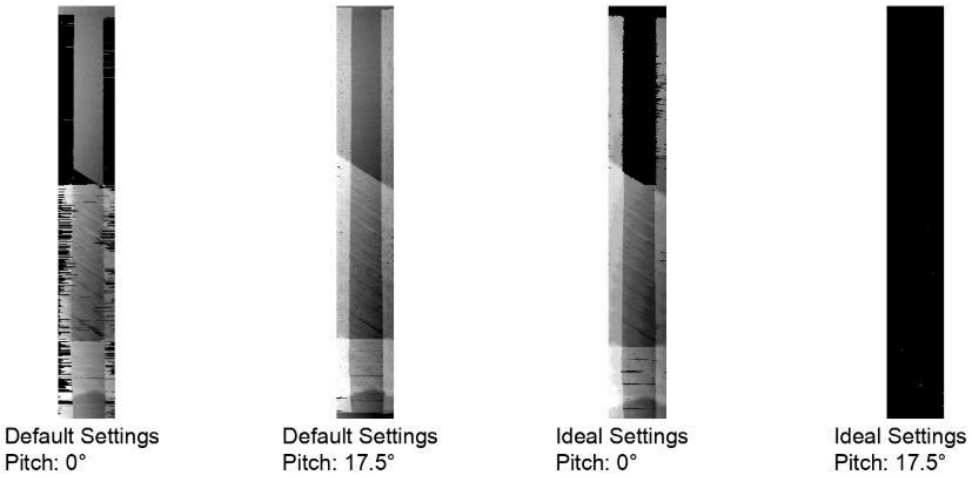


*Figure E.2: Script Created Images Generated by Scanning with Combinations of Default/Ideal Settings and 0°/17.5° Pitch – Material A Simulated Layup Error Samples*

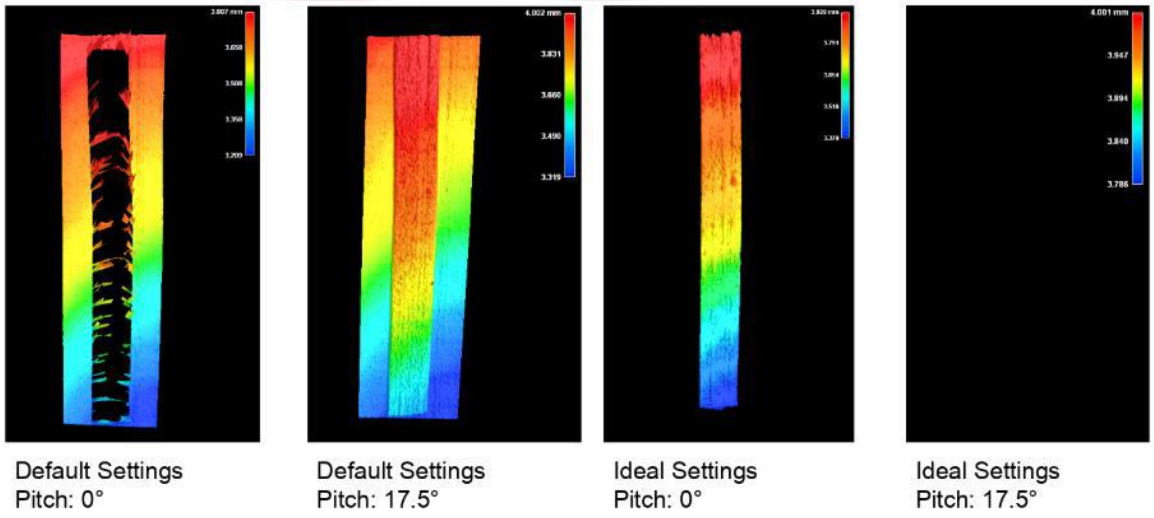


*Figure E.3: Keyence Software 3D Images Generated by Scanning with Combinations of Default/Ideal Settings and 0°/17.5° Pitch – Material A Single Tow Samples*

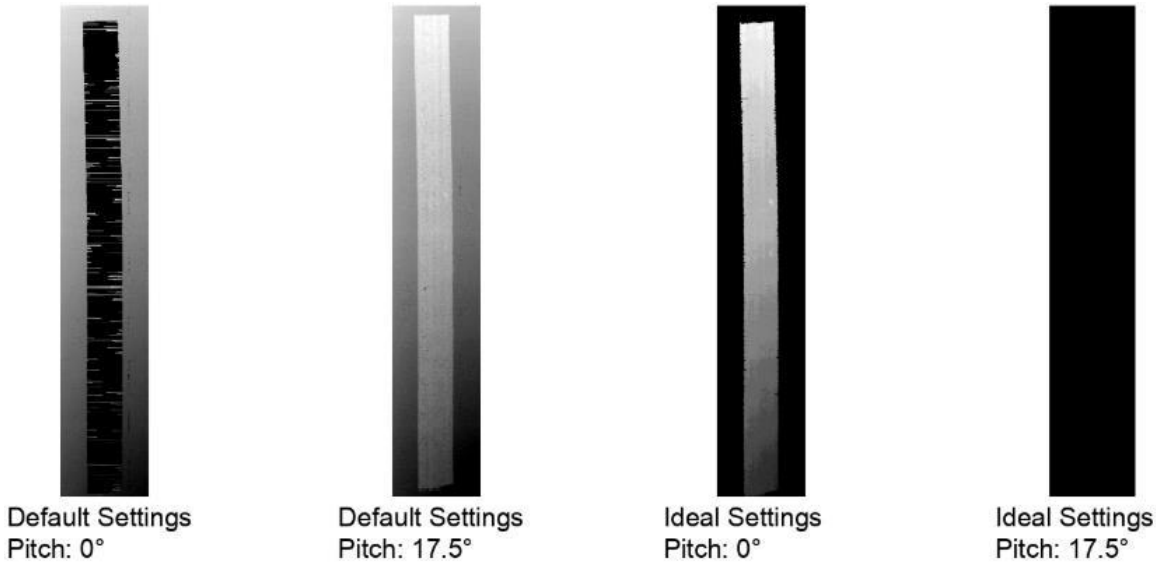


*Figure E.4: Script Created Images Generated by Scanning with Combinations of Default/Ideal Settings and 0°/17.5° Pitch – Material A Single Tow Samples*

## E.2 MATERIAL B

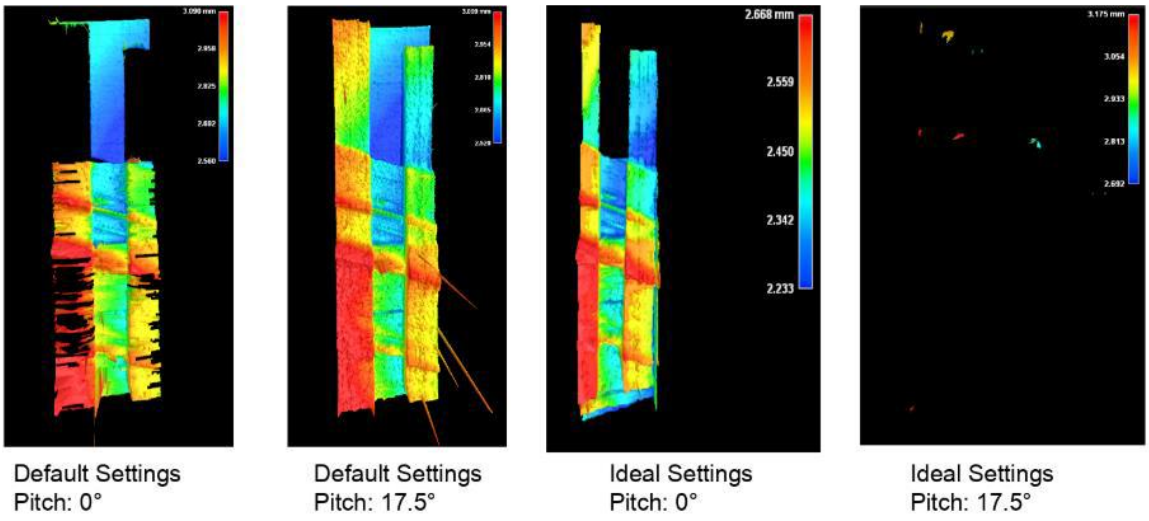


*Figure E.5: Keyence Software 3D Images Generated by Scanning with Combinations of Default/Ideal Settings and 0°/17.5° Pitch – Material B Simulated Layup Error Samples*

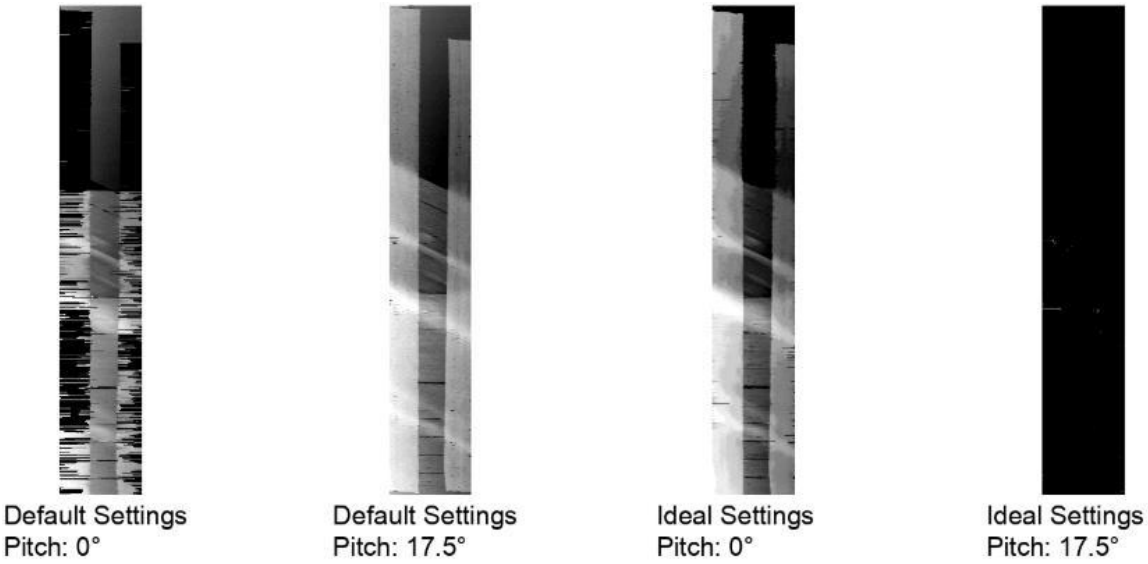


*Figure E.6: Script Created Images Generated by Scanning with Combinations of Default/Ideal Settings and 0°/17.5° Pitch – Material B Simulated Layup Error Samples*

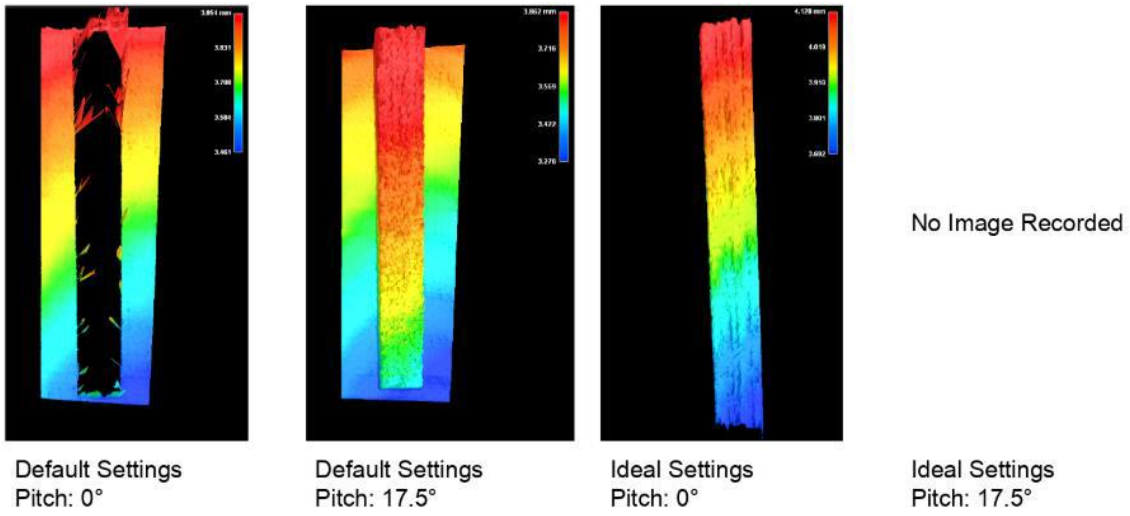


*Figure E.7: Keyence Software 3D Images Generated by Scanning with Combinations of Default/Ideal Settings and 0°/17.5° Pitch – Material B Single Tow Samples*

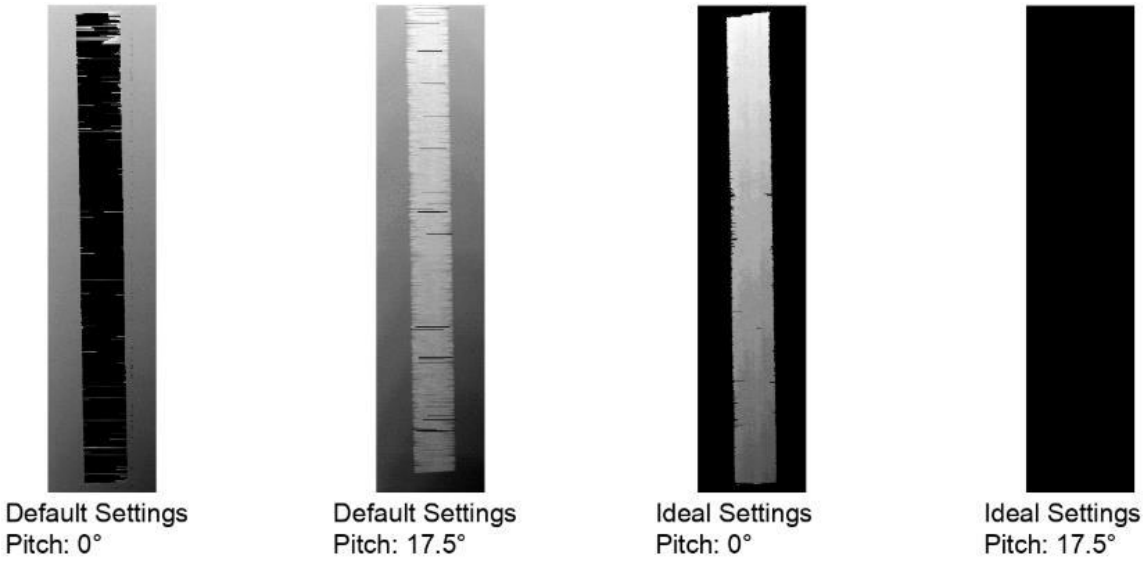


*Figure E.8: Script Created Images Generated by Scanning with Combinations of Default/Ideal Settings and 0°/17.5° Pitch – Material B Single Tow Samples*

## E.3 MATERIAL C

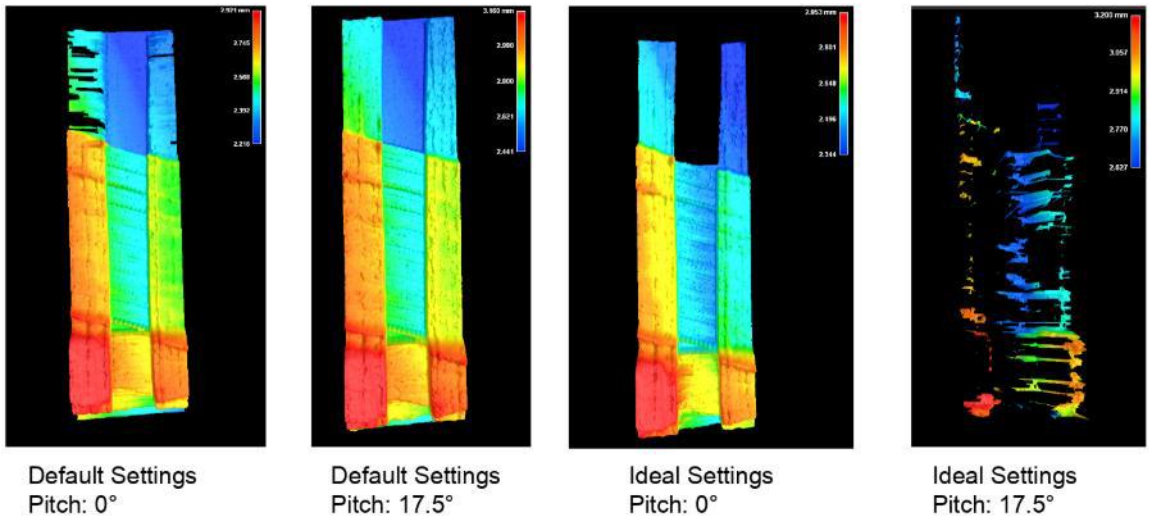


*Figure E.9: Keyence Software 3D Images Generated by Scanning with Combinations of Default/Ideal Settings and 0°/17.5° Pitch – Material C Simulated Layup Error Samples*

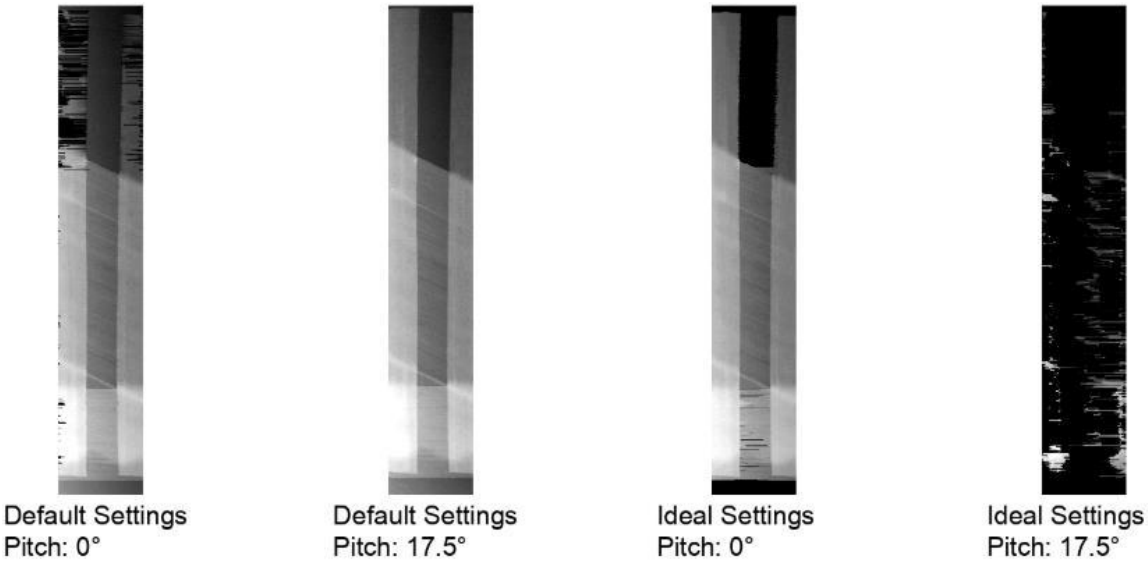


*Figure E.10: Script Created Images Generated by Scanning with Combinations of Default/Ideal Settings and 0°/17.5° Pitch – Material C Simulated Layup Error Samples*

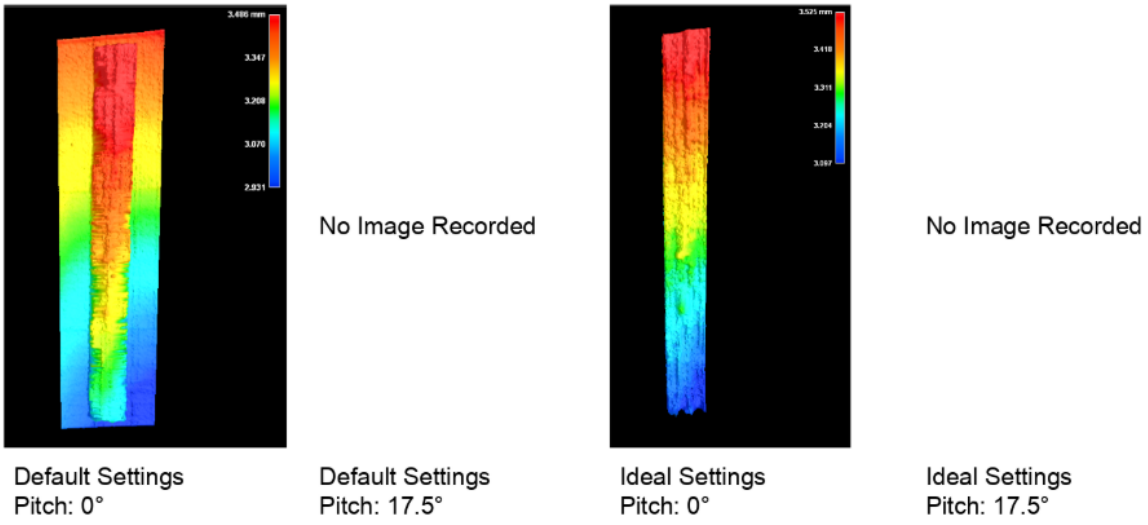


*Figure E.11: Keyence Software 3D Images Generated by Scanning with Combinations of Default/Ideal Settings and 0°/17.5° Pitch – Material C Single Tow Samples*

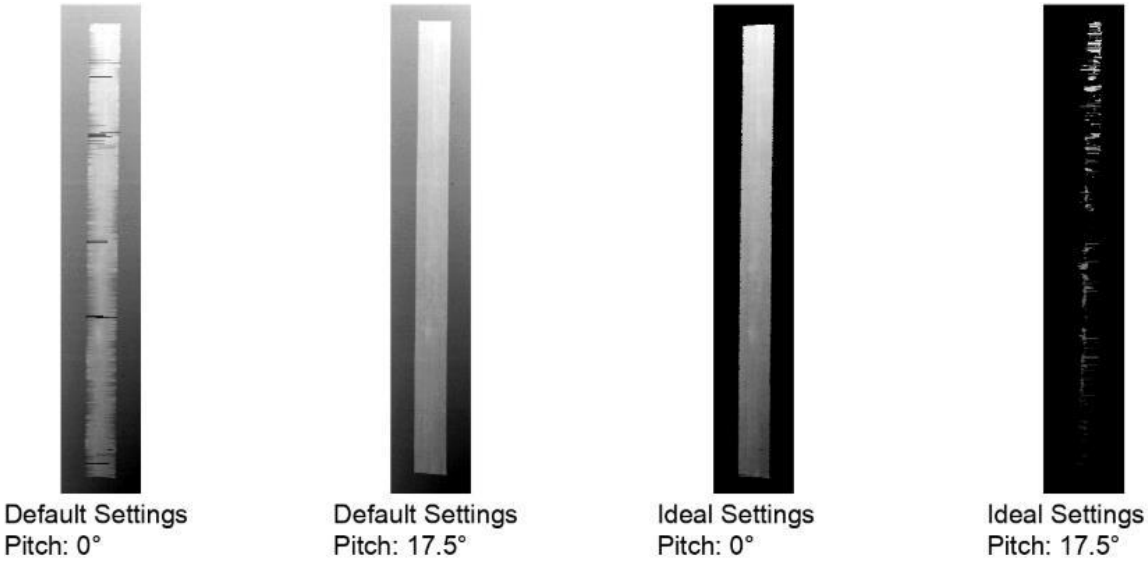


*Figure E.12: Script Created Images Generated by Scanning with Combinations of Default/Ideal Settings and 0°/17.5° Pitch – Material C Single Tow Samples*